U.PORTO

MESTRADO INTEGRADO EM BIOENGENHARIA
Ramo de Biotecnologia Molecular

DISSERTAÇÃO

Immunomodulatory nanoenabled 3D scaffolds for chondral repair

Cristiana Maria Sousa Couto

UNIVERSIDADE DO PORTO
Faculdade de Engenharia
Instituto de Ciências Biomédicas Abel Salazar
Instituto de Engenharia Biomédica

Immunomodulatory nanoenabled 3D scaffolds for chondral repair

Cristiana Maria Sousa Couto

Master's Dissertation

Integrated Masters in Bioengineering – Molecular Biotechnology

Faculty of Engineering of the University of Porto

School of Medicine and Biomedical Sciences

Supervisor: Susana G. Santos, PhD

Co-supervisor: Juliana Alves, PhD

September, 2021

This work was financially supported by the European Union's Horizon 2020 research and innovation programme under the RESTORE Project, grant agreement Nº 814558. I also thank all partners that kindly provided the materials used for the experimental work.

This project received funding from the European Union's Horizon 2020 research and innovation programme under grant agreement No 814558.

Agradecimentos

Em primeiro lugar, um agradecimento especial à minha orientadora, Susana Santos, por quem guardo um grande carinho. Foi um prazer ter aprendido tanto num período tão curto de tempo. Sem a sua motivação e partilha de conhecimento esta dissertação não seria possível. E à minha coorientadora, Juliana Alves pelas sugestões e revisão do manuscrito.

Ao Professor Mário Barbosa por acolher todos os elementos do grupo de braços abertos, nos fazer questionar e incentivar todos os dias a ser melhores cientistas. E a todos do grupo Microenvironments for New Therapies por me terem recebido tão bem e por estarem sempre dispostos a ajudar. Em especial à Silvana que me orientou no começo, à Kaoutar, minha colega de projeto que me ajudou inúmeras vezes, à Mafalda, por todas as dúvidas que me tirou e ao Nuno e Filipe, pela companhia. Não posso deixar de fazer um agradecimento especial à María Lázaro do Bioimaging Centre por toda a orientação no microscópio confocal e por me avisar sempre que havia uma vaga disponível. A sua ajuda foi preciosa neste trabalho.

Aos meus amigos de faculdade que fizeram com que estes 5 anos passassem a voar. Ao "Party Hits", Miguel, Carol, Pipa, Dri, Catx, Eva e Inês, por estarem sempre prontos para a festa. Ao "Bambora", Nocas, Martim, Rita e Inês, pelos jantares e lanches. Um agradecimento especial às minha amigas de Biotec, Lina e Filipa que tornaram a experiência de faculdade mais especial. Ao Filipe, que me acompanha desde o 9º ano e que está ao meu lado (e na minha turma) desde então.

Um parágrafo especial para o Matias, que me apoiou incansavelmente durante estes 5 anos de faculdade. Aturou todas as minhas crises existenciais e fez-me acreditar em mim quando eu duvidava. Foste minha força e em ti não teria sido a mesma coisa. Obrigada.

Não posso deixar de agradecer aos patudos daqui de casa, porque são uma presença constante. Ao papagaio Juca, por interromper todas as minhas reuniões Zoom. Ao Zeus, por estar sempre pronto para um passeio junto ao rio para me ajudar a limpar as ideias. Ao Dragão, pelas sonecas que fez enquanto eu estudava. E uma obrigada especial ao Boss, que me fez perceber que quando queremos arranjamos tempo para o mais importante. Tenho muitas saudades tuas.

Por último, um obrigado muito especial à minha família. Ao meu avô Silvério que estava sempre pronto para me levar à faculdade. À minha avó Maria pela preocupação constante. Ao meu pai, por me incentivar a fazer sempre melhor. E à minha mãe. A minha fã número um, sempre lá para mim. Obrigada pelos lanchinhos surpresa a meio do estudo, obrigada pelo bolinho que fazias quando sentias que eu precisava e por todas as vezes que me dizias para parar e descansar. Muito obrigada!

Foram todos uma contribuição muito importante nesta jornada que agora chega ao fim e ser-vos-ei eternamente grata por tudo.

Abstract

Articular cartilage lesions in the knee remain a challenge for orthopedic surgeons to treat and often lead to osteoarthritis (OA). OA is a painful and disabling disease that affects millions of patients and is associated with an increasing socioeconomic impact. The surgical approaches currently in use have a limited capacity for tissue regeneration and yield only short-term symptom relief. Therefore, there is an urgent need to develop more effective alternatives.

To effectively promote cartilage regeneration, it is critical to develop strategies that skew inflammation towards a pro-regenerative and pro-chondrogenic microenvironment. Merging biomaterials with recent progress in nanotechnology can be helpful to develop efficient immunomodulatory scaffolds. Macrophages are recognized as key players in resolving inflammation after implantation and can polarize towards a more pro-inflammatory (M1) or anti-inflammatory (M2) phenotype, depending on the stimuli received. In this work, the immunomodulatory properties of nanoenabled scaffolds with anti-inflammatory and stimuli responsive nanomaterials were investigated.

First, collagen-polylactic acid (Col-PLA) scaffolds nanoenabled with poly (lactic-co-glycolic) acid (PLGA) NPs, loaded with ibuprofen (PLGA-Ibuf), a commonly prescribed non-steroid anti-inflammatory drug (NSAID), were explored. Internalization of fluorescein isothiocyanate (FITC) loaded PLGA NPs was initially confirmed using conventional and imaging flow cytometry, indicating a dose-dependent uptake of NPs at early time points, up to 3h. Also, FITC-loaded PLGA NP internalization within nanoenabled Col-PLA scaffolds was evaluated by confocal microscopy. Results show macrophage colonization of nanoenabled scaffolds and PLGA NPs were observed inside of macrophages. Next, the anti-inflammatory and immunomodulatory properties of Col-PLA scaffolds nanoenabled with PLGA-Ibuf was studied by a combination of confocal microscopy, evaluating phenotypic markers CCR7 (M1) and CD163 (M2). When monocytes were seeded on Col-PLA scaffolds and allowed to differentiate towards macrophages directly on empty and nanoenabled scaffolds, their stimulation towards M1 phenotype could not be counteracted by the presence of PLGA-Ibuf. The proportion of CCR7 positive cells was high in unstimulated and M1 stimulated cells cultured in Col-PLA scaffolds nanoenabled with PLGA-Ibuf. Also, levels of prostaglandin E2 (PGE2) and the pro-inflammatory cytokine interleukin-1β (IL-1β) were significantly increased by M1 stimulation in Col-PLA empty or nanoenabled with PLGA-Ibuf. Thus, we tested if ibuprofen could have been consumed during macrophage differentiation and before their stimulation. For that, monocytes were initially differentiated towards macrophages in Petri dishes and seeded on nanoenabled Col-PLA scaffolds at day 10 and then stimulated towards M1 phenotype. This led to high CCR7 expression in all conditions tested, stimulated and non-stimulated, and again no significant impact of

PLGA-Ibuf presence. Interestingly, PGE2 levels were not significantly increased by M1 stimulation in cells cultured in Col-PLA scaffolds nanoenabled with PLGA-Ibuf, but IL-1β levels were significantly increased after M1 stimulation.

Thus, we questioned if ibuprofen was not available when PLGA-Ibuf NPs were incorporated in Col-PLA scaffolds and investigated if the addition of the NPs and the free ibuprofen on top of the scaffolds would be able to modulate macrophages M1 polarization. The analysis of M1 and M2 phenotypic markers was inconclusive, with high proportions of cells expressing CCR7, even in unstimulated conditions. Nonetheless, PLGA-Ibuf NPs added on top were capable of inhibit PGE2 levels increase in M1 activated macrophages but levels of IL-1β still increased significantly with M1 stimulation.

Recruitment of mesenchymal stromal/ stem cells (MSCs) to cartilage lesions could promote their repair/regeneration, as these cells are known to differentiate into the chondrogenic lineage and to modulate immune cells, including macrophages. Hence, the capacity of macrophages cultured on nanoenabled Col-PLA scaffolds to recruit MSCs was investigated, as well as the influence of a pro-inflammatory M1 stimuli in this crosstalk. Matrigel-coated membranes were used in transwell invasion assays to study MSCs recruitment. Our results showed that seeded macrophages promoted MSCs recruitment, with slight increases for M1-stimulated macrophages, but no significant differences were observed between macrophages cultured on empty or nanoenabled scaffolds.

Lastly, we studied the effects of COPLA® Scaffolds nanoenabled with multi-walled carbon nanotubes (MWCNT) on macrophages inflammatory response. This class of stimuli-responsive nanobiomaterials might have the ability to enhance cartilage regeneration through external stimulation, while providing enhanced mechanical stability. Confocal microscopy images demonstrated that macrophages populated the scaffolds after 13 days of culture and presented normal morphology. More detailed analysis by transmission electron microscopy (TEM) clearly shows the presence of CNTs inside the cells and some evidence of cellular and mitochondrial stress. The presence of CNTs in the scaffolds resulted in an increase of the proportion of macrophages expressing pro-inflammatory markers upon M1 stimulation, and in comparison with pristine scaffolds.

Taken together, our results show that incorporation of PLGA-Ibuf NPs in Col-PLA scaffolds did not lead to the expected anti-inflammatory effect and positive immunomodulatory shift from M1 to M2 macrophages. On another note, preliminary results indicate that CNT functionalized scaffolds might have a pro-inflammatory effect in macrophages that requires further investigation.

Keywords: Cartilage Regeneration; Scaffold; Nanoparticles; Macrophage; Phenotype; Mesenchymal Stem Cells; Carbon Nanotubes.

Resumo

As lesões da cartilagem articular do joelho continuam a ser um desafio para cirurgiões ortopédicos e muitas vezes levam à progressão para osteoartrite (OA). A OA é uma doença dolorosa e incapacitante que afeta milhões de pacientes e está associada a um grande impacto socioeconómico. As abordagens cirúrgicas atualmente em uso têm uma capacidade limitada de regeneração do tecido e apenas promovem um alívio dos sintomas a curto prazo. Há, portanto, uma necessidade urgente de desenvolver alternativas mais eficazes.

Para promover eficazmente a regeneração da cartilagem, é fundamental desenvolver estratégias que inclinem a inflamação em direção a um microambiente pró-regenerativo e pró-condrogénico. A combinação de biomateriais com os recentes progressos da nanotecnologia pode ser útil para desenvolver scaffolds imunomoduladores eficientes. Os macrófagos são reconhecidos pelo seu papel chave na resolução da inflamação após a implantação e podem polarizar em direção a um fenótipo mais pró-inflamatório (M1) ou anti-inflamatório (M2), dependendo dos estímulos recebidos. Neste trabalho, foram investigadas as propriedades imunomodulatórias de scaffolds funcionalizados com nanomateriais anti-inflamatórios e responsivos a estímulos.

Primeiro, scaffolds de colagénio-ácido polilático (Col-PLA) nanofuncionalizados com nanopartículas (NPs) de ácido poli (lático-co-glicólico) (PLGA), carregadas com ibuprofeno (PLGA-Ibuf), um medicamento anti-inflamatório não esteroide comumente prescrito (NSAID), foram explorados. A internalização das NPs de PLGA carregadas com isotiocianato de fluoresceína (FITC) foi inicialmente confirmada por citometria de fluxo convencional e de imagem e indicou uma internalização dependente da dose em pontos de tempo iniciais, até 3h. Adicionalmente, a internalização de NPs de PLGA carregadas com FITC após incorporação em scaffolds de Col-PLA nanofuncionalizados foi avaliada por microscopia confocal. Os resultados mostram a colonização dos macrófagos nos scaffolds e as NPs de PLGA foram observadas dentro dos macrófagos. Em seguida, as propriedades anti-inflamatórias e imunomodulatórias dos scaffolds Col-PLA nanofunciolazidados com PLGA-Ibuf foram estudadas por microscopia confocal, avaliando os marcadores fenotípicos CCR7 (M1) e CD163 (M2). Quando os monócitos foram cultivados em scaffolds Col-PLA e se diferenciaram em macrófagos diretamente nos scaffolds vazios e nanofuncionalizados, a sua estimulação para o fenótipo M1 não pôde ser contrariada pela presença de PLGA-Ibuf. A proporção de células positivas para CCR7 foi elevada em células não estimuladas e M1 estimuladas, quando cultivadas em scaffolds Col-PLA nanofuncionalizados com PLGA-Ibuf. Além disso, os níveis de prostaglandina E2 (PGE2) e da citocina pró-inflamatória interleucina-1β (IL-1β) foram significativamente aumentados pela estimulação M1 em Col-PLA vazios ou nanofuncionalizados com PLGA-Ibuf. Assim, testamos se o ibuprofeno poderia ter sido consumido durante a diferenciação dos macrófagos e antes de sua estimulação. Para

isso, os monócitos foram inicialmente diferenciados para macrófagos em placas de Petri e cultivados em scaffolds Col-PLA ao dia 10 e, em seguida, estimulados para o fenótipo M1. Isto levou a uma alta expressão de CCR7 em todas as condições testadas, estimuladas e não estimuladas, e novamente não houve nenhum impacto significativo da presença de PLGA-Ibuf. Curiosamente, os níveis de PGE2 não foram significativamente aumentados pela estimulação M1 em células cultivadas em scaffolds Col-PLA nanofuncionalizados com PLGA-Ibuf, mas os níveis de IL-1β aumentaram significativamente após a estimulação M1.

Assim, questionamos se o ibuprofeno não estava disponível quando NPs de PLGA-Ibuf foram incorporados em scaffolds Col-PLA e investigamos se a adição de NPs e ibuprofeno livre no topo dos scaffolds seria capaz de modular a polarização M1 de macrófagos. A análise dos marcadores fenotípicos M1 e M2 foi inconclusiva, com altas proporções de células a expressar CCR7, mesmo em condições não estimuladas. No entanto, as NPs de PLGA-Ibuf adicionadas no topo foram capazes de inibir o aumento dos níveis de PGE2 em macrófagos ativados M1, mas os níveis de IL-1β ainda aumentaram significativamente com a estimulação M1.

O recrutamento de células estaminais / tronco mesenquimais (MSCs) para lesões da cartilagem pode promover a sua regeneração, já que estas células são conhecidas por se diferenciarem na linhagem condrogénica e por modularem células imunes, incluindo macrófagos. Assim, a capacidade de macrófagos cultivados em scaffolds Col-PLA nanofuncionalizados para recrutar MSCs foi investigada, bem como a influência de um estímulo M1 pró-inflamatório neste crosstalk. Membranas revestidas com Matrigel foram utilizadas em ensaios de invasão transwell para estudar o recrutamento de MSCs. Os nossos resultados mostraram que macrófagos cultivados promoveram recrutamento de MSCs, com um ligeiro aumento para macrófagos estimulados para M1, mas nenhuma diferença significativa foi observada entre macrófagos cultivados em scaffolds vazios ou nanofuncionalizados.

Por último, estudamos os efeitos de COPLA® Scaffolds nanofuncionalizados com nanotubos de carbono de paredes múltiplas (MWCNT) na resposta inflamatória dos macrófagos. Esta classe de nanobiomateriais responsivos a estímulos pode ter a capacidade de aumentar a regeneração da cartilagem por meio de estimulação externa, enquanto melhora a estabilidade mecânica. Imagens de microscopia confocal demonstraram que os macrófagos se encontram distribuídos nos scaffolds após 13 dias e apresentaram uma morfologia normal. Uma análise mais detalhada por microscopia eletrónica de transmissão (TEM) mostra claramente a presença de CNTs dentro das células e algumas evidências de stress celular e mitocondrial. A presença de CNTs nos scaffolds resultou num aumento da proporção de macrófagos que expressam marcadores pró-inflamatórios após estimulação M1, e em comparação com os scaffolds vazios.

Os nossos resultados mostram que a incorporação de NPs de PLGA-Ibuf em scaffolds Col-PLA não levou a um efeito anti-inflamatório esperado e ao shift imunomodulador positivo de macrófagos M1 para M2. Por outro lado, resultados preliminares indicam que os scaffolds funcionalizados com CNT podem ter um efeito pró-inflamatório em macrófagos que requer uma investigação mais aprofundada.

Palavras-chave: Regeneração de cartilagem; Scaffold; Nanopartículas; Macrófagos; Fenótipo; Células estaminais mesenquimais; Nanotubos de carbono.

Table of Contents

List of Figures

List of Tables

List of Abbreviations

3D	Three-dimensional
ACI	Autologous chondrocyte implantation
ADAMTS	A disintegrin and metalloproteinase with thrombospondin motifs
APC	Antigen presenting cells
BC	Buffy coats
BCP	Basic calcium phosphate
BM	Bone marrow
BSA	Bovine serum albumin
CCL	Chemokine CeC motif ligand
CD	Cluster of differentiation
CHUSJ	Centro Hospitalar Universitário de São João
CNT	Carbon nanotube
Col-PLA	Collagen-poly (lactic-co-glycolic) acid
COX	Cyclooxygenase
CSF-1R	Colony-stimulating factor-1 receptor
CX3CR1	CX3C chemokine receptor 1
CXCL	Chemokine (C-X-C motif) ligand
DAMP	Damage-associated molecular pattern
DAPI	4', 6-diamidino-2-phenylindole
DC	Dendritic cell
DMEM	Dulbecco's modified Eagle's medium
DMSO	dimethyl sulfoxide
ECM	Extracellular matrix
EDTA	Ethylenediaminetetraacetic acid
FBS	Feral bovine serum
FITC	Fluorescein isothiocyanate
GAG	Glycosaminoglycans
HLA	Human leukocyte antigen
Ibuf	Ibuprofen
IDO	Indoleamine 2,3-dioxygenase
IGF	Insulin-like growth factor
IL	Interleukin
INF-γ	Interferon-γ
iPSC	Induced pluripotent stem cell
IRF	Interferon regulatory factor

ISCT	International Society for Cellular Therapy
LPS	Lipopolysaccharide
M-CSF	Macrophage colony-stimulating factor
MACI	Matrix-assisted autologous chondrocyte implantation
MARCO	Macrophage receptor with collagenous structure
MHC	Major histocompatibility complex
MMP	Matrix metalloproteinase
MSC	Mesenchymal stem/stomal cell
MWCNT	Multi-walled carbon nanotube
NF-κB	Nuclear factor-κB
NK	Natural killer
Nkd	Naked
NO	Nitric oxide
NP	Nanoparticle
NSAID	Non-steroid anti-inflammatory drug
OA	Osteoarthritis
OSM	Oncostatin
PBMC	Peripheral blood monocyte
PBS	Phosphate buffer saline
PCL	Polycaprolactone
PEG	Poly (ethylene glycol)
PES	Polyethersulfone
PFA	Paraformaldehyde
PGE2	Prostaglandin E2
PLA	Polylactic acid
PLGA	Poly (lactic-co-glycolic) acid
PLLA	Poly-L-lactid acid
RPMI	Roswell Park Memorial Institute
RT	Room temperature
SWCNT	Single-walled carbon nanotube
TE	Tissue engineering
TEM	Transmission electron microscopy
TGF-β	Transforming growth factor β
TLR	Toll-like receptors
TNF-α	Tumor necrosis factor alpha
TSG	TNF-α-stimulated gene/protein 6

CHAPTER 1. Introduction

1.1. Cartilage in health and disease

Diarthrodial joints connect two adjoining bones and their unique structural properties and components make them extraordinary load bearing and motion devices. Each mature diarthrodial joint is a complex structure that adjusts to its environment and mechanical demands. The different functions played by the joints in the body determine their structural differences[1].

A typical joint encompasses the synovium, muscles, tendons, ligaments, bursae, meniscus, subchondral bone and articular cartilage (Figure 1A)[1, 2]. The synovium lines the joint cavity and is where the production of synovial fluid takes place. The fluid provides nutrition for the articular cartilage and lubricates the cartilage surfaces. Joints are encased in connective tissue, the synovial capsule, that is lined by a thin cell layer of macrophages and fibroblasts, the synovial membrane[2]. Skeletal muscles support and allow movement of the body, under the control of the central nervous system. Tendons provide the functional and anatomic bridges between the muscles and bones, while ligaments are the stabilizing link between bones, allowing a limited range of movement. Some joints also include bursae, closed sacs that facilitate gliding of a tissue over another and meniscus, wedge-shaped fibrocartilaginous structures with important functions such as stability joint, load distribution and shock absorption[1].

The bones are protected by articular cartilage, which is a layer of a firm, visco-elastic tissue that allows low-friction and high-velocity movement in the joints[1]. The subchondral bone comprises a layer of compact cortical bone and an underlying system of cancellous bone, organized into a trabecular network. Histologically, cartilage tissue can be clearly distinguished from calcified cartilage and underlying subchondral bone (Figure 1B and C). The tidemark is a histological defined zone that separates the articular cartilage from the underlying calcified cartilage [1].

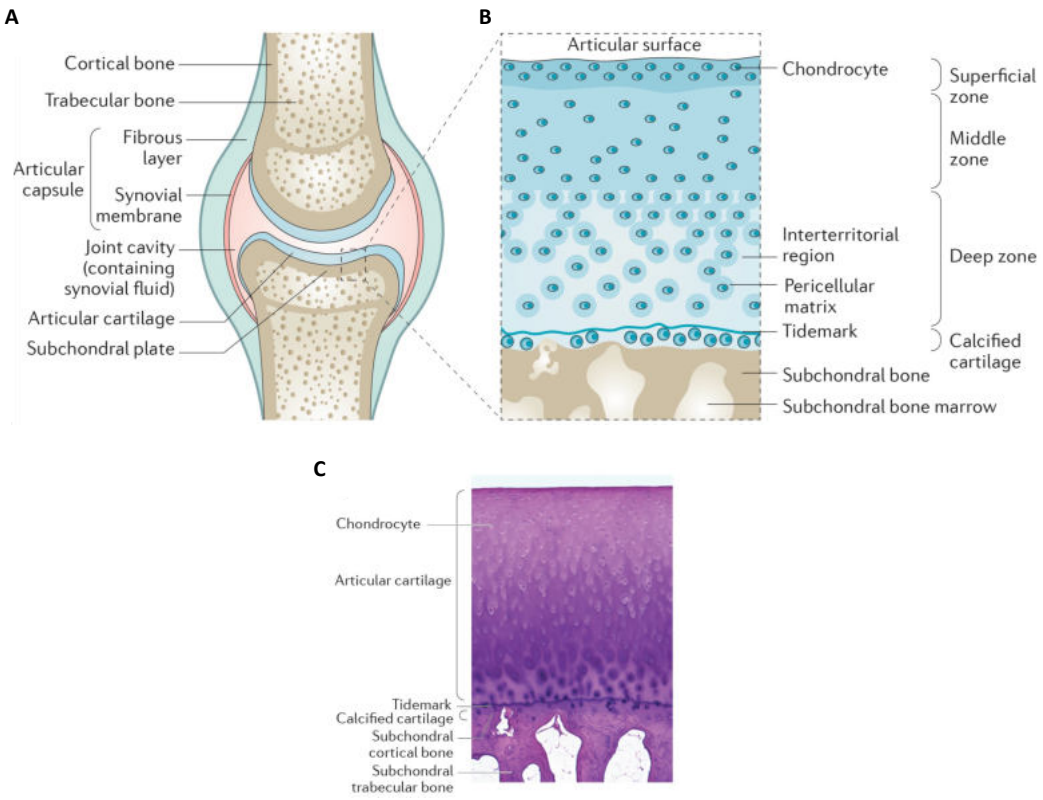

Figure 1. Healthy diarthrodial joint. A. Normal joint joining two adjacent bones that are covered by a layer of specialized articular cartilage and encased in a connective tissue capsule lined by a thin cell layer of macrophages and fibroblasts, the synovial membrane**. B, C.** Schematic illustration and histological representation of a diarthrodial joint articular surface cross-section illustrating the main structural elements, including the chondrocytes embedded in articular cartilage, tidemark, calcified cartilage and subchondral cortical and trabecular bone. From Martel-Pelletier, Barr, Cicuttini, Conaghan, Cooper, Goldring, Goldring, Jones, Teichtahl and Pelletier [3].

The cartilage is an organized and specialized connective tissue that can be classified into three types: fibrocartilage, elastic and hyaline. Articular hyaline cartilage covers the weight-bearing surfaces of diarthrodial joints. It has a high-water content (>70%) and is composed of organic extracellular matrix (ECM) components produced by the single cellular component of adult hyaline articular cartilage, the chondrocyte[1]. The ECM is essentially made of collagens (type II and IX) and non-collagenous proteins such as glycoproteins, glycosaminoglycans (GAGs) and proteoglycans (e.g., hyaluronan and aggrecan) (Table 1)[4].

Table 1. Extracellular matrix (ECM) components of articular cartilage. Adapted from Firestein, Kelley, Budd, McInnes and O'Dell [1].

Collagens
Type II
Type IX
Type XI
Type VI
Types XII, XIV
Type X (hypertrophic chondrocytes)
Proteoglycans
Aggrecan
Versican
Link protein
Biglycan (DS-PGI)
Decorin (DS-PGII)
Epiphycan (DS-PGIII)
Fibromodulin
Lumican
Proline/arginine-rich and leucine-rich repeat protein (PRELP)
Chondroadherin
Perlecan
Lubricin (SZP)
Other Non-collagenous Proteins (Structural)
Cartilage oligomeric matrix protein (COMP) or thrombospondin-5
Thrombospondin-1 and thrombospondin-3
Cartilage matrix protein (matrilin-1) and matrilin-3
Fibronectin
Tenascin-C
Cartilage Intermediate layer protein (CILP)
Fibrillin
Elastin
Other Non-collagenous Proteins (Regulatory)
Glycoprotein (gp)-39, YKL-40
Matrix Gla protein (MGP)
Chondromodulin-I (SCGP) and chondromodulin-II
Cartilage-derived retinoic acid-sensitive protein (CD-RAP)
Growth factors
Cell-Membrane Associated proteins
Integrins
Anchorin CII (annexin V)
Cell determinant 44 (CD44)
Syndecan-1, -3 and -4
Discoidin domain receptor 2

ECM components are essential for cartilage biomechanical properties[1]. The extensive collagen fiber network provides tensile strength, while the interlocking mesh of proteoglycans entraps and extrudes large quantities of water through its hydrophilic GAG side chains, providing compressive resilience[3]. These features render cartilage a smooth, gliding structure, that also serves as a cushion between the two bones[5]. It allows absorption of transmitted forces associated with locomotion, while contributing to joint stability.

The cartilage is populated by one single cell type, the chondrocyte[1]. Chondrocytes are spheroidal cells with a diameter raging between 10 to 13 μm, that make up only about 5% of the tissue volume, and are embedded in a highly organized and dense ECM[6]. They are responsible for synthesizing and maintaining specialized cartilage matrix macromolecules.

Under healthy conditions, chondrocytes remain in a state of low mitotic and metabolic activity[1, 3]. They are encased in a pericellular matrix that consists of type VI collagen and other ECM proteins[3]. This specialized matrix helps to maintain chondrocytes in a differentiated low-turnover state by protecting them from interacting with ECM components from the interterritorial cartilage matrix. Chondrocytes maintain minimal collagen turnover and replace the GAG constituents on aggrecan and small proteoglycan proteins as these components undergo changes in response to external stimuli[3]. They exhibit primary cilia located on their surface, as well as other mechanosensitive receptors that allows them to sense and adapt their metabolic activity in response to physical forces[3].

Cartilage is avascular and aneural, so chondrocytes exist in an environment with low oxygen tension and receive nutrients by diffusion from adjacent connective tissue capillaries. Consequently, cartilage tissue has limited access to circulating progenitor cells and exhibits limited capacity to spontaneously self-repair upon injury[7, 8]. Even if the lesion has relatively small proportions, cartilage features hinder their ability to regenerate. Consequently, it can progress rapidly and lead to cartilage structure destruction and whole joint mechanical instability.

1.1.1. Pathogenesis of Osteoarthritis

Cartilage lesions can have multiple causes, from trauma to degenerative pathologies, which frequently result in gradual tissue deterioration, affecting joint integrity and stability[2, 9].

The management of chondral lesions is a challenging clinical problem for orthopedic surgeons. Chondral and osteochondral defects due to injury or other pathologies commonly lead to the development of osteoarthritis (OA). OA is one of the most common musculo-skeletal diseases and the main cause for joint pain and physical disability. About 10-12% of the adult population have symptomatic OA and it has been suggested that 250 million people globally are affected by knee OA[10, 11].

The word's population is growing older, with the number of people aged 65 years or more expected to almost double by 2050 and the number of people 80 years or over projected to triple[12]. As the average life-expectancy has increased significantly over the past decades, the population is increasingly suffering from diseases associated with age. Combining the aging population with increasing obesity and number of joint injuries, OA prevalence is expected to become the greatest cause of chronic disability by 2030[13].

Chondral lesions greatly affect patient's quality of life and account for a substantial burden on healthcare systems globally. It is typically accompanied by two common forms of pain: one that is intermittent and usually severe or intense, and another that is a persistent background pain. Furthermore, it is estimated that about 80% of individuals with OA have some degree of movement limitation and 25% are not able to perform major daily life activities[10].

OA burden can be measured in direct and indirect costs. The direct costs of OA are mostly related to hospital stays and elective orthopedic surgery. A smaller percentage is accounted for medications, physician visits and diagnosis procedures. The indirect costs are more difficult to assess and, consequently, the true burden of OA is often underestimated. These include costs associated with productivity losses, premature death, early retirements and compensation for household work performed by others[10].

OA can be classified as primary or secondary according to its major predisposing factor or cause. Primary OA is the most common type and develops due to aging and the wear and tear in the joints that comes along with it. As such, there are no identifiable etiology or predisposing cause associated with primary OA. This type of OA is often seen in people aged above 55. Secondary OA has an identifiable underlying cause such as a metabolic condition (e.g., calcium crystal deposition) or the sequelae of an inflammatory disorder (e.g., septic arthritis). Additionally, secondary OA can be associated with anatomic abnormalities that include joint deformities and mal-alignments or with traumatic events such as major joint trauma (e.g., sports injury, traffic accident) and joint surgery[9]. This type of OA typically affects younger individuals. Besides its classification, both types have in common an altered cartilage physiology and are pathologically indistinguishable[1].

Chondral lesions can be described based on their location, size and associated damage, which influence the clinical treatment choice[14]. Considering the depth of the lesion, they can be classified as mild or partial thickness and severe or full thickness, that leave the underlying subchondral bone exposed[9]. Ultimately, the worst scenario are osteochondral defects that extend into the subchondral bone. In these lesions, bone derived mesenchymal stem/ stromal cells (MSCs) form a fibrocartilaginous tissue to counterweight the loss, that is associated with increased pain, mobility limitations and structural changes[9, 15].

OA can evolve through time, arising from an imbalance between repair and destruction of joint tissues[16]. Cell-derived or matrix-derived factors are able to alter the composition and structural properties of joint tissues. Abnormalities in a single tissue can ultimately affect all joint tissues because of their intimate physical and functional association. Therefore, OA remains to date a challenging condition to treat[2].

Chondral lesions often evolve to OA, that is considered a disease of the whole joint. Besides marked changes in hyaline articular cartilage, it comprises alterations in the

subchondral bone, ligaments, capsule and synovial membrane (Figure 2A)[3]. Pathogenesis is complex and involves mechanical, inflammatory and metabolic factors. The structural damages found in the joints include loss of cartilage, osteophyte formation and subchondral bone and meniscus alterations[3]. Structural destruction eventually leads to synovial joint failure. It is usually accompanied by joint pain, transient morning stiffness and crepitus during joint motion (a sound produced in the joint). As mentioned, OA leads to joint instability and physical disability of patients, impairing their quality of life[3].

In OA, cartilage structure undergoes noticeable changes[3, 17]. Surface fibrillations become visible, and the exfoliation of cartilage fragments results in deep fissures. Fissures lead to delamination and exposure of the underlying calcified cartilage and bone (Figure 2A)[3]. Additionally, the zone of calcified cartilage expands and replaces the overlying articular cartilage, duplicating the tidemark (Figure 2B)[3].

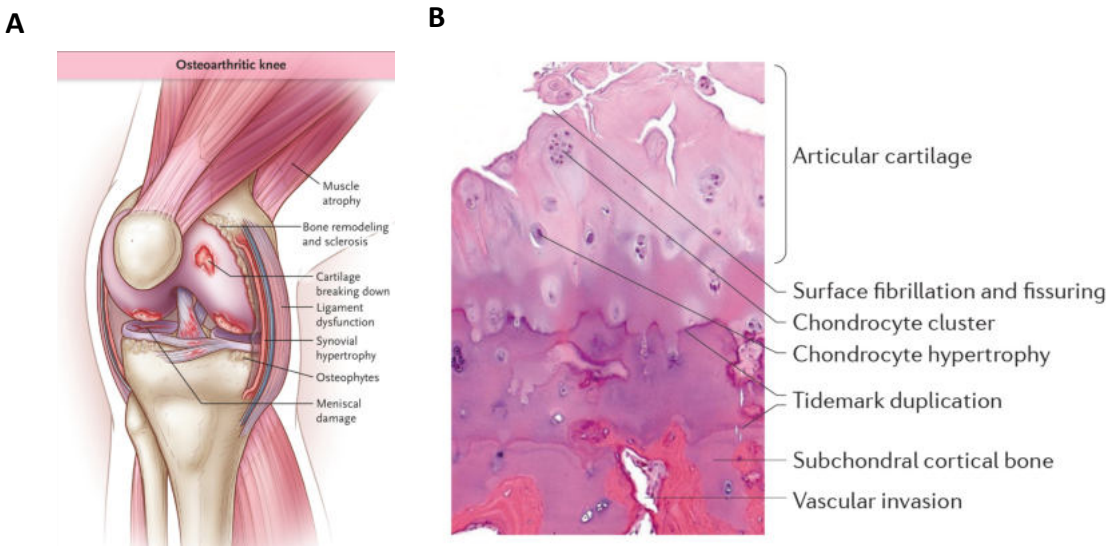

Figure 2. Osteoarthritic joint. A. In OA, the articular cartilage shows fissures, there are signs of synovial inflammation and bone remodeling that can lead to bony outgrowth and subchondral sclerosis. **B.** Histopathological cross-section of an osteoarthritic cartilage surface, showing characteristic changes such as the fissuring and fragmentation of the articular surface, chondrocyte proliferation and hypertrophy and advancement and duplication of the tidemark. From Sharma [18] and Martel-Pelletier, Barr, Cicuttini, Conaghan, Cooper, Goldring, Goldring, Jones, Teichtahl and Pelletier [3].

Cartilage ECM undergoes striking alternations in OA. Disease progression is marked by proteoglycan depletion from the matrix and collagen network erosion. This is accompanied by chondrocyte production of several different matrix metalloproteinases and aggrecanases that further disrupt the ECM[19, 20]. Alterations in cartilage composition lead to changes in material properties, which render it more susceptible to disruption by external physical forces. Genes encoding proteins associated with inflammatory and catabolic responses are upregulated. Signal transduction involves nuclear factor-κB (NF-κB), mitogen-activated protein kinase and other inflammation and stress-induced pathways[21, 22].

Chondrocytes are deregulated in OA. The disruption of the chondrocyte pericellular matrix is an early OA event. When chondrocytes are exposed to the components of the interterritorial matrix, its function is deregulated through cell surface receptors, and they exhibit increased synthetic activity[3]. Their hypertrophic state, with increased synthetic activity, comes as an attempt at repair[17]. Additionally, chondrocyte catabolic activity generates matrix degradation products and pro-inflammatory mediators[17]. These act in an autocrine and paracrine way, further deregulating chondrocytes. These mediators are also able to act on adjacent synovium, stimulating proliferative and pro-inflammatory responses[17]. Chondrocytes can also assume a senescence-associated secretory profile, marked by the increased production of reactive oxygen species, cytokines, chemokines and other pro-inflammatory products[23].

1.2. Inflammatory response in cartilage damage

Synovitis, the inflammation of the synovium, is a common feature of chondral damage. The synovium comprises the synovial membrane and fluid. The synovial membrane is a major source of synovial fluid components, that nourishes and lubricates chondrocytes, contributing to the articular surface unique low-friction properties[24, 25]. Two cell types compose the synovial membrane: fibroblasts that secrete hyaluronan and lubricin and macrophages with phagocytic activity [26].

Upon cartilage damage, dysfunctional chondrocytes release proteinases that lead to the generation of pro-inflammatory cartilage degradation products. They act as damage-associated molecular patterns (DAMPs), interacting with receptors expressed on chondrocytes, such as Toll-like receptors (TLR) and integrins that further increase the expression of catabolic and inflammatory products. Cartilage matrix degradation products play a role in the activation of the immune system[27].

Macrophages are innate immune system phagocytic cells found in almost every tissue. Their primary role is to maintain tissue homeostasis and protect the host against infection. They express an extended repertoire of strategically located innate immunity receptors, such as toll-like receptors (TLR), inflammasomes and lectin-like receptors[28]. Macrophages collaborate with other innate immunity cells, including natural killer (NK) cells and neutrophils[29]. They also bridge and instruct adaptative immune system responses through cell interactions and various secreted mediators[30]. To perform their roles, macrophages are highly plastic, continuously adapting and responding to specific local stimuli[31]. As macrophages play a critical part of the innate immune system, they have long been considered an important participant in OA[32].

Synovial macrophages can have an embryonic or bone marrow (BM) origin. Tissue resident macrophages are embryonically derived, and their primary role is to maintain tissue homeostasis during adulthood[30]. Resident synovial CX3C chemokine receptor 1 ($CX3CR1^{+}$) macrophages derived from proliferating mononuclear cells of the synovial

tissue were showed to physically isolate the joint and restrict inflammation, thereby exhibiting an anti-inflammatory profile[33]. In a healthy knee joint, there is only a small number of constitutively resident macrophages. However, in OA joints, the synovium is intensely populated by infiltrating macrophages[34].

Infiltrating monocyte-derived macrophages seem to be responsible for joint inflammatory response[33]. Synovium infiltrating macrophages are mainly migratory BM-derived, rather than tissue-resident macrophages[30]. In response to inflammation, circulating monocytes are recruited to the inflammation site and subsequently differentiate into macrophages upon contacted with local inflammatory mediators[35]. Non-tissue resident macrophages have been shown to differentiate into pro-inflammatory and anti-inflammatory phenotypes after homing to tissue, influencing both inflammation and repair based on the stimuli provided[36].

Macrophages are involved in the joint inflammation associated with chondral damage. These innate immune cells secrete cytokines and other molecular mediators in the joint microenvironment that trigger inflammation and influence chondrocyte's response[37]. Synovial tissue macrophages express lineage markers such as CD14 and CD68[38]. Macrophages are antigen presenting cells (APC) that express major histocompatibility complex (MHC) class II molecules, which gives them the ability to initiate adaptative immune responses through CD4+ T cell activation[39]. They also express or their cellular surface macrophage receptor with collagenous structure (MARCO) which is a scavenger receptor that mediates binding and ingestion of unopsonized environmental particles, including nano-sized materials[40]. In addition, macrophages possess colony-stimulating factor-1 receptor (CSF-1R), which is activated by macrophage colony-stimulating factor (M-CSF), a glycoprotein know to stimulate the formation of macrophage colonies[41]. Macrophages release inflammatory cytokines, such as tumor necrosis factor alpha (TNF-α) and interleukin (IL)-1β, and promote the production of matrix degrading enzymes that disrupt synovial tissue homeostasis and increase cartilage and bone resorption[42].

Synovial lining macrophages play a crucial role in cartilage damage. Cartilage breakdown leads to the release of molecular fragments into the synovial fluid. Resident macrophages present in the synovial membrane remove these fragments from the synovium, and signal in a positive feedback loop that triggers apoptosis in chondrocytes[26]. This articular inflammatory environment is a key factor in cartilage lesion initiation and progession[43]. It is also associated with clinical symptoms such as pain and dysfunction[43, 44].

Macrophage's plasticity enables them to adjust to local microenvironments and respond to a broad range of stimuli, under physiological and pathological conditions[32]. Two macrophage phenotypes have been defined at the edges of the continuum of their polarization status, when confronted with different stimuli. Both have been extensively characterized in terms of gene expression, surface molecules patterns and production

of biological mediators and metabolites[45]. Depending on their phenotype, they play different roles during cartilage damage: pro-inflammatory M1-like macrophages are associated with chronic inflammation and joint destruction, while anti-inflammatory M2-like macrophages promote tissue repair and inflammation resolution (Table 2)[31].

During the inflammatory phase, classically activated M1 macrophages are recruited to the inflammation site[32]. M1 macrophages can be induced by interferon-γ (IFN- γ), lipopolysaccharide (LPS) and tumor necrosis alpha (TNF-α)[46]. They are associated with the production of high levels pro-inflammatory cytokines and chemokines[43]. After stimuli, transcription factors such as interferon regulatory factor 5 (IRF5) activate transcription of genes encoding pro-inflammatory cytokines such as IL-1β, IL-6, IL-12, IL-23 and TNF-α, while repressing genes encoding anti-inflammatory cytokines such as IL-10[47, 48].

Alternatively activated M2 macrophages promote an anti-inflammatory response. They are also known as wound-healing macrophages, contributing to the resolution of inflammation. They can be further divided into specific subtypes, based on the stimuli used to activate them. M2a is induced by IL-4 or IL-13, M2b by TLRs agonists and M2c by IL-10[49]. The anti-inflammatory factors produced by M2 macrophages, such as IL-10 and transforming growth factor β (TGF-β), reverse the inflammatory process. Inducting stimuli leads the activation of transcription factors such as IRF4 that favor polarization[50]. M2 macrophages express CD163 and CD206 markers and produce arginase 1[51].

Table 2. Macrophage polarization in cartilage repair and OA. Adapted from Fernandes, Gomoll, Lattermann, Hernandez, Bueno and Amano [38].

Macrophage polarization	Stimuli	Transcription factors	Phenotype	Released products	Functional roles	Potential tools for treatment
M1	INF-g, microbial infection (mimicked by LPS), TNF-a	IRF1, IRF5, IRF8, Pu. 1, STAT1, STAT2, NF-kB	CD80, CD86, CD40, MHC-II	TNF-a, IL-1b, IL-6, IL-12, IL-23, OSM, NO, CXCL10, IL-8, CCL5, CXCL9, CXCL11, MMP1, MMP3, MMP9, MMP13, ADAMTS	Inflammation, type 1 response and tissue injury microbicidal **OA progression**	M1 blocker** Depletion of CD14+ Macrophages**
M2	IL-4, IL-13, IL-10 and TLRs agonists, MSCs (?)	IRF4, Pu.1, SOCS1, STAT6, JMJD3, PPARd, GATA3, C/ EBPb	ARG-1, CD163, CD206	IL-10, IL-1RA, TGF-b, IGF, CCL18, CCL4, CCL13, CCL17, MMP1, MMP12	Anti-inflammatory response, type 2 response, tissue repair, chondrogeneic and turnover of extracellular matrix **Cartilage regeneration**	M2 inducers: oxLDL, collagen type II, MSCs* Blocking mTOR pathway?**

** The M2 polarization can be halt by the microenvironment.*
*** Further studies are required for confirmation.*

The polarization of macrophages during inflammation might account several pathological processes[32]. Upon damage, macrophages M1 act as cleaners during the early stages of repair and promote inflammation. As the repair process continues, there needs to be a shift from M1 to M2 macrophages, that are considered promoters of regenerative homeostasis[52].

M1 macrophages have a pro-inflammatory role and contribute to chondral damage. During cartilage damage, M1 macrophages inhibit genes associated with matrix production, upregulate expression of matrix degrading enzymes and induce/perpetuate an inflammatory microenvironment. M1 macrophages produce cytokines such as IL-6, TNF-α and Oncostatin (OSM) that induce destructive processes in chondrocytes[25]. They also down regulate chondrocyte's collagen type II and aggrecan synthesis. In addition, synovial M1 macrophages up regulate the production of cyclooxygenase-2, that mediates inflammation, and matrix-degrading proteolytic enzymes that include matrix metalloproteinase (MMP)-1, MMP3, MMP13, MMP9 and aggrecanases (ADAMTS)[53, 54]. Furthermore, synovial and monocyte-derived pro-inflammatory macrophages negatively affect chondrogenic differentiation of MSCs[25].

Thus, a shift towards M2 macrophages during chondral damage might contribute to cartilage repair[38]. They exert an immunomodulatory effect on tissue healing by producing anti-inflammatory cytokines, such as IL-10, IL-1RA, chemokine (CeC motif) ligand 18 (CCL18) and TGF-β, as well as pro-chondrogenic factors, including TGF- β1, TGF- β2, TGF- β3, insulin-like growth factor 1 (IGF1) and 2 (IGF2)[25, 38, 55].

However, anti-inflammatory molecules secreted by M2-like macrophages are often not enough to counter the catabolic inflammatory response. A higher ratio of pro-inflammatory M1 macrophages compared to anti-inflammatory M2 macrophages shifts the cytokine profile of joint synovial fluid in favor of inflammation, observed by high levels of IL-β1, IL-6 and IL-8. This stimulates chondrocytes to produce ECM-degradative enzymes, which further aggravates cartilage destruction and accelerate the onset of OA and related symptoms[30].

There is a growing interest in controlling inflammation in different diseases by targeting the phenotypic changes in macrophages. An emerging therapeutic strategy for macrophage-involved diseases, such as atherosclerosis, lung cancer and bone diseases, is to normalize the M1/M2 ratio[32].

Mahon et al. showed recently that peripheral blood monocyte (PBMC)-derived naïve macrophages, stimulated with OA-related metabolites, such as basic calcium phosphate (BCP) crystals, exhibited an increased expression of M1 surface markers, such as CD86 and CD40, as well as increased production of chemokine (C-X-C motif) ligand 9 (CXCL9) and CXCL10 chemokines[56]. In accordance with these findings, Liu at al. reported an increased proportion of pro-inflammatory macrophages in circulation in OA patients compared with healthy individuals, while the number of anti-inflammatory CD206+ macrophages was considerately lower in OA patients[57]. Similarly, synovium-resident macrophages seem to follow the same activation and cytokine releasing pattern, contributing to OA progression[32].

In the light of this knowledge, therapeutic manipulation of M1-like macrophages toward M2-like effectors appears as a promising strategy to revert chondral damage-associated

inflammation and promote repair. Furthermore, during biomaterial implantation, adequate activation of macrophages is essential to promote an adequate response and some biomaterials have shown potential to induce a M2 macrophage phenotype[55, 58]. The interaction between implanted biomaterials and macrophages is crucial for successful cartilage repair.

1.3. Macrophages and their crosstalk with cell tissue populations

MSCs are undifferentiated, self-renewing cells with potential for multilineage differentiation. They are considered multipotent due to their ability to differentiate into more committed cell types from the mesodermal embryonic layer[59]. These stem cells can be obtained from BM and adipose tissue, which are the most used sources for the isolation of MSCs. Additionally, they can be isolated from postnatal tissues that include skeletal muscles, periosteum, articular cartilage, synovium and peripheral blood[60, 61]. MSCs are heterogenous cells, presenting variable growth potential and distinct morphologic and functional characteristics[61]. Consequently, the proliferation and differentiation capacity of MSCs varies according to their isolation source[59].

Although diverse antigens have been found on the surface of MSCs, none of them appears to be a unique molecular signature for these stem cells. As a result, the International Society for Cellular Therapy (ISCT) has proposed minimal criteria to define human MSCs. MSCs must be plastic-adherent when maintained in standard culture conditions using tissue culture flasks. They must be able to differentiate into adipocytes, osteoblasts and chondrocytes under standard in vitro in functional tests when cultured in appropriated differentiating conditions. Lastly, MSCs must express specific surface antigens: more than 95% of the cell population must express CD105, CD73 and CD90, while lacking expression ($\leq$ 2% positive cells) of lineage markers CD45, CD34, CD14 or CD11b, CD79β or CD19 and MHC class II that are expressed on thrombocytes, endothelial cell and leucocytes[62].

MSCs maintain adult tissues and are responsible for their normal turnover under physiological conditions. Upon damage, MSCs migrate to injured tissues and contribute to their repair by secreting cytokines, chemokines and ECM proteins[63]. Upon biomaterial subcutaneous implantation in a murine model, there is first recruitment of inflammatory cells, which is then correlated with MSCs recruitment[64]. In addition to their chondrogenic potential, MSCs exhibit known immunomodulatory properties, influencing the recruitment and activity of immune cells[65]. Therefore, these stem cells represent a powerful tool for chondral repair.

MSCs exhibit immunoregulatory capacity and favor an immunosuppressed environment[38]. MSCs are capable to suppress all immune cells that play pathophysiological role in the development and progression of OA. They can

downregulate effector innate immune cells such as macrophages, dendritic cells (DCs) and NK cells, as well as adaptative immune cells such as B and T lymphocytes.

MSCs can influence immune cells through several mechanisms. They can secrete immune regulating molecules such as TGF- β, human leukocyte antigen G (HLA-G), prostaglandin (PGE2), indoleamine 2,3-dioxygenase (IDO) and IL-10, that act in a paracrine manner in surrounding cells[63, 65]. Additionally, they can modulate inflammatory response in a juxtacrine manner (cell-to-cell contact)[51]. Through these mechanisms, MSCs are able to attenuate proliferation and cytotoxicity of NK cells, suppress activation of autoreactive B cell and production of autoreactive antibody, prevent activation of inflammatory CD4+ Th1 cells and assist generation of immunosuppressive CD4+ T regulatory cells[61].

In vitro, MSCs inhibit the activation of inflammatory M1 macrophages, while promoting their polarization to an anti-inflammatory M2 phenotype. MSCs secrete several chemokines, cytokines and growth factors that act on macrophages and push them to polarize towards an anti-inflammatory phenotype. MSCs induce conversion of TNF-α and IL-1 producing M1 macrophages towards IL-10 producing, immunosuppressive M2 cells. This shift attenuates joint inflammation and promotes a pro-regenerative environment for cartilage repair (Figure 3)[61].

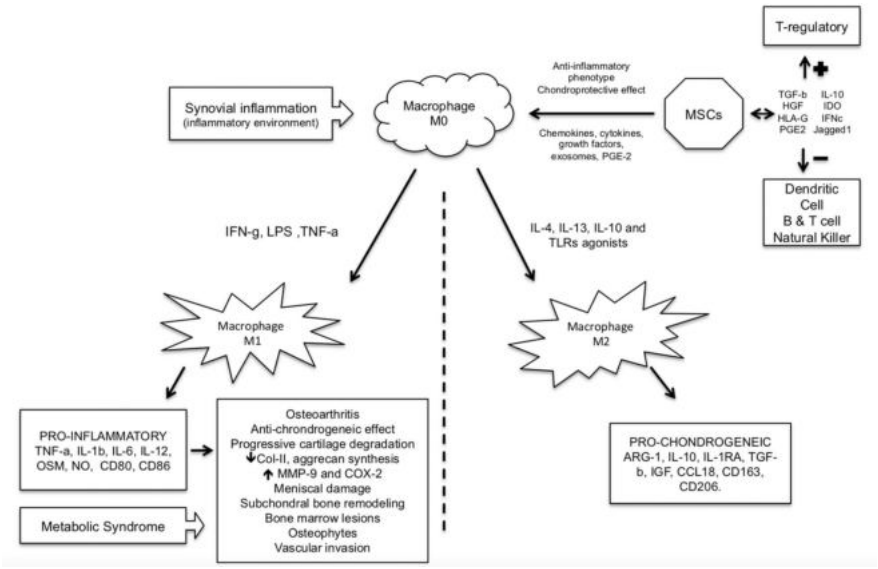

Figure 3. Macrophage's polarization and crosstalk with MSCs in cartilage injury/repair. From Fernandes, Gomoll, Lattermann, Hernandez, Bueno and Amano [38].

During joint inflammation, MSCs secretome influences macrophages phenotype. MSCs secrete TNF- α-stimulated gene/protein 6 (TSG-6) in response to TNF-α released by activated M1 macrophages. TSG-6 interacts with CD44 on macrophages and decreases TLR2/NFκ-B signaling, consequently alleviating production of inflammatory mediators such as nitric oxide (NO), TNF-α and IL-1[66]. Furthermore, MSC-derived PGE2 binds to its receptor on macrophages, promoting the production of IL-10. MSC-derived PGE2 is also

involved in immunomodulation of cytokine profile of other effector immune cells[61]. MSC-induced IDO, produced after exposure to the inflammatory joint environment, catalyzes the degradation of tryptophan into kynurenine. Kynurenine has immunomodulatory effects and promotes conversion of M1 macrophages into CD206+ anti-inflammatory phenotype[61].

On the other hand, the destructive inflammatory environment found in OA seems to halt the MSCs properties to promote cartilage repair. Osteoarthritic-conditioned media and synovial fluid were shown to inhibit the chondrocyte differentiation of MSCs[67, 68]. Moreover, M1 macrophages were shown to inhibit chondrocyte differentiation of MSCs, which indicates that synovial macrophages regulate the chondrogenesis potential of MSCs[25].

Under an already inflamed environment, MSCs fail to induce an M2 response and have their properties impaired[38]. Therefore, additional stimuli might be required to promote an M2 macrophage response, improving MSCs therapeutic effects and cartilage repair.

1.4. Importance of chondral repair treatments

The individual and socioeconomic impact of OA is further aggravated by the current lack of available cure. OA is a complex chronic disease, and its management is best characterized as palliative and reactive. Topical, oral and injectable pharmacological treatments are used to alleviate the symptoms of individuals with OA. However, they are considered only moderately effective pain relievers and are not suitable for every patient. Indeed, studies report that most people suffering from OA experience persistent pain, despite prescribed therapies[3].

Pharmacological therapies include nonsteroidal anti-inflammatory drugs (NSAIDs) and paracetamol. Oral NSAIDs and selective cyclooxygenase 2 (COX2) inhibitors are customary oral pharmacological agents in OA. As they are associated with considerable toxicity, particularly gastrointestinal and cardiovascular complications, factors such as age, current medications and comorbid conditions (i.e., gastrointestinal and cardiovascular problems) need to be considered before NSAIDs prescription. Paracetamol is often prescribed as an analgesic alternative to NSAIDs, although it was proven less effective[69].

NSAIDs can also be applied topically and exhibit safer profiles than oral, systemic therapies. However, their effectiveness decreases since it is limited by joint penetration. It also requires multiple daily applications, which reduces patient compliance with the therapeutic[70].

Arthroplasties or joint replacement surgeries, have increased over the years and proved effective for the knee and hip joint[10]. Unfortunately, joint surgeries have their own drawbacks, such as the possibility of site infection, prosthesis rejection and persistent pain after total joint replacement. Surgical referral is reserved for patients with critical

functional limitations and severe pain, in which less invasive options have been delivered without providing adequate symptom relief.

Furthermore, joint replacement surgeries are generally delayed in younger active patients (<60 years), since prosthesis have a limited life expectancy and high-impact activity following arthroplasties is restricted. Additionally, revision surgeries have less-favorable outcomes due to their complexity [71, 72]. Therefore, younger individuals are left with fewer therapeutic options and become more prone to safety issues that arise from prolonged pharmacological treatment.

The quest for disease-modifying therapies for OA has several years, but no drug has yet proven efficient. Since OA is a multifactorial disease, some argue that a single compound for its efficient treatment will never exist. Therefore, an adequate OA treatment might require the localized combination of drugs and factors with distinct mechanisms of action[2].

The significant unmet need of successful OA treatments led to the development of new therapeutic options. There are currently no effective treatments for chondral lesions that avoid progression to OA. Tissue engineering (TE) approaches to repair and regenerate articular cartilage emerged as a promising strategy and have gained relevance in OA treatment over the last years[73].

1.5. Present cartilage repair techniques

Multiple surgical techniques are available for cartilage repair. They limit the progression of cartilage lesions and minimize associated health conditions. Each of them presents its own advantages and limitations. Unfortunately, there are still many obstacles that hinder proper tissue repair after injury and current clinical methods are not satisfactory.

During arthroscopic debridement, the surgeon removes loose intraarticular tissue debris and inflammatory mediators from the damage cartilage (Figure 4). This helps to reduce inflammation, thus reducing pain and improving movement. This technique is often paired with bone marrow stimulation through perforations and microfractures, since arthroscopic debridement procedure alone shows discouraging results[74].

The microfracture technique is a subchondral bone marrow stimulation method in which a blood clot fills the defect (Figure 4). It enhances the migration of MSCs from bone marrow to the cartilage defect site, facilitating the access of cells to the injury to assist the formation of cartilage tissue. The induced microfractures seem to be effective in small injuries, where the subchondral plate remains intact[75].

Unfortunately, microfracture often leads to the formation of fibrocartilage. Fibrocartilage is made of collagen type I and is biochemically and biomechanically inferior compared to hyaline articular cartilage. The repaired tissue is more vulnerable to mechanical joint forces due to the lack of mechanical robustness and typically

deteriorates soon after the procedure. Deterioration is more evident when treating larger chondral defects[75]. Studies show that microfracture is only able to delay cartilage degeneration in the short-term and treatment failure is expected 5 years after surgery, regardless of the lesion size[76].

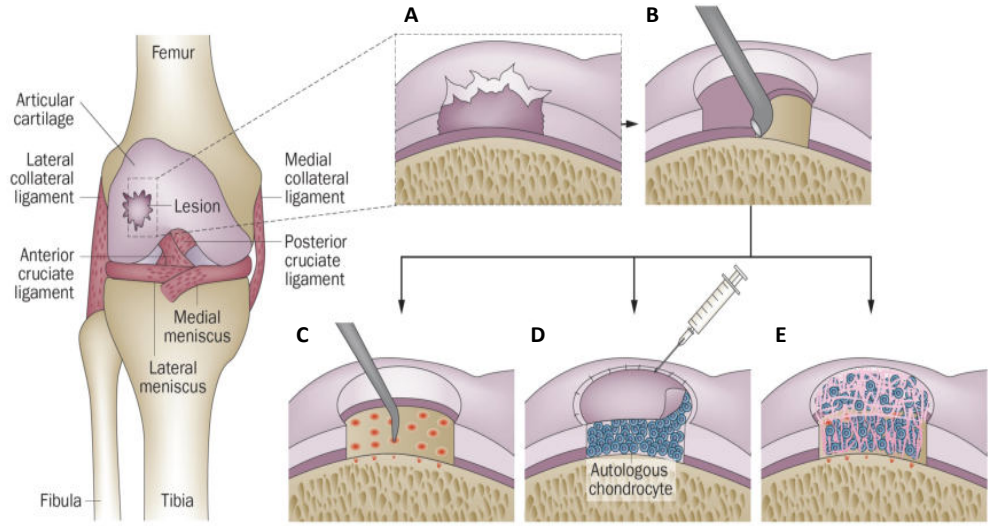

Figure 4. Present cartilage repair techniques. A. Full-thickness cartilage lesion. **B.** Arthroscopic debridement procedure is used to remove unwanted cartilage products and enhance the integration of host tissue. **C.** Microfracture. Channels penetrate the subchondral bone and allow MSCs migration to the cartilage defect. **D.** ACI. The lesion is filled with autologous chondrocytes and covered with a periosteal flap or a collagen membrane. **E.** MACI. Autologous chondrocytes are expanded in vitro and seeded onto 3D scaffolds prior to implantation. ***Abbreviations:*** *ACI, autologous chondrocyte implantation; MACI, matrix-assisted autologous chondrocyte implantation; MSC, mesenchymal stem cell.* Adapted from Makris, Gomoll, Malizos, Hu and Athanasiou [77].

Both techniques are straightforward, fast and inexpensive. However, they only delay degradation and repair the tissue to a certain point. The number of available cartilage progenitor cells from the bone marrow is too small to achieve full cartilage regeneration with original cartilage properties. To circumvent that, more promising techniques were developed.

Osteochondral mosaicplasty involves transplantation of multiple small cylindrical osteochondral plugs to resurface a defected area of the cartilage (Figure 5A). The plugs are harvested from a less weight-bearing area of the articular cartilage[7].

This procedure offers several advantages but also has limiting downsides. During transplantation, viable hyaline cartilage is transplanted in a single operation with a relatively brief rehabilitation period. However, this procedure is associated with donor site morbidity and limited availability of graft harvesting areas. The donor cartilage site must be healthy, but patients in need of a graft usually have their overall cartilage in bad shape. Other limitations include significant differences between donor and recipient cartilage in terms of orientation, thickness and mechanical properties. Furthermore, during donor site healing, the defects are filled with cancellous bone and fibrocartilage, which decreases the quality of donor site articular cartilage[7].

Osteochondral allograft transplantation involves the resurfacing of a cartilage defect with intact, viable cadaveric cartilage graft and its underlying subchondral bone (Figure 5B). The procedure can be done a single-stage operation and it is possible to tailor donor graft critical factors such as the size, depth and location to fit the defect. They can also be obtained from weight-bearing areas that are more identical to the damaged area. As such, a precise surface architecture is achieved, with no donor site morbidity[7].

However, this procedure has high costs and the risk of immunological rejection. Grafts also have very limited availability and have the potential for disease transmission. Additionally, the harvested cartilage must be used within a short period of time, as it is kept fresh in serum, but only up to a few weeks after extraction. To extend the usage window, cryopreservation techniques were developed. Unfortunately, cryopreserved cartilage shows fewer viable cells which affects cartilage recovery after surgery[7].

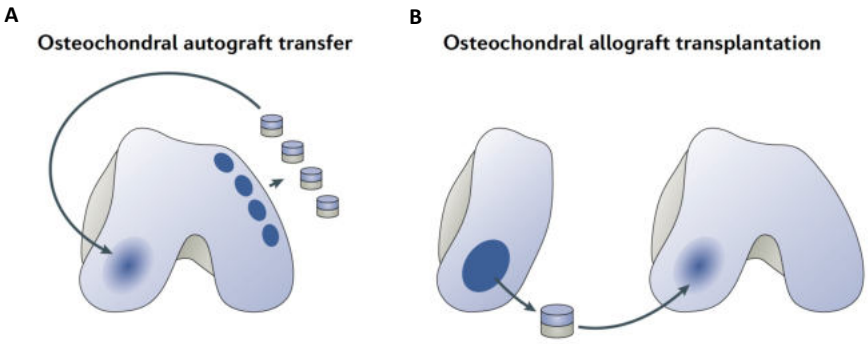

Figure 5. Osteochondral transplantation techniques. A. Osteochondral autograft transfer. During osteochondral autograft transfer, multiple small cylindrical osteochondral plugs are transferred from a less weight-bearing area of cartilage to resurface the defect. **B. Osteochondral allograft transplantation.** Osteochondral allograft transplantation involves resurfacing of a cartilage defect with a cadaveric cartilage graft. Adapted from Kwon, Brown, Lee, Wang, Paschos, Hu and Athanasiou [73].

Autologous chondrocyte implantation (ACI) is a technique used to restore cartilage cells into full-thickness chondral defects (Figure 4D). Its main theoretical goal is to promote the formation of hyaline cartilage rather than fibrocartilage[7]. First, an initial arthroscopic operation is performed to collect a full-thickness sample from a low-weight-bearing cartilage region. After the procedure, chondrocytes are expanded in vitro to yield a population of approximately 12-48 million cells. Chondrocytes are implanted during a second surgery, after cartilage debridement. The area is then covered with a periosteal membrane to seal the implanted cells in the cartilage defect and provide factors for cartilage regeneration[77].

ACI uses patient's own cells, which avoids potential immune complications and infections related to allogenic cell and foreign material transplantation. Additionally, the smaller biopsy minimizes complications associated with chondrocyte donor site morbidity. However, this technique involves two surgeries and a longer recovery time after transplantation to ensure neotissue maturation. Moreover, it is associated with an

increase in cartilage volume (hypertrophy) and ossification of the grafted area. Since this problem seems to be associated with the periosteal membrane, alternative approaches were developed[77].

A second generation of repair techniques was developed to circumvent the lack of supportive scaffold material to guide matrix synthesis. It is focused on scaffold-based approaches for chondrocyte delivery. The tissue-engineered matrix carried the cells to maintain and support crucial tissue characteristics.

Scaffold-based approaches have many advantages over scaffold-free techniques. For instance, it allows better control to fill the cartilage defect, has fewer donor site complications and is technically less challenging. Additionally, it provides increased graft stability and chondrocytes cultured in a three-dimensional (3D) environment are less prone to dedifferentiate, producing a more hyaline-like cartilage[77].

Matrix-induced autologous chondrocyte implantation (MACI) is a scaffold-based cartilage repair technique currently in clinical practice (Figure 4E). Similar to ACI, it also involves two surgical procedures: a first to collect autologous tissue for chondrocyte isolation and expansion, and a second for cell-seeded scaffold implantation. Prior to implantation, chondrocytes are seeded for 3 days on an absorbable porcine-derived collagen type I and II membrane. Hyaluronic-acid-based scaffolds are also used to implant chondrocytes in a 3D biodegradable environment. However, despite the added costs of this procedure compared to other alternatives, MACI superiority remains unproven[77].

Unfortunately, no current technique for articular cartilage repair has recreated a tissue with the same characteristics of native hyaline cartilage.

1.6. Emerging articular cartilage repair approaches

An ideal treatment for cartilage injuries must recreate a healthy hyaline-type cartilage with similar biomechanical features as the pre-injury tissue such as strength and durability. Often, the previously described techniques are not long-term clinical solutions and do not provide adequate tissue quality, which prompted the development of TE and regenerative approaches for chondral repair[77].

Cartilage TE aims to reconstitute damaged cartilage tissue through the combination of relevant cells, biomaterials and extraneous signals in a harmonious manner. A variety of different cell sources such as autologous cells, allogenic cells and stem cells has been tested in vitro. They can be cultured ex vivo with different stimuli and chemicals to enhance chondrogenic potential and synthesis. Scaffolds improve the integrity of the neotissue by creating a 3D environment that helps cells to maintain their phenotype and recruit cells from their host environment. The combination of these elements results in three major cartilage TE strategies: scaffold-free, cell-based techniques; cell-seeded scaffolds and cell-free, scaffold-based implants[77].

The utilization of cells for articular cartilage repair techniques is promising but encounters some limitations. Autologous chondrocytes, MSCs and more recently alternative cell sources such as induced pluripotent stem cells (iPSCs) must be extracted, proliferated and differentiated, which can be time consuming and expensive. Furthermore, the use of cells renders the regulatory approval longer and more expensive. These drawbacks led to an increasing interest in cell-free products for cartilage repair. Biomaterials can be utilized off-the-shelf, and many components have established precedence of clinical use[77, 78]. Furthermore, when implanted directly into the organism they can act as a medium for the colonization by host cells[79].

Biomaterials for chondral repair are developed to mimic the cartilage matrix and restore function at the defected site. To do so, they must meet important criteria. Their mechanical properties must be tailored to match those of existing cartilage in terms of compressive strength and frictionless motion. Additionally, they must integrate with adjacent cartilage and last throughout the patient's life[80]. Appropriate scaffold production methods result in desired architecture, pore interconnectivity, mechanical parameters and scaffold forms. Scaffold forms include 3D membranes/sponges, hydrogels, nanofibrous (nonwovens) and combinations thereof[79].

Biomaterials for chondral repair are in general biodegradable. After providing the necessary functional support for cartilage regeneration, the biomaterial is eventually eliminated from the body. The rate and mechanisms of biodegradation are tunable in many biomaterials. This allows the kinetics of biomaterial resorption to match neotissue formation[78].

Articular cartilage is a highly hydrated tissue, with up to 80% of its wet weight consisting of water[81]. Hydrogels are water-rich 3D polymeric networks that are a popular option for in situ cartilage regeneration because they are able to replicate the hydrophilic cartilage environment. Hydrogels can be classified based on their polymer composition as natural or synthetic. The combination of both allow to maximize the benefits of each component[78].

In order to minimize the severity of orthopedic interventions, there is an increasing interest in the use of arthroscopic procedures instead of open joint surgery. They reduce the risk of infection and shorten recovery time[78]. For smaller, partial thickness chondral lesions, injectable hydrogels that are compatible with arthroscopic methods have gained particular relevance.

The regenerative hydrogel can be injected into the defect thought the joint capsule[78]. The main advantage is their ability to be injected as a prepolymer solution and polymerize in vivo, filling irregularly shaped defects anatomically with low invasiveness and possibility to precise adjust to the defect. In addition, recent 3D bioprinting techniques allow hydrogels to be assembled ex vivo into physically relevant structures and geometry for chondral defect repair with adequate biomechanical requirements[82].

Severe lesions comprising larger defects have higher biomechanical demands. Full thickness chondral lesions require scaffolds with sufficient mechanical strength to withstand high loads while the repaired cartilage tissue is being formed. A 3D scaffold for cartilage TE must have tailored features that include porosity, pore size, interconnectivity and permeability. These play a key role in cell adhesion, migration and tissue ingrowth. The porous structure ensures oxygen diffusion, nutrients and metabolic products. More importantly, scaffolds must display appropriate mechanical parameters such as stiffness, strength and stability. They must also integrate correctly with the native tissue when implanted and support neotissue development[79].

1.7. Nanocarriers for cartilage repair

Pharmacological treatments commonly focus on the administration of one or two drugs locally (topical or intra-articular) or systemically. Although local application of these drugs reduces inflammation upon administration, the drugs are rapidly cleared from the joint by blood and/or lymphatic drainage, which restricts target location and effectiveness. On the other hand, high oral doses of anti-inflammatory drugs are commonly prescribed besides their side effects[4].

Nanotechnological strategies are being explored to target specific immune cell populations such as macrophages. Engineered biomaterials can be designed to load and deliver therapeutic molecules in a controlled manner[31]. Macrophages, owing to their phagocytic nature, have demonstrated significantly higher uptake and accumulation of nanostructures during inflammation, when compared to other immune cells[83]. Therefore, the past decade witnessed the development of several different nanocarriers for improve the delivery of drugs to macrophages in the joint[31].

As discussed, the M1/M2 macrophage ratio is an important factor to promote inflammation resolution. Some drugs have shown ability to decrease this ratio, however, they are not yet capable of an appropriate spatial-temporal manipulation of the immune response. New drug delivery and administration tools, focused in a therapeutic intervention of macrophages, can guarantee an effective drug concentration inside the joint for a sustained period of time, therefore achieving higher therapeutic efficacy[31]. These systems comprise many advantages such as a dose and time-controlled release of specific drugs at the desired location, reduction of systemic biodistribution and related adverse effects and improved drug solubility and efficacy , [31].

Nanoparticle (NP) physicochemical properties such as size and surface charge can be tuned to favor macrophage uptake and their therapeutic manipulation[31]. Most nanotechnological approaches developed to inhibit macrophage-induced inflammation in the joint have used natural or synthetic polymers with good regulatory profile[84]. Biodegradable and bioeliminable biomaterials can be engineered as drug delivery

systems to increase drug solubility, prolong their retention in the articular cavity, decrease toxicity and improve their pharmacokinetics[4].

Poly (lactic-co-glycolic) acid (PLGA) is a linear and biodegradable aliphatic polyester copolymer often used as a delivery carrier[85]. PLGA is suitable for the encapsulation of a wide range of biomolecules with controlled substances release and is already approved by regulatory agencies for many drug delivery applications, including TE [4, 85]. It demonstrated low toxicity, mostly because in the body it is degraded into lactic and glycolic acid[86].

PLGA biocompatibility and versatility make it one of the most used synthetic polymers in the field of regenerative medicine[85]. It can be processed into several different shapes or sizes and its degradation period can be tuned to match the rate of the neotissue formation or to achieve a desired drug release behavior. Loaded PLGA NPs were showed not only improve bioavailability of encapsulated active biomolecules, but also boost their pharmacological effects[87]. Moreover, the negative surface charge of PLGA NPs makes them highly internalized by phagocytic cells, such as macrophages, while poorly internalized by nonphagocytic ones[88].

Cartilage degradation is associated with an inflammatory environment, where joint infiltrating macrophages contribute to an increase of pro-inflammatory cytokines and prostaglandins[16]. Furthermore, the body produces a natural inflammatory reaction in response to biomaterials implantation[89]. An increasing body of evidence suggests that modulating, rather than inhibiting inflammation, has a more beneficial effect in tissue repair/regeneration[16, 38, 90]. As a result, new implantable biomaterials are being modified to target specific immune cell populations and/or modulate cell activation and secretion of pro-/anti-inflammatory cytokines to control inflammation[91].

NSAIDs are acknowledged for their potent anti-inflammatory effect[92]. They act on various pathways and cellular signaling systems involved in inflammation. NSAIDs main pharmacodynamic actions relate to the reduction in prostaglandin production. Prostaglandins are key inflammatory mediators that contribute to pain and inflammation. They derive from arachidonic acid in a process that involves cyclooxygenases enzymes, COX-1 and COX-2 (Figure 6)[93, 94] .

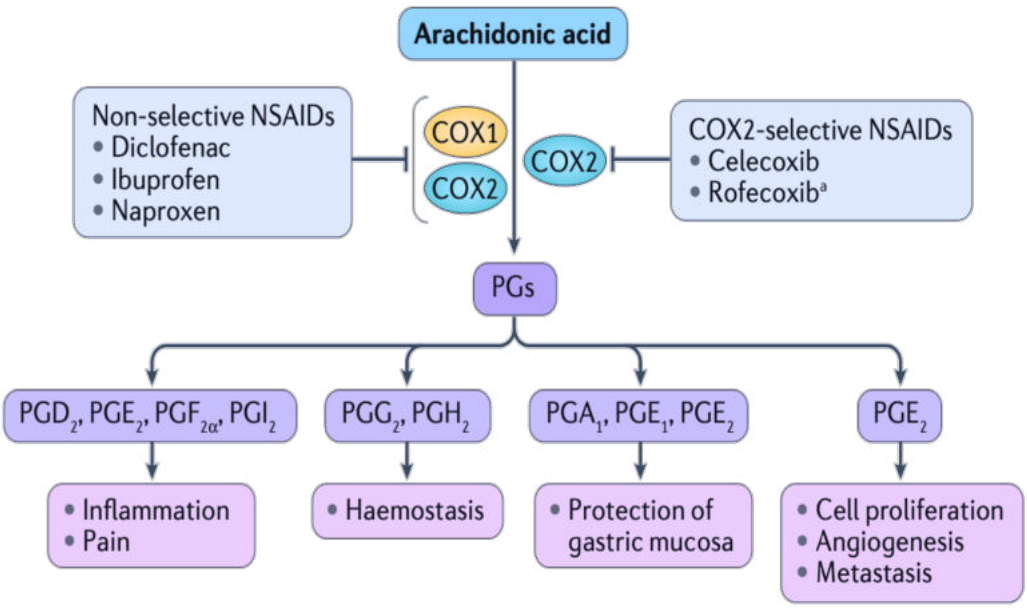

Figure 6. Mechanism of action of NSAIDs. Nonsteroidal anti-inflammatory drugs (NSAIDs) inhibit the conversion of arachidonic acid to prostaglandins (PGs), by inhibiting the cyclooxygenase isoenzymes COX1 and COX2. Adapted from Schjerning, McGettigan and Gislason [94].

Ibuprofen is a commonly prescribed NSAID with analgesic, anti-inflammatory and antipyretic properties. It is a member a class of drugs referred as 2-arylpropionic acid derivatives, also known as propionic acids[93]. At low doses, it is indicated to relieve minor pain and inflammation. Higher prescription doses are used for the long-term treatment of chronic conditions such as rheumatoid arthritis and OA[95]. Ibuprofen downregulates proinflammatory mediators in OA, such as IL-1β, TNF-α, NO, MMP-13, cathepsin K and aggrecanases[4]. Usually it is administered orally, although other administrations routes are available[93].

As discussed, NSAIDs are associated with several side effects in gastrointestinal, hepatic, renal and cardiac systems, especially over longer periods of administration. These side effects are related to the high doses used in patients due to the short biological half-life, rapid metabolism and high percentage of protein binding of NSAIDs. Additionally, cartilage drug delivery is challenging since drugs are rapidly cleared from the joint due to synovial fluids exchange. Furthermore, cartilage characteristics, such as its avascularity, difficult drug bioavailability[4]. Therefore, local application could overcome some of the drugs limitations, potentiating its efficiency[96].

Several strategies have been proposed to carry the drugs directedly to the target tissue thereby reducing adverse reactions. For example, intra-articular injections of anti-inflammatory drugs have been investigated to ameliorate joint inflammation[97]. However, frequent injections are necessary, which is painful for patients, leads to alteration and damage of the cartilage and substantially increases the financial burden of the treatment[4].

Ibuprofen-loaded scaffolds for are being proposed as a next generation of engineered tissues[98]. Cardea et al. developed a poly-L-lactid acid (PLLA) and ibuprofen composite scaffold with a homogeneous drug distribution and controlled released of the drug[98, 99]. Similarly, Yuan et. al prepared an ibuprofen-loaded electrospun PLLA scaffold to inhibit inflammation and promote muscle wound healing in vivo. Implanted scaffolds showed slighter inflammation and earlier reparation in a rat muscle wound model. Other polymers have also been combined with ibuprofen in the production of drug releasing scaffolds for TE[100, 101].

The incorporation of anti-inflammatory drugs in biomaterials for cartilage repair can modulate the inflammatory response towards a more pro-regenerative environment[91]. In particular, nanocarriers can be used for sustained local anti-inflammatory drug delivery[96]. They allow a decrease of the dose used and minimized the side effects of incorporated drugs. At the same time, drug release is not dependent upon scaffold degradation, since loaded NPs can be internalized with compromising its mechanical integrity.

During the healing process, a key factor that influences cartilage regeneration is the mechanical strength and stability of the 3D scaffold[102]. Polymeric scaffolds often do not have the mechanical properties needed to support long-term cartilage regeneration. In recent years, polymeric scaffolds have been combined with high strength, carbon derived materials such as carbon nanotubes (CNTs) and graphene oxide for TE applications[102]. These biocompatible nanomaterials reinforce the polymeric matrix, enhancing the functionality and strength of the scaffolds. In CNTs, the carbon atoms are arranged in tubular formations with pentagon and hexagon structures that provide mechanical and electrical properties. The C-C covalent bonds in the carbon rings offer CNTs the outstanding mechanical strength since they are considered the most constant chemical links[103]. Moreover, CNTs are strong, flexible, biocompatible, and chemically stable, which renders them appropriate for cell attachment, proliferation, and differentiation in TE. CNTs exist in two different forms: single-walled (SWCNTs) and multi-walled (MWCNTs). Both exhibit high aspect ratio, high elastic modulus, high tensile strength, elasticity and electrical and thermal conductivity[104].

CNTs have been used to strengthen polymeric biomaterials and reinforce their structural integrity and biomechanical strength. For example, Karbasi et al. developed a polycaprolactone (PCL)-gelatin scaffold for cartilage TE containing 1 wt% of multi-walled CNTs (MWCNTs) through electrospinning technique[104]. The hydrophilic nature of MWCNTs increased the hydrophilicity and bioactivity of the scaffold. Moreover, the CNTs addition enhanced the biomaterial mechanical strength, when compared to PCL-gelatin alone[104].

Although the incorporation of CNTs in scaffolds for TE is well characterized in terms of mechanical behavior, the immunological response is poorly described. MWCTNs are

capable of stimulate macrophage migration, induce cytokine secretion, and activate inflammatory pathways[105]. Furthermore, MWCNTs characteristics such as size (length and/or diameter), functionalization and purification influence macrophage's bioactivity[105]. To the author's knowledge there are no published works that explore the macrophage phenotype upon contact with scaffolds containing CNTs.

1.8. Scaffolds for cartilage TE

Scaffolds for cartilage TE should provide an appropriate microenvironment for cell adhesion, survival, and function. Several scaffolds with different compositions have been proposed to accelerate the cartilage regeneration process[106]. Biomaterials for scaffolds should be biocompatible and biodegradable into non-toxic and non-inflammatory components for the host organism, while exhibiting adequate mechanical parameters. Furthermore, they should resist body conditions such as pH and temperature. Scaffolds can be made of natural or synthetic polymers or a combination thereof (i.e., hybrid materials)[79].

Natural materials include collagen, hyaluronic acid and chitosan. They are widely explored due to their biocompatibility and bioactivity. Some natural materials, such as collagen naturally occurs in the human body, and therefore have properties similar to those of native tissues[79]. Approved products for cartilage regenerative medicine are mainly made of natural materials (Table 3)[79].

Collagen is a popular natural polymer that is recognized by mammalian cells. It has been acknowledged as an indispensable articular cartilage component[55]. Therefore, collagen has been extensively studied for chondral repair and cartilage TE. As Table 1 shows, commercially available scaffolds are mostly made of collagen[107]. Collagen naturally supports cell attachment and stimulates synthesis and assembly of ECM molecules. Furthermore, it has been shown that type II collagen increases chondrocyte secretion of cartilage matrix in vitro[108].

However, natural materials have some disadvantages. Since they rapid hydrolyze, natural materials quickly lose their mechanical stability, which impairs their cellular support and renders the scaffold susceptible to future damage[79]. Implanted collagen hydrogels are mechanically weak and degrade relatively too rapidly for tissue regeneration applications[78]. Thus, collagen membranes alone do not have suitable properties to create hyaline cartilage.

Synthetic polymers such as poly (ethylene glycol) (PEG), polylactic acid (PLA) and polyethersulfone (PES) show promising features for cartilage TE and some of them have been approved by regulatory agencies. Synthetic polymers can be used to produce several shapes of membranes to provide cell attachment and good mechanical, chemical and physical properties. Additionally, most of them degrade into components that are

metabolized by the body and allow a better control of compositional, structural, and mechanical properties[79, 109].

Table 3. Commercialized natural scaffolds for cartilage TE. Adapted from Wasyleczko, Sikorska and Chwojnowski [79].

Product (Company)	Materials	Characteristic
Hyalofast® (Anika)	Benzyl ester of hyaluronic acid	A bioresorbable 3D scaffold used through a one-step procedure after a microfracture. It can be used even for deep cartilage lesions. The scaffold's non-woven structure allows it to be cut and adaptively matched into uneven lesions.
NeoCart® (Histogenics)	Bovine type I collagen	Bioresorbableelectrospun scaffold used in MACI, a two-step procedure. The patient's chondrocytes are expanded into scaffolds. Then, they are incubated in Bovine type I the Tissue Engineering Processor (TEP), which collagen simulates the variation of mechanical forces and reduces oxygen pressure, allowing the maintenance of the chondrocyte phenotype forming the appropriate proteins of the ECM.
ChondroGide (Geistlich)	Type I/III collagen	The first described matrix for the ACI method. It is used in a one-step procedure. ChondroGide's role is to support and promote the chondrogenic differentiation of MSCs released after the microfracture method.
ACI-Matrix™ (MACI)	Type I/III collagen	The procedure is a two-step process. Expanded autologous chondrocytes (2 or 3 passage) are cultured collagen into the scaffold for 3 or 4 days before implantation into the patient.
Cartipatch® (Xizia Biotech)	Agarose and alginate	The cylindrical scaffold of a single layer of hydrogel with expanded cartilage cells. The clinical procedure is the same as that for the two-step method. The alginate polymer provides elasticity to the matrix, which facilitates handling during the surgical procedure.
NOVOCART® 3D AesculapOrthopaedics (BBraun)	Type I collagen, chondroitin sulfate	A sponge scaffold with a bilayer structure and interconnected pores, used in a two-step procedure. This scaffold is desirable in young patients,<16 years old, to avoid eventual secondary injuries, such as early osteoarthritis.
CaReS (Arthrokinetics)	Type I collagen gel	The scaffold is used in a two-step clinical procedure. Isolated autologous chondrocytes are mixed with a fluid matrix. Then, after 14 days, it is set in the lesion using fibrin glue. The height, thickness, and size of the hydrogel can be easily adjusted to the lesion.
CARTISTEM® (Medipost)	Hyaluronic acid	Allogeneic human umbilical cord blood (hUCB)-derived MSCs and HA hydrogel products for cartilage regeneration for repeated traumas or degenerative osteoarthritis. A 7-year follow-up study of 104 patients showed promising efficacy in terms of durable cartilage regeneration with no significant adverse effects.

PLA is a synthetic polyester extensively utilized in TE. It degrades by simple hydrolysis and has been approved for clinical use in sutures. Unfortunately, synthetic polymers lack specific and desirable biological functions, and some degradation products can result in toxic side-effects for the host organism.

Hybrid scaffolds combine the advantages of natural and synthetic materials. Blending collagen and PLA can lead to optimal desirable biodegradation, viscoelasticity, hydrophilicity and mechanical properties. They combine the desired mechanical properties with retaining the biofunctionality an tunability necessary for cartilage repair. The combination of PLA with a highly hydrophilic natural polymer facilitates cell attachment and stimulates matrix production[110]. Therefore, a hybrid scaffold presents an optimal structure for cartilage TE[111].

Nanofibrous scaffolds biomimic the natural ECM, providing an appropriate environment for cell attachment and proliferation. COPLA® Scaffold is a porous 3D biodegradable scaffold developed for chondral repair in weight-bearing joints. It can be used to regenerate full thickness chondral and osteochondral defects and is already in use for veterinary patients. COPLA® Scaffold is implanted after the traditional cartilage debridement procedure and secured to the chondral repair with fibrin glue. It is a hybrid scaffold made of collagen and polylactic acid (PLA) tailored to withstand mechanical loading and unloading, a biological phenomenon of the native tissue[111, 112].

1.9. Nanoenabled scaffolds for cartilage repair

Given the poor self-repair capability of cartilage tissue, 3D scaffolds arise as a promising strategy to provide an artificial ECM for its regeneration[79]. Nanoenabled scaffolds can offer a more appropriate microenvironment for the attachment, growth and phenotype modulation of cells.

Implantation of tissue-engineered scaffolds simultaneously triggers two different host responses. The scaffolds cause an immune reaction against the foreign material and tissue repair mechanisms are activated at the injured area. Perpetuated inflammation can be detrimental, aggravating tissue damage. At the same time, inflammation of essential to promote progenitor cell recruitment and healing mechanisms.

Optimal biomaterials should provide both structural support for regeneration and act as a reservoir for the release of bioactive molecules[113]. This way, the behavior of scaffold colonizing cells can be directly influenced, increasing tissue adaptation. The development of complex 3D biomaterials, enabled with nanocarriers that deliver active anti-inflammatory molecules can have a key immunomodulatory role in macrophages, towards an M2-like anti-inflammatory phenotype, while promoting a pro-regenerative microenvironment for chondrocytes.

1.10. Objectives

The main goal of this work is to study the immunomodulatory impact of a nanoenabled bioengineered 3D scaffold on macrophage polarization and its possible implications for cartilage repair. In order to accomplish this aim, four specific objectives were delineated:

1. **Macrophage internalization of nanocarriers alone.**

   Analysis of the macrophage's capacity to internalize FITC-loaded nanocarriers by conventional and imaging flow cytometry.

2. **Culture primary human monocyte-derived macrophages in pristine and nanoenabled 3D scaffolds, functionalized with FITC-loaded nanocarriers loaded or CNTs.**

   Analysis of macrophage morphology, differentiation and internalization of nanocarriers after culture on 3D biomaterials using confocal and electron microscopy.

3. **Evaluate the impact of nanoenabled 3D biomaterials on macrophage polarization, when exposed to pro-inflammatory conditions.**

   Assessment of the anti-inflammatory properties of the bioengineered scaffolds by culturing macrophages on scaffolds in naïve or pro-inflammatory conditions. Investigation of macrophage phenotype by labeling cells with M1 and M2 markers (CCR7, CD163) and analyzing them using confocal microscopy. Assessment of macrophage's cytokine secretion profile by through ELISA.

4. **Analyze the impact of macrophages cultured on nanoenabled 3D biomaterials on MSC/chondrocyte cell recruitment.**

   Evaluation of the extent of MSC mobilization induced by macrophages differentiated on pristine of nanoenabled 3D biomaterials using transwell recruitment assays.

CHAPTER 2. Materials and Methods

2.1. Ethics statement

Human samples and procedures were conducted in agreement with the principles established by the Declaration of Helsinki. Monocytes were obtained from surplus buffy coats (BC) from healthy and anonymized blood donors, kindly donated by *Serviço de Imunohemoterapia, Centro Hospitalar Universitário de São João (CHUSJ)*, Porto. Human mesenchymal stem/ stromal cells (MSCs) were isolated from healthy and anonymized human bone marrow of patients undergoing knee ligament surgery, kindly provided by *Serviço de Ortopedia*, CHUSJ, Porto. All experimental protocols were performed following the approval and recommendations of the CHUSJ Ethics Committee for Health (references 90/19 and 260/11), and patient identification was not provided to researchers.

2.2. Primary human monocyte isolation

Human monocytes were isolated from BC of health blood donors by negative selection, adapting previously described methods [114, 115]. In brief, BC were centrifuged for 20 min at room temperature (RT) and 1200 g (Eppendorf Centrifuge 5810R, VWR International LLC), with acceleration at 5 and brake set to 0, for blood components separation. Gradient separation formed 3 layers and the middle layer, enriched in peripheral blood mononuclear cells (PBMC) was collected. PBMCs were incubated with RosetteSep™ Human Monocyte Enrichment Cocktail (67 μL/mL, Stem-Cell Technologies™) for 20 min at RT under slow orbital agitation (Figure 7). The mixture was then diluted with equal volume of 2% heat inactivated fetal bovine serum (FBS) (Biowest) in phosphate buffer saline (PBS), carefully layered over Histopaque-1077 (Sigma-Aldrich Co.) and centrifuged for 20 min at room temperature (RT) and 1200g, with acceleration at 2 and brake set to 0. Three new layers were formed, and the enriched monocyte layer was collected and washed at least three times with PBS by centrifugation for 7 min at RT and 1300 rpm until the supernatant was clear. Cell pellet was resuspended in complete Roswell Park Memorial Institute (RPMI) 1640 media with L-glutamine (Corning) supplemented with 100 U mL^{-1} penicillin and 100 $\mu g/mL^{-1}$ streptomycin (1% P/S, both from Invitrogen) and 10% heat-inactivated FBS (Biowest). The number of viable cells was then counted in a Neubauer chamber.

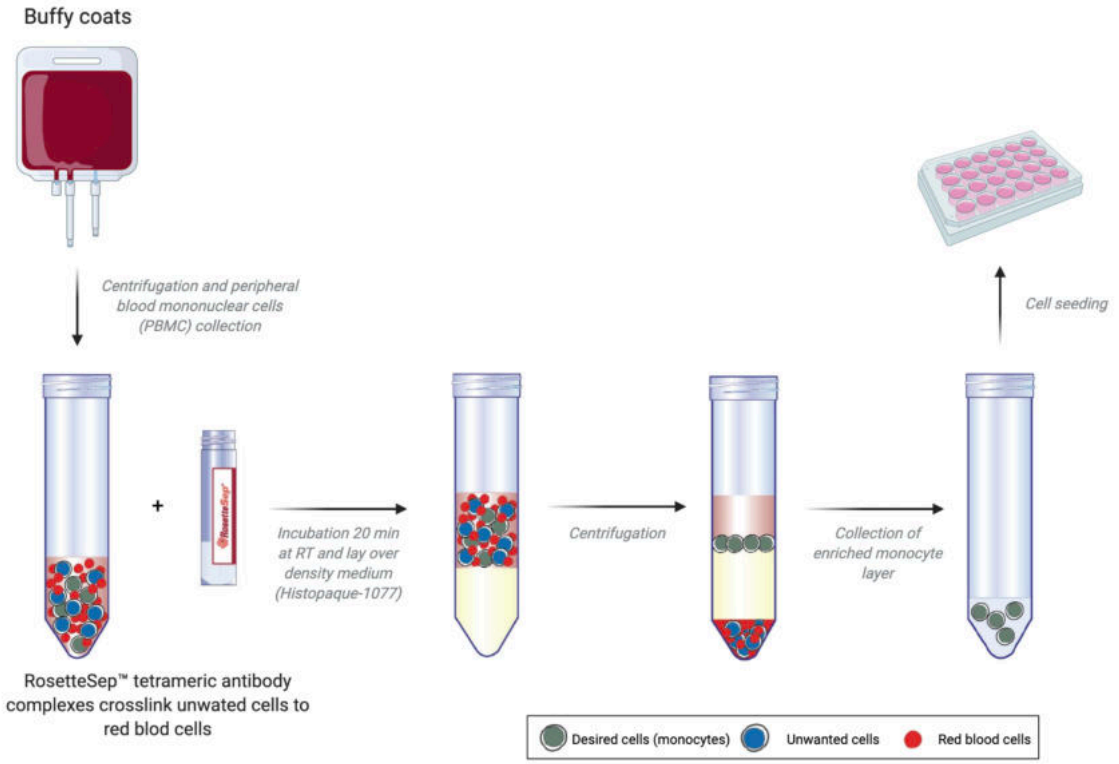

Figure 7. RosetteSep™ protocol diagram for the recovery of human primary monocytes from buffy coats (BC). After BC centrifugation, an interface enriched in peripheral blood mononuclear cells (PBMCs) is formed. RosetteSep™ tetrameric antibody links cells in the mix that bear CD2, CD3, CD8, CD19, CD56, CD66b, CD123 and glycophorin A (unwanted cells) to red blood cells. After density gradient centrifugation with Histopaque-1077, these complexes are removed and an interfaced enriched in monocytes collected. Cells are cultured in medium supplemented with macrophage differentiating factors. Adapted from StemCell Technologies[116].

2.3. Internalization/ phagocytosis of PLGA nanoparticles by human macrophages

For macrophage differentiation, 0.5 x 10^6 or 2 x 10^6 monocytes were seeded on glass coverslips in 24- or 6-well plates, respectively, and cultured for 7 days in complete RPMI media in the presence of 50 ng/mL of human macrophage colony-stimulating factor (M-CSF, ImmunoTools). After 7 days, cell culture media was replaced, and M-CSF removed. In order to assess NPs internalization/ phagocytosis by human macrophages, PLGA NPs loaded with fluorescein isothiocyanate (FITC) were prepared (C. Leite Pereira et al., INEB). At day 13, human macrophages were incubated with 15 μg/mL or 30 μg/mL FITC-loaded PLGA NPs for 1, 3 or 24h. Afterwards, detached macrophages were collected and centrifuged for 10 min at 300 g with acceleration and break set to maximum. The supernatant was collected under sterile conditions and stored at -80°C for further analysis. The remaining cells were washed with PBS and incubated with PBS-50 nM ethylenediaminetetraacetic acid (EDTA, VWR International LLC) for 15 min at RT. After, macrophages were harvested by scrapping the coverslips and used in further experiments.

2.4. Evaluation of macrophage NP internalization by flow cytometry

Previously collected and washed macrophages were resuspended in FACS buffer (PBS, 2% FBS, 0.01% sodium azide (Sigma-Aldrich Co.)) and stained with specific fluorochrome-conjugated antibodies: anti-human CD14-APC (2 μL in 50 μL) or CD14-PE (2 μL in 50 μL) (both from Immuno-Tools) for 30 min, in the dark at 4°C. Control samples were prepared using only FACS buffer (unstained), only CD-14 (macrophages without NPs) and only FITC. After labeling, cells were washed 3 times with FACS buffer and fixed with 1% paraformaldehyde (PFA, Sigma-Aldrich). Fixed and stained cells were analyzed by imaging flow cytometry (ImageStream^x, Amnis) after sample filtration (40 mm mesh) using INSPIRE software (Amnis). FITC fluorescence was assessed in channel 2 (505-560 nm) and CD14-PE in channel 3 (560-595 nm). Analysis was performed using IDEAS software (Amnis). For each sample, total of 20,000 events were acquired and > 5,000 single focused cells were analyzed for NP internalization, using the Internalization wizard. Cells were also analyzed by traditional flow cytometry in using a FACSCanto II™ Flow Cytometer (Becton Dickinson) and FACSDiva™ software (both from BD Biosciences). A total of 10,000 events were acquired and gated according to forward and side scatter parameters. Data were analyzed using FlowJo software (BD Biosciences, version 10).

2.5. Monocyte/ macrophage culture on Col-PLA scaffolds

Nanoenabled Col-PLA scaffolds were previously prepared (C. Leite Pereira et al, INEB). Col-PLA scaffolds were cut into 4- or 8-mm diameter discs using sterile biopsy punchers. Before cell seeding, scaffolds were allowed to incubate at 37°C in complete RPMI media for 1h.

For monocytes seeding (Figure 8A), a total of 1 x 10^6 cells, resuspended in 5 μL of complete RPMI media were seeded directly on top of the scaffolds. Cells were allowed to attach for 2h at 37°C. After, complete RPMI media supplemented with of 50 ng/mL of M-CSF (ImmunoTools) was added and cells were kept at 37°C in a humidified 5% CO_2 incubator for 13 days. At day 7, cell culture media was replaced, and M-CSF removed. At day 10, media was replaced, and half of the scaffolds were stimulated with 10 ng/mL LPS, Escherichia coli O55:B5 (Sigma-Aldrich Co.) and 50 ng/mL IFNγ (ImmunoTools) for M1 macrophage activation. Supernatants were collected under sterile conditions at day 7, 10 and 13, centrifuged at 10,000 rpm for 5 min at 4°C (Eppendorf Centrifuge 5810R, VWR International LLC) to remove any cellular debris and stored at -80°C until further analysis.

For macrophage seeding (Figure 8B), a total of 10 x 10^6 monocytes were seeded on Petri dishes after isolation from BCs and cultured for 7 days in complete RPMI media in the presence of 50 ng/mL of human M-CSF (ImmunoTools) for macrophage differentiation.

After 7 days, cell culture media was replaced, and M-CSF removed. At day 10, macrophages were washed twice with PBS and harvested by incubating with Accutase (Grisp) for 15 min at 37°C. Cell suspension was centrifuged at 300xg for 10 min with acceleration and brake set to 9 (Eppendorf Centrifuge 5810R, VWR International LLC) and the pellet resuspended in RPMI media for scaffold seeding. After seeding, cells were allowed to attach for 2h and complete RPMI media was added afterwards. The next day, half of the scaffolds was stimulated with LPS and IFNγ as described above for M1 macrophage activation. Supernatants were collected under sterile conditions at day 11 and 13, centrifuged as previously described and stored at -80°C until further analysis.

At day 13, after media collection, all samples were washed three times with warm PBS (5 min each) and fixed with PFA 4% for 15 min at room temperature. Afterwards, scaffolds were washed three times with PBS (5 min each) and stored in PBS at 4°C until further use.

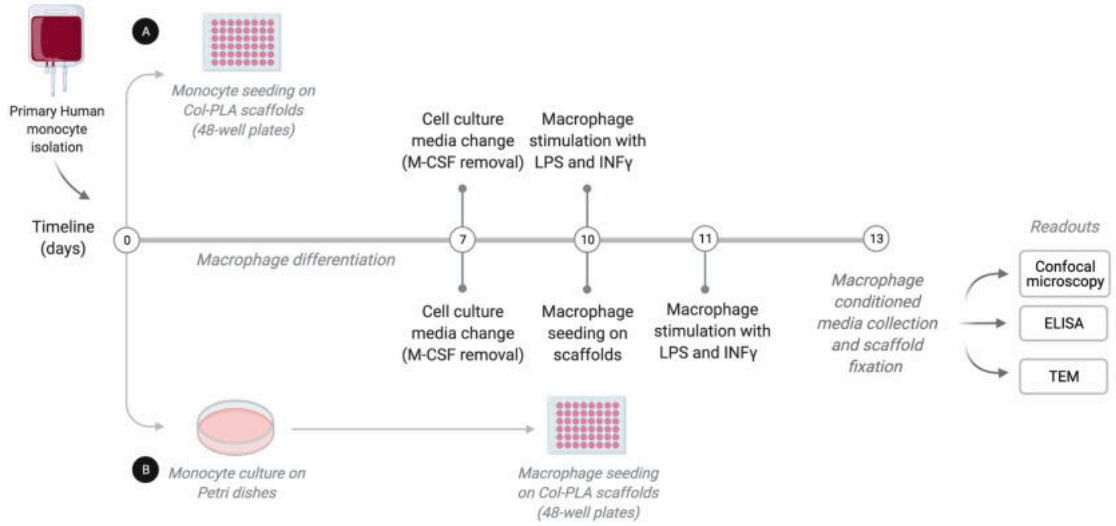

Figure 8. Experimental timeline and readouts. A. Freshly isolated monocytes are seeded on Col-PLA scaffolds with media supplemented with M-CSF for macrophage differentiation. M-CSF is removed at day 7 and cells stimulated with LPS and INFγ at day 10. **B.** Monocytes are seeded initially on Petri dishes for macrophage differentiation. M-CSF is removed at day 7 and macrophages are gently harvested and seeded on Col-PLA scaffolds at day 10. Macrophage M1 activation takes place a day later.

2.6. Nuclei and actin staining for confocal microscopy

After 13 days, coverslips with adherent macrophages and Col-PLA scaffolds were washed three times with PBS and fixed with PFA 4% (Sigma-Aldrich) for 15 min at RT. Afterwards, samples were washed three times with PBS (5 min each) and cell membranes were permeabilized with Triton X-100 0.2% (Sigma-Aldrich) in PBS for 15 min at RT. After, cells were washed three times with PBS (5 min each) and blocked with bovine serum albumin (BSA) 1% (VWR International LLC) in PBS for 60 min at RT to reduce nonspecific background staining. For the immunofluorescence staining, samples were incubated for 60 min at RT with a solution with 16:1000 Alexa®594-conjugated phalloidin (Invitrogen) for actin staining and 1:500 4', 6-diamidino-2-phenylindole (DAPI)

for nuclei staining. Afterwards, cells were a washed three times with PBS (5 min each). Coverslips were mounted onto microscope slides and sealed. Samples were store at 4°C until visualization by confocal laser scanning microscope (Leica SP5) using Leica Application Suite X (LAS X) software. Images were processed with Fiji (ImageJ).

2.7. M1/ M2 macrophage polarization by immunofluorescent staining

To assess the impact of nanoenabled Col-PLA scaffolds on macrophage polarization, macrophages were labelled for pro-inflammatory M1 markers and anti-inflammatory M2 markers using an immunofluorescent staining. After fixation, scaffolds were incubated with Triton X-100 0.2% (Sigma-Aldrich) in PBS for 15 min at RT for cell membrane permeabilization, followed by three washes with PBS (5 min each). After, samples were blocked with BSA 1% (VWR International LLC) in PBS for 1h at RT to reduce nonspecific background staining. For the immunofluorescence staining, samples were first incubated with primary antibody rabbit anti-human CCR7 (M1 marker) (Abcam) at a 1:100 ratio at 4°C. The following day, samples were washed 3 times with PBS (5 min each) and incubated with secondary antibody Alexa Fluor 647 goat anti-rabbit (ThermoFisher scientific) at a 1:300 ratio for 1h at RT, protected from light. Samples were then washed three times with PBS (5 min each) and blocked again with BSA 1% in PBS for 1h at RT. After, scaffolds were incubated with primary antibody mouse anti-human CD163 (M2 marker) (Bio-rad) at a 1:100 ratio at 4°C. The following day, samples were washed 3 times with PBS (5 min each) and incubated with secondary antibody Alexa Fluor 594 goat anti-mouse (ThermoFisher scientific) at a 1:300 ratio for 1h at RT, protected from light. After, scaffolds were washed 3 times with PBS (5 min each) and stored protected from light at 4°C until visualization by confocal laser scanning microscope (Leica SP5) using Leica Application Suite X (LAS X) software. Images were processed with Fiji (ImageJ).

2.8. Macrophage secretion profile

PGE2 was quantified by ELISA using the high sensitivity format of DetectX® Prostaglandin E2 Enzyme Immunoassay Kit (Arbor Assays™), according to the manufacturer's instructions. Optical density generated from each sample was measured at 450 nm using a multiplate reader (Synergy Mx, BioTek).

The concentration of the pro-inflammatory cytokine IL-1β produced by macrophages cultured on Col-PLA scaffolds was quantified using ELISA MAX™ Deluxe Set Human IL-1β kit, according to manufacturer's instructions (Biolegend). Optical density generated from each sample was measured at 450 nm using a multiplate reader (Synergy Mx, BioTek).

2.9. Multipotent mesenchymal stem/stromal cell (MSC) culture

Primary human MSCs used in this work were previously isolated from the BM of patients undergoing knee ligament surgery by density gradient centrifugation followed by selection of adherent cells, as previously described[117]. Following isolation, MSCs were characterized according to ISCT criteria. MSCs at passage 6 were stored in freezing medium (MSC growth medium with 10% dimethyl sulfoxide (DMSO), Sigma-Aldrich), in liquid nitrogen until further use. Prior to the assay, frozen aliquots of MSCs were thawed and cultured in MSCs growth medium (Dulbecco's modified Eagle's medium (DMEM; low glucose with Glutamax (Corning)), supplemented with 10% FBS Gibco MSC qualified (Fisher Scientific) and 1% P/S (Invitrogen). For MSC culture and maintenance, cells were seeded in 175 cm^2 tissue culture flasks (Falcon) with MSCs growth medium that was changed twice a week. At 70-80% confluence, cells were passaged by washing with warm PBS and detached using Gibco trypsin-EDTA 0.05% (Fisher Scientific) for 5 min at 37°C. After viable cell count using trypan blue exclusion dye (Sigma-Aldrich), MSCs were seeded at a density of 3000 cells/ cm^2 in 175 cm^2 tissue culture flasks. Experiments were performed using MSCs between passages 8 and 9.

2.10. Multipotent mesenchymal stem cell (MSC) transwell invasion/ recruitment assay

The capacity of macrophages cultured on nanoenabled Col-PLA scaffolds to recruit MSCs and the crosstalk between the two cell populations was evaluated in transwell assays. Boyden chambers with 8 μm pore size, coated with Matrigel™ (Corning) were used as inserts for 24-well plates (Figure 9). In all experiments, the bottom compartment contained Col-PLA scaffolds in 750 μL of MSC medium, that were previously seeded and cultured as described above. In the top compartment, $4x10^4$ MSCs were seeded in 500 μL of MSC medium. Assays were performed for 24h (macrophages in the scaffolds at day 12 of differentiation). Unseeded Col-PLA scaffolds (empty, PLGA-nkd and PLGA-Ibuf) in MSC medium and MSCS medium alone were used as controls.

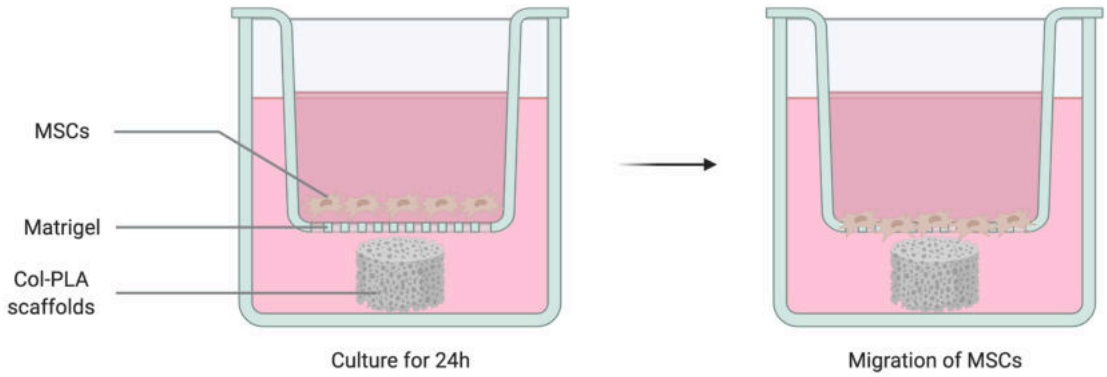

Figure 9. Experimental setup of the transwell assays. Col-PLA scaffolds with or without macrophages in DMEM are placed in the bottom compartment of a 24-well plate, being the stimuli for MSC invasion over the Matrigel™-coated membrane of the Boyden camber insert (top compartment).

MSCs were allowed to invade the membrane for 24h. Afterwards, culture medium was removed and stored at -80°C, membranes were washed twice with PBS 1x and fixed for 15 min with 4% PFA. The membrane side facing the interior of the insert was then thoroughly scrubbed with a cotton swab and washed again twice with PBS 1x. For nuclei visualization, membranes were carefully cut using a surgical blade and placed on a microscope slide with the migrated cells facing upwards. The slides were previously prepared with DAPI-containing mounting media (VectaShield, Sigma-Aldrich) and afterwards covered with a coverslip. Samples were stored at 4°C until further analysis. Nuclei were visualized using a fluorescence widefield microscope (IN Cell Analyzer 2000) with IN Cell Translator software. Images were then processed using IN Cell Developer Toolbox 1.9.3 software. First, images were collapsed into a single one using the Collage 50% protocol. Afterwards, nuclei were counted using the following inclusion criteria: form factor superior to 0.7, density levels superior to 140 and nuclei size between 35 and 300 μm.

2.11. Morphological analysis by transmission electron microscopy (TEM)

Cells cultured on the empty and CNT functionalized Col-PLA scaffolds were observed using transmission electron microscopy (TEM). Scaffolds were fixed using 2.5% glutaraldehyde/2% paraformaldehyde in cacodylate buffer 0.1M (pH 7.4), post-fixed with 1% osmic acid, dehydrated and then embedded in epon resin (TAAB). Semi-thin sections of the scaffolds with 50 nm thickness were prepared on a RM Ultramicrotome (PowerTome, Labtech) using a diamond knife. Sections were stained with uranyl acetate and lead citrate and electron micrographs were obtained using a Jeol-1400 TEM (JEOL USA, Inc.) operating at 200 kV in 200 mesh size formvar carbon supported copper grids coupled with a Orius SC 1100W digital camera (Orius). TEM was equipped with Energy-Dispersive X-ray Spectroscopy (EDS) system to trace intracellular iron associated with CNTs.

2.12. Statistical analysis

Statistical analysis of the results obtained was accomplished using GraphPad Prism 8.3.2 (GraphPad Software, Inc.). Data obtained was first tested for normality using Shapiro-Wilk normality test. Statistical differences between conditions were compared using a one-way ANOVA and *post hoc* multiple comparisons corrections were performed with Sidak or Fisher's LSD test. When normal distribution of data was not verified, the non-parametric Friedman test was performed followed by Dunn's, for multiple comparisons. A $p<0.05$ value was accepted as being statistically significant.

CHAPTER 3. Results

3.1. FITC loaded PLGA nanoparticles are readily internalized by primary human macrophages

In order to study the immunomodulatory impact of a nanoenabled bioengineered 3D scaffold on macrophage polarization, first the internalization of PLGA NPs by macrophages was studied by using FITC loaded PLGA NPs. FITC is a commonly used fluorochrome to assess NPs internalization by immune cells[96, 118]. Two different NPs concentrations were selected, to test the amounts necessary to later deliver 15 μg/mL and 30 μg/mL of ibuprofen. Also, 3 different internalization time-points (1h, 3h and 24h) were chosen to determine the cumulative accumulation of NPs on macrophages.

FITC-loaded PLGA NPs internalization was initially analyzed qualitatively by confocal microscopy (Figure 10). FITC fluorescence was found inside the cells for all conditions studied and appeared more evident for the higher concentration (30 μg/mL) of NPs used, independent of incubation time. This technique provides excellent spatial resolution and allows to confirm the presence of particles inside the macrophages. Furthermore, the concentrations of NPs and time-points used in this study did not result in alterations in macrophage morphology (Figure 10).

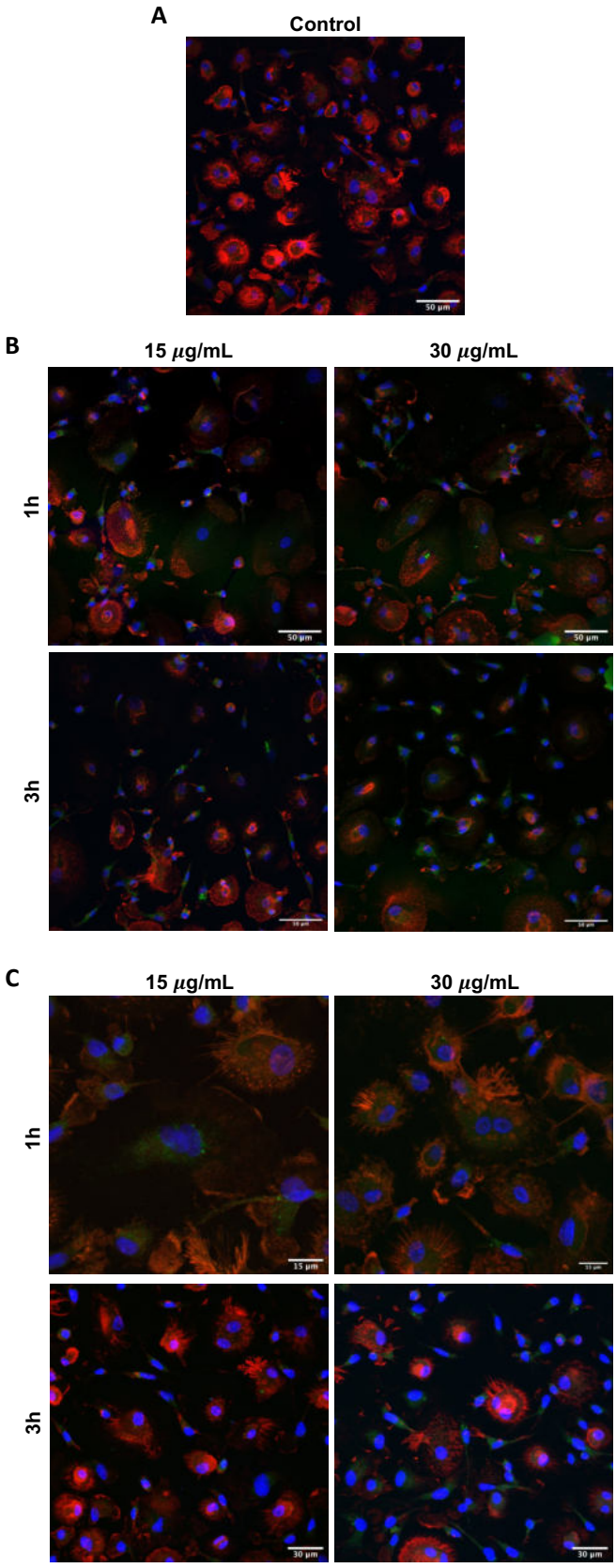

Figure 10. Representative confocal microscope images of FITC-loaded PLGA NPs internalization by primary human macrophages. A. Macrophages without NPs were imaged as a control. **B.** and **C.** FITC-loaded PLGA NPs can be identified within the cell cytoplasm in both lower and higher magnifications, respectively. Actin fibers were stained in red, cell nuclei in blue with DAPI and FITC is represented in green. Images are representative of 2 independent experiments.

Internalization of FITC loaded PLGA NPs by primary human macrophages was quantified using two different cytometry techniques. Internalization was first quantified using Imaging Flow Cytometry. Supplementary Figure A1 illustrates the workflow used for the analysis in IDEAS software, the "Internalization Wizard", and results exemplified in Figure 11A show that FITC loaded NPs can be readily observed within the cells. Although the cells have been detached and the level of cell detail is not comparable to confocal microscopy shown above, the surface staining for macrophage lineage marker CD14 clearly shows that PLGA NPs were internalized by macrophages. When the percentage of cells with internalized NPs was quantified along different donors it is clear that those that were not incubated with NPs (control) showed only residual fluorescence (0.43 $\pm$ 0.39 %) (Figure 11B), while those that were incubated with FITC-PLGA NPs at both concentrations, for 1 and 3h, as expected showed significantly more cells with internalized NPs. At 24h of incubation, particularly for the higher concentration, NPs were still found inside macrophages, but their fluorescence intensity levels were decreased. The higher concentration (30 μg/mL) led to almost 80% of macrophages having detectable FITC-NPs at 1h and 3h, with no statistical differences along time (Figure 11B). Albeit there were also no significant statistical differences between the two NP concentrations, the lower concentration of NPs (15 μg/mL) resulted in a lower percentage of FITC-positive cells, close to 60% at 1h and 3h (Figure 11B).

Additionally, internalization of FITC loaded PLGA NPs was quantified using regular flow cytometry for the same donors. Results illustrated in Figure 11C show that the CD14 population of macrophages becomes positive for FITC when cells were incubated with NPs, with a decrease in FITC fluorescence clear for the 24h incubation with the lower concentration. When the percentage of FITC positive macrophages was quantified across different donors (Figure 11D) the results are similar to these obtained for imaging flow cytometry. However, there were only significant differences for the higher NP concentration. Both techniques reveal a dose-dependent increase in PLGA NPs internalization, so the 30 μg/mL concentration of PLGA NPs was further used in subsequent experiments.

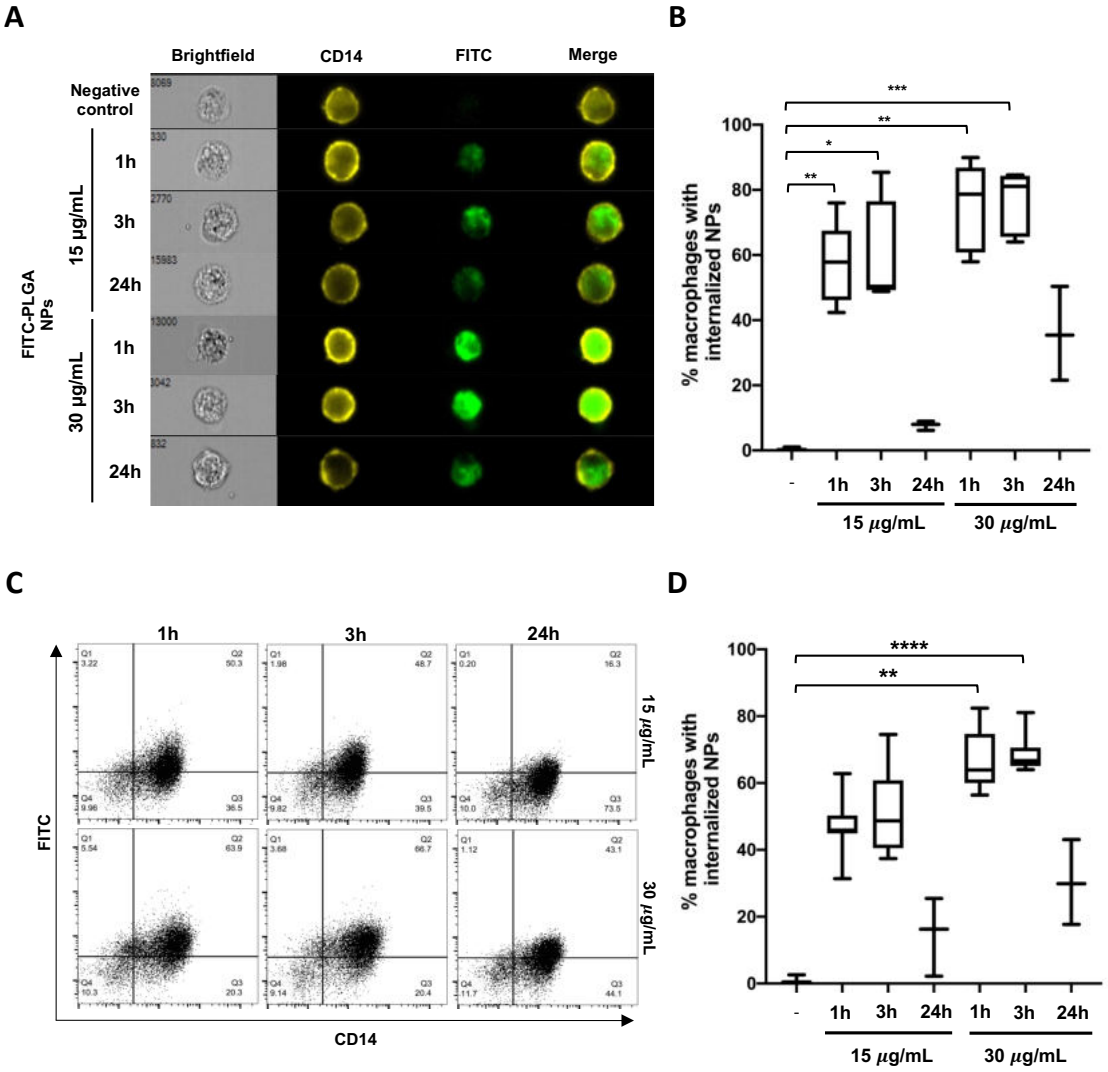

Figure 11. FITC-loaded PLGA NPs internalization by human macrophages, analyzed by Imaging Flow Cytometry (ImageStream^x) and regular flow cytometry. Macrophages were differentiated for 13 days prior to incubation with FITC-loaded PLGA NPs (15 μg/mL and 30 μg/mL) for 1h, 3h and 24h. Afterwards, cells were harvested, and surface stained for the marker CD14 before analysis. **A.** Representative images of CD14 positive (yellow) macrophages incubated without NPs (top) and 15 μg/mL (middle) or 30 μg/mL (bottom) of PLGA NPs loaded with FITC (green). Only residual fluorescence is observed in control (no NPs), whereas evident intracellular green fluorescence is observed for cells incubated with FITC-NPs (both concentrations). **B.** Quantification of the results illustrated in A, across independent donors. *p<0.05, **p<0.01, ***p<0.001 (n=3-5, Mixed-effects analysis, followed by Sidak's multiple comparisons test). **C.** Representative plots of the flow cytometry analysis. The numbers in the gates indicate the percentage of these populations. All samples show good expression of the surface marker CD14. **D.** Quantification of the flow cytometry results illustrated in C across different donors. **p<0.01, ****p<0.0001 (n=3-7, Friedman test, followed by Dunn's multiple comparisons test). The horizontal lines in the bars of the plot represent the median value for that distribution.

3.2. FITC loaded PLGA nanoparticles incorporated in Col-PLA scaffolds are internalized by primary human macrophages

With the purpose of assessing the internalization of PLGA NPs by primary human macrophages when the particles are incorporated in 3D scaffolds, FITC loaded PLGA NPs were incorporated in Col-PLA scaffolds. Two different experimental setups were

studied. First, monocytes were seeded directly after isolation (day 0) on top of empty and FITC-PLGA NPs Col-PLA scaffolds and differentiated to macrophages directly on the scaffolds. The second consisted in seeding macrophages, previously differentiated on Petri dishes, on FITC-PLGA NPs Col-PLA scaffolds, at day 10. Macrophages were stimulated towards M1 phenotype (LPS+INFγ) at day 10 or 11, respectively. Both experiments were carried out until day 13.

An area scan fluorescence reading after 13 days of culture demonstrated that control (no cells) FITC-PLGA Col-PLA scaffolds had higher fluorescence intensity compared to cell-seeded ones, both for monocyte (day 0) and macrophage (day 10) seeding (Figure 12). Moreover, no significant differences in fluorescence were found between scaffolds seeded with monocytes/macrophages at day 0 or day 10. Macrophage polarization towards an M1 phenotype also did not have an impact on scaffold fluorescence.

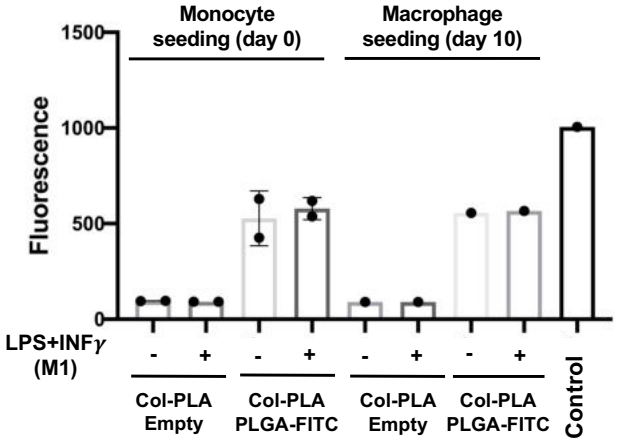

Figure 12. Fluorescence reading of empty and FITC-PLGA Col-PLA scaffolds. After 13 days of culture, a fluorescence area scan with excitation at 488 nm and reading at 520 nm was performed, both in scaffolds with monocytes seeded at 0 or macrophages at day 10 (n=1-2). In the control scaffold, no cells were seeded. ***Abbreviation:*** *Collagen-polylactic acid, Col-PLA;*

To evaluate NP internalization by macrophages seeded on the scaffolds, confocal microscopy was performed (Figure 13). Results show that, as expected, empty Col-PLA scaffolds had no fluorescence, while FITC-PLGA Col-PLA scaffolds for both experimental setups were fluorescent (Figure 13). Macrophages, that were labelled for their cytoskeleton (red) and nuclei (blue), are visible and well distributed in the 2 types of scaffolds. When macrophages were seeded at day 10, scaffolds seem to preserve more of their green fluorescence (Figure 13B). Most importantly, zooming in on the macrophages, FITC-PLGA NP internalization can be observed at day 10 (Figure 13C), which shows that FITC loaded PLGA NPs incorporated in Col-PLA scaffolds are also internalized and can be found inside macrophages.

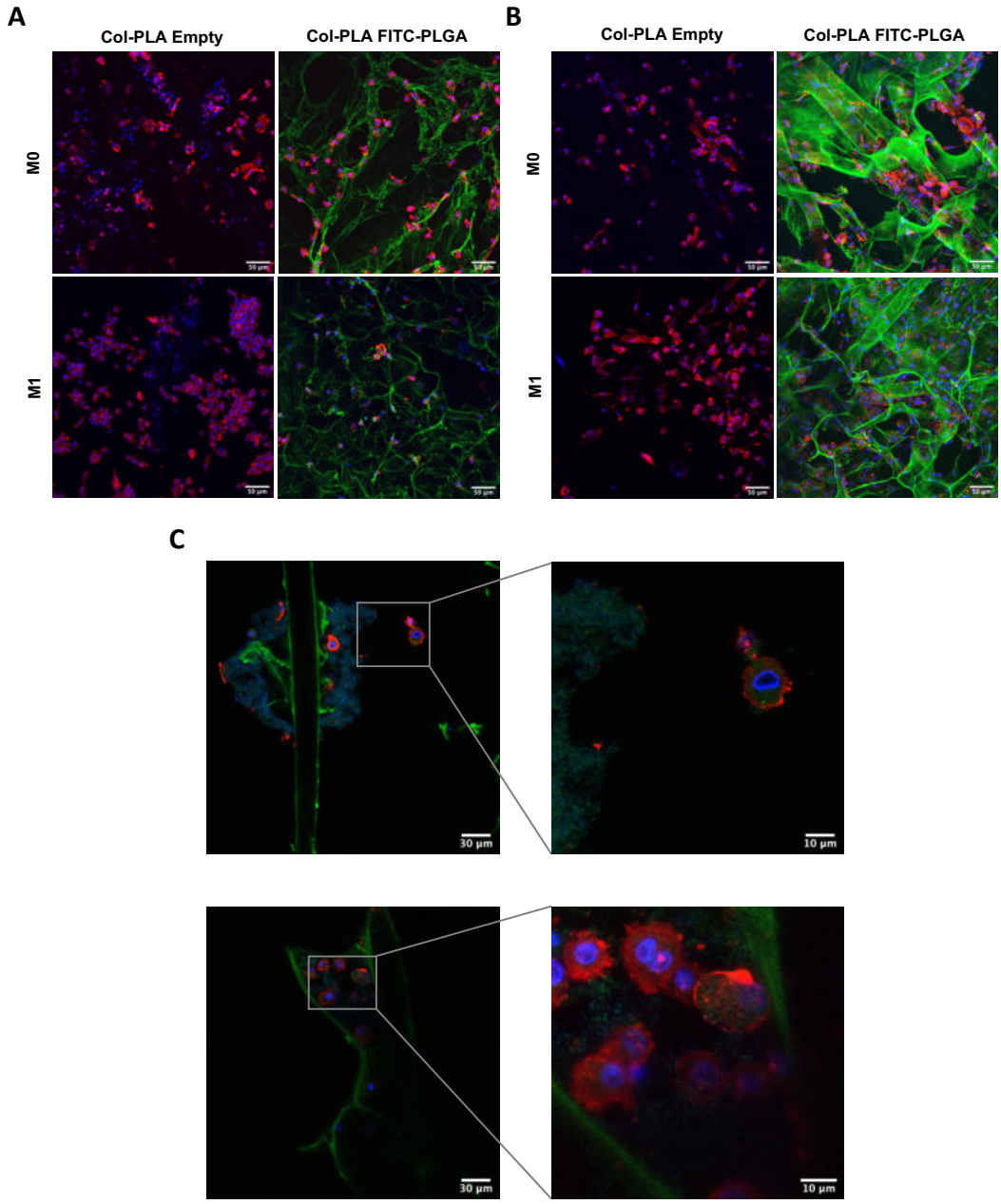

Figure 13. Representative confocal microscope images of macrophages grown in empty and FITC-loaded PLGA Col-PLA after 13 days of culture. Macrophages in the scaffolds were fixed and stained for cytoskeleton (red) and nuclei (blue). FITC-PLGA NPs can be seen in green and confer scaffolds their green fluorescence. **A.** Monocytes were seeded directly on Col-PLA scaffolds after isolation and allowed to differentiate to macrophages. **B.** Macrophages were seeded on Col-PLA scaffolds at day 10, after differentiation in Petri dishes. **C.** Higher magnification of B showing FITC-PLGA NPs internalization. Images are representative of 3 independent experiments. ***Abbreviations:*** *Collagen-polylactic acid, Col-PLA.*

3.3. The anti-inflammatory and immunomodulatory effect of nanoenabled Col-PLA scaffolds

Inflamed tissues can be characterized by the presence of inflammatory mediators, cytokines, and growth factors. Additionally, in these tissues there are elevated infiltrations of macrophages and lymphocytes. For diseases where inflammation plays

an important role in tissue damage, such as OA, macrophages could be a promising target for therapeutic approaches[119].

In this study, empty PLGA NPs (PLGA-nkd) and PLGA NPs carrying an anti-inflammatory drug (ibuprofen) (PLGA-Ibuf) were incorporated in a collagen-PLA scaffold (Col-PLA) and macrophage response to this biomaterial-based delivery system was investigated. We hypothesized that nanoenabled Col-PLA scaffolds containing PLGA-Ibuf NPs could effectively promote an anti-inflammatory environment and modulate macrophage polarization away from the M1 phenotype. Monocytes were seeded directly on top of Col-PLA scaffolds at day 0 and allowed to differentiate towards macrophages. M1 (LPS and INFγ) macrophage activation was used to simulate the joint inflammatory environment.

The capacity of nanoenabled Col-PLA scaffolds to modulate macrophage polarization was investigated. Scaffolds were fixed and stained for specific macrophage markers: M1 marker CCR7 (red) and M2 marker CD163 (green). Scaffolds were visualized using Confocal Microscopy to investigate the phenotypic profile of macrophages. Figure 14A shows representative confocal images of empty, PLGA-nkd and PLGA-Ibuf Col-PLA scaffolds, with or without M1 macrophage activation. Some macrophages present double staining and the colocalization is shown in yellow. Unstimulated scaffolds show a higher presence of cells expressing CD163 marker (green), while M1 stimulation led to an increase of CCR7 marker (red), and this increase is more significative in PLGA-Ibuf Col-PLA scaffolds. Cells positive for each marker or both were counted and are presented as a percentage of the total of stained cells for each condition and for two different donors (Figure 14B).

In Col-PLA empty scaffolds, M1 activation for 72h led to a significant increase in the proportion of M1 macrophages. The percentage of M2 macrophages was similar between both conditions, while the number of cells expressing both markers decreased after M1 stimulation. Interestingly, in unstimulated PLGA-nkd scaffolds we observed the highest percentage of M2 macrophages. In these scaffolds, for M1 stimulated conditions, the percentage of M1 and M2 macrophages decreased significantly, while the number of cells expressing both markers increased. Unexpectedly, the percentage of M1 macrophages was considerably high for both unstimulated and stimulated PLGA-Ibuf Col-PLA scaffolds.

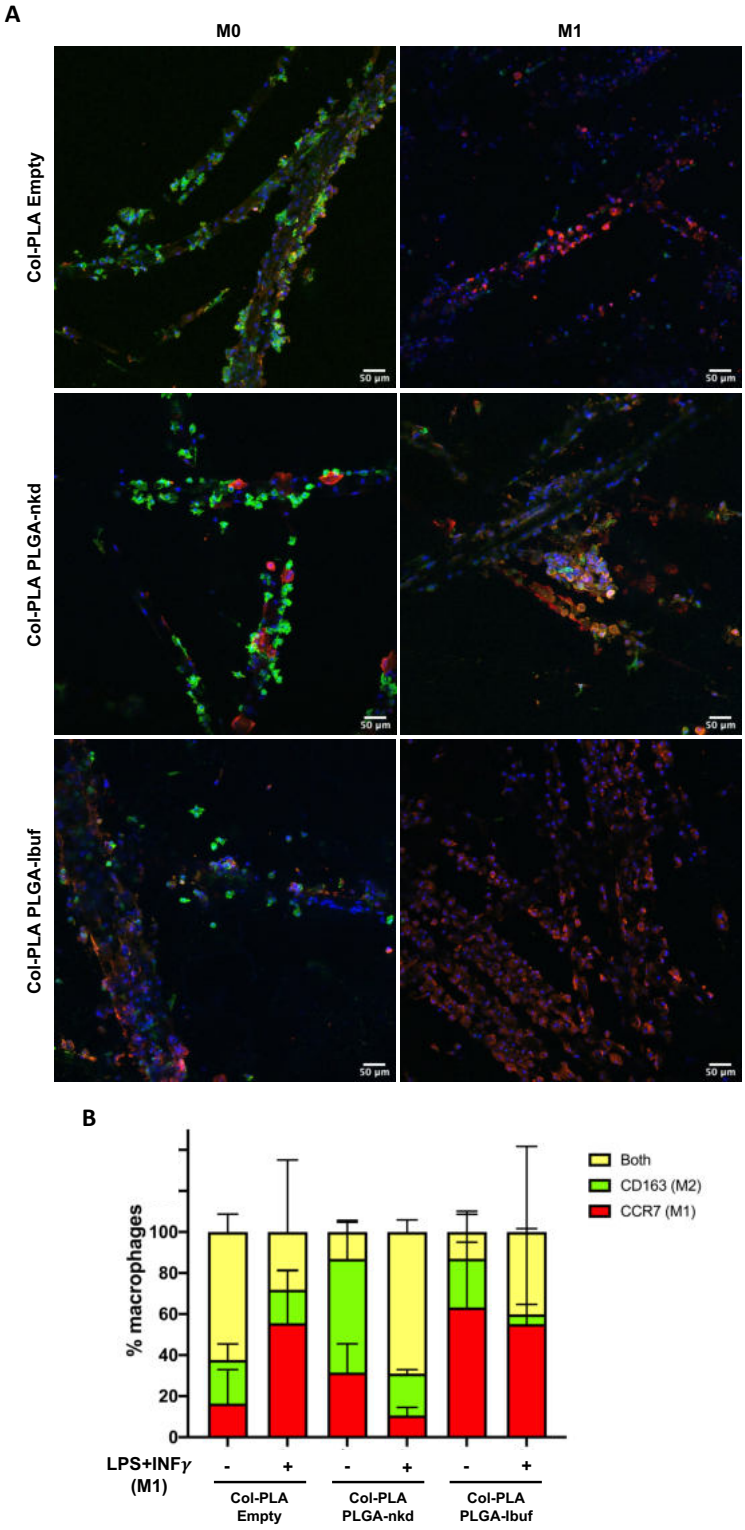

Figure 14. Macrophage polarization in Col-PLA scaffolds nanoenabled with PLGA-Ibuf NPs cultured for 13 days with and without M1 stimulation. Monocytes were previously isolated and seeded on Col-PLA empty, PLGA-nkd and PLGA-Ibuf scaffolds at day 0. Monocytes were allowed to differentiate towards macrophages and M1 stimulation (LPS+INFγ) was performed at day 10. Macrophages in the scaffolds were fixed at day 13, stained for M1 marker CCR7 (red), M2 marker CD163 (green) and nuclei (blue) and visualized using Confocal Laser Scanning Microscopy. **A.** Representative confocal microscope images of 2 independent experiments. **B.** Quantification of the results illustrated in A. The number of macrophages positive for M1, M2 or both markers were counted for each condition and expressed as a percentage of the total of stained cells. A total of 5 images per scaffold were acquired (n=2). ***Abbreviations:*** *naked, nkd; ibuprofen, ibuf, collagen-polylactic acid, Col-PLA.*

The anti-inflammatory potential of nanoenabled Col-PLA scaffolds was further evaluated by their ability to revert PGE2 levels of M1 activated macrophages. M1 stimulation of macrophages is known to induce COX-2 expression, consequently generating prostanoids that include PGE2[120, 121]. On the other hand, NSAIDs, including ibuprofen can effectively inhibit the production of PGE2 by inhibiting the enzymatic activity of COX-2[122].

PGE2 concentrations were analyzed by ELISA. Results indicate that, as expected, M1 macrophage stimulation for 72h led to a statistically significant increase in PGE2 production by macrophages. This increase was significant across all types of Col-PLA scaffolds investigated (Figure 15A), which shows that the ibuprofen-loaded PLGA NPs present in nanoenabled scaffolds were not able to attenuate the pro-inflammatory M1 stimulation.

The production of the pro-inflammatory cytokine IL-1β by macrophages was also investigated. In accordance with the PGE2 results, M1 macrophage stimulation for 72h (LPS+INFγ) also resulted in a statistically significant increase in IL-1β secreted by macrophages across all types of Col-PLA scaffolds investigated, including those functionalized with PLGA-Ibuf NPs (Figure 15B).

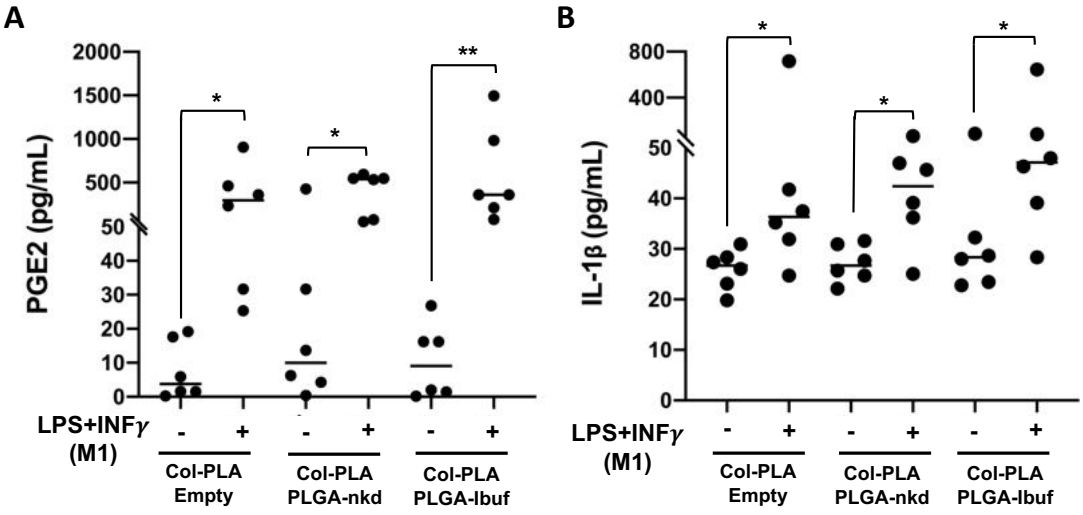

Figure 15. Anti-inflammatory potential of Col-PLA scaffolds nanoenabled with PLGA-Ibuf NPs on macrophages cultured for 13 days with and without M1 stimulation. Monocytes were previously isolated and seeded on Col-PLA empty, PLGA-nkd and PLGA-Ibuf scaffolds at day 0. Monocytes were allowed to differentiate towards macrophages and M1 stimulation (LPS+INFγ) was performed at day 10. **A. PGE2 concentration.** PGE2 was quantified in the medium at day 13 by ELISA. *p<0.05, **p<0.01 (n=6, Friedman test, followed by Uncorrected Dunn's test). **B. Concentration of the pro-inflammatory cytokine IL-1β.** IL-1β was quantified in the medium at day 13 by ELISA. *p<0.05 (n=6, Friedman test, followed by Uncorrected Dunn's test). Horizontal bars represent the mean for each condition. ***Abbreviations:*** *naked, nkd; ibuprofen, ibuf; Collagen-polylactic acid, Col-PLA.*

Collectively, these results indicate that Col-PLA scaffolds nanoenabled with PLGA-Ibuf NPs were not able to promote an anti-inflammatory environment and attenuate macrophages M1 polarization. In previous work by our group, macrophages were incubated with PLGA-Ibuf NPs for 72h only (unpublished). Thus, we hypothesized that

the anti-inflammatory effect of the nanoenabled scaffolds could have been transient and more evident in the initial days after cell seeding. Therefore, next we seeded previously differentiated macrophages on Col-PLA scaffolds, empty or nanoenabled, and activated the cells 24h later, evaluating macrophage activation 48h afterwards.

An immunofluorescent staining, followed by visualization by confocal microscopy was again used to investigate the immunomodulatory capacity of nanoenabled scaffolds on macrophages seeded at day 10. Figure 16A shows representative confocal images of empty, PLGA-nkd and PLGA-Ibuf Col-PLA scaffolds, with or without M1 macrophage activation. As cells had less time to colonize the scaffolds, more were visible at their surface, and their expression of CD163 (green) appears reduced when compared with those seeded at day 0. Cells positive for each marker were counted across two different donors and are presented as a percentage of the total of stained cells (Figure 16B). In all conditions studied, the percentage of M1 macrophages was consistently high, which was not the case when macrophages were seeded at day 0. Surprisingly, M1 stimulation (LPS+INFγ) led to a decrease in the percentage of M1 macrophages in all types of scaffolds in study, compared to unstimulated ones, while the percentage of cells expressing both M1 and M2 markers (yellow) increased. The number of M2 macrophages did not vary significantly between conditions (Figure 16B).

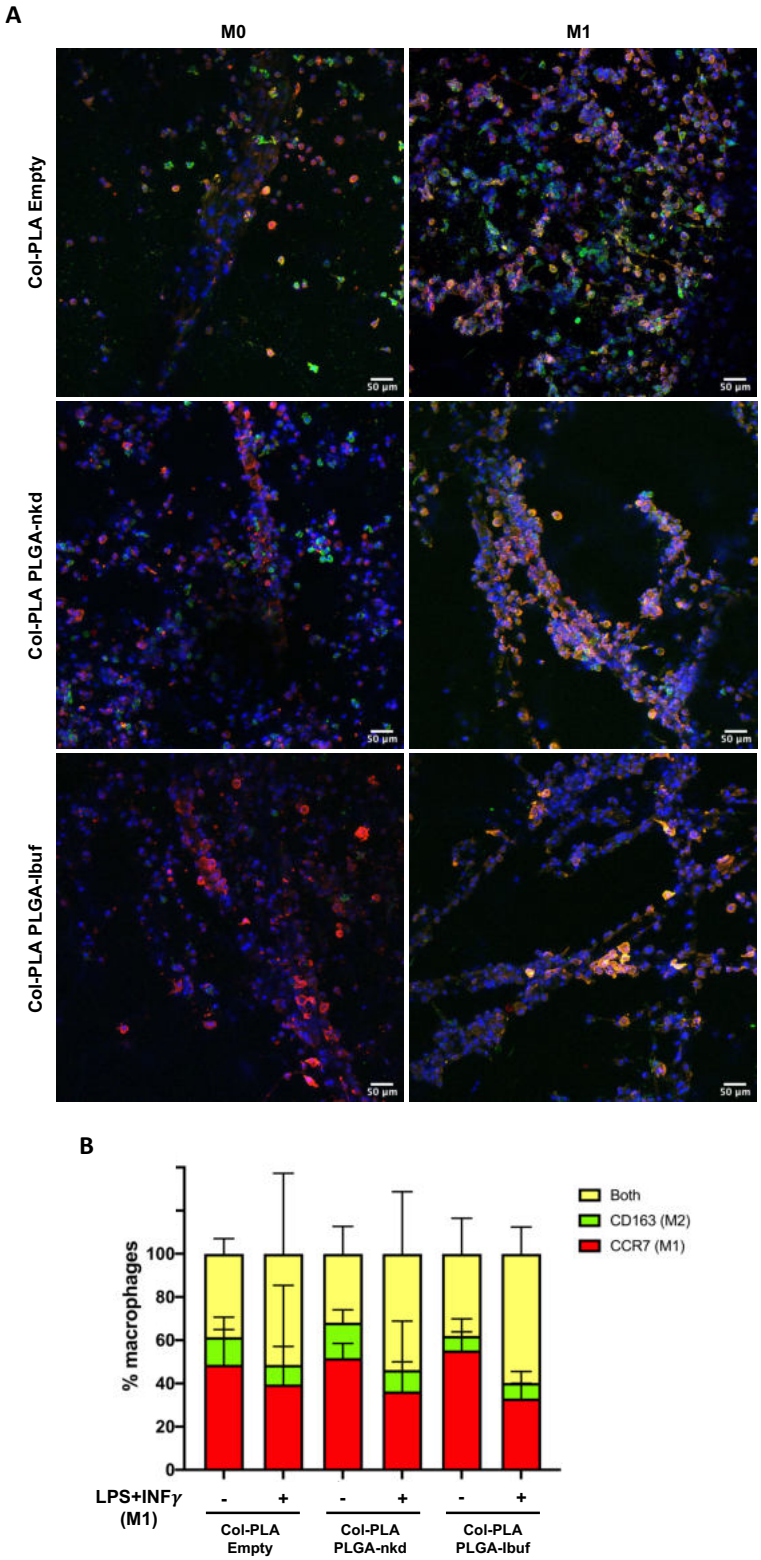

Figure 16. Polarization of macrophages seeded at day 10 in nanoenabled Col-PLA scaffolds with and without M1 stimulation. Monocytes were previously isolated, cultured on Petri dishes for 10 days and allowed to differentiate towards macrophages prior to seeding in Col-PLA scaffolds. M1 stimulation (LPS+INFγ) was performed at day 11. Macrophages in the scaffolds were fixed at day 13, stained for M1 marker CCR7 (red), M2 marker CD163 (green) and nuclei (blue) and visualized using Confocal Microscopy. **A.** Representative confocal microscope of 2 independent experiments. **B.** Quantification of the results illustrated in A. The number of macrophages positive for M1, M2 or both markers were counted for each condition and expressed as a percentage of the total of stained cells. A total of 5 images per scaffold were acquired (n=2). ***Abbreviations:*** *naked, nkd; ibuprofen, ibuf; collagen-polylactic acid, Col-PLA.*

To clarify the results of the confocal microscopy, PGE2 concentrations were measured to investigate the anti-inflammatory potential of nanoenabled Col-PLA scaffolds after 72h of culture. M1 macrophage stimulation (LPS+INFγ) resulted in an increase in PGE2 production by macrophages in both empty (non-statistically significant) and PLGA-nkd Col-PLA scaffolds (Figure 17A). No increase in PGE2 production was observed between unstimulated and stimulated PLGA-Ibuf Col-PLA scaffolds. However, the mean PGE2 concentration in both conditions was considerably high and was similar to the mean of the stimulated scaffolds of empty and PLGA-nkd Col-PLA (Figure 17A).

Macrophage production of the pro-inflammatory cytokine IL-1β was also studied. The results followed a similar trend, showing an increased concentration of IL-1β after macrophage M1 stimulation in all types of scaffolds that was statistically significant for empty and PLGA-Ibuf Col-PLA (Figure 17B).

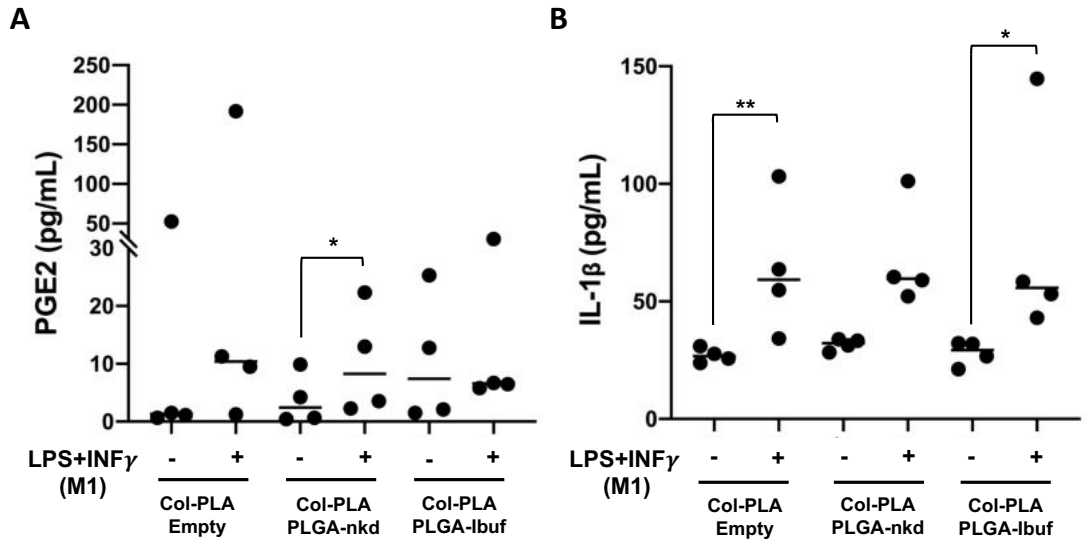

Figure 17. Anti-inflammatory potential of Col-PLA scaffolds nanoenabled with PLGA NPs on macrophages seeded at day 10 and with and without M1 stimulation. Monocytes were previously isolated, cultured on Petri dishes for 10 days and allowed to differentiate towards macrophages prior to seeding in Col-PLA empty, PLGA-nkd and PLGA-Ibuf scaffold. M1 stimulation (LPS+INFγ) was performed at day 11. **A. PGE2 concentration.** PGE2 was quantified in the medium at day 13 by ELISA. *p<0.05 (n=4, Friedman test, followed by Uncorrected Dunn's test). **B. Concentration of the pro-inflammatory cytokine IL-1β.** IL-1β was quantified in the medium at day 13 by ELISA. *p<0.05, **p<0.01 (n=4, Friedman test, followed by Uncorrected Dunn's test). Horizontal bars represent the mean for each condition. ***Abbreviations:*** *naked, nkd; ibuprofen, ibuf; collagen-polylactic acid, Col-PLA.*

Previous results from our group indicate that ibuprofen loaded PLGA NPs have an effective anti-inflammatory effect on M1 polarized macrophages (unpublished results) that has not been observed when NPs are incorporated in Col-PLA scaffolds for both cells seeded at day 0 and day 10. Taking these results together with the high fluorescence of the FITC-PLGA NPs functionalized Col-PLA scaffolds, we hypothesized that maybe the ibuprofen in the PLGA NPs inside the Col-PLA scaffolds would not be accessible for macrophages.

To test our hypothesis, PLGA NPs were added directly on top of the scaffold. Col-PLA with entrapped PLGA NPs and with the free drug added directly to the scaffolds were used as controls. Differentiated macrophages were seeded on the different scaffolds at day 10, and M1 stimulation was performed at day 11.

Figure 18A shows representative confocal images of macrophage polarization upon culture on nanoenabled Col-PLA scaffolds with or without M1 macrophage activation. The CCR7 (red) staining appears more abundant than CD163 (green), across all conditions. Cells positive for each marker were counted across two donors and are presented as a percentage of the total of stained cells (Figure 18B). The results indicate that the percentage of M1 macrophages was high in all conditions studied. Surprisingly, M1 macrophage stimulation led to a decrease in the percentage of CCR7+ M1 macrophages in empty and NP-functionalized scaffolds compared to unstimulated conditions, while the percentage of cells expressing both M1 and M2 markers (yellow) increased. In scaffolds with free ibuprofen CCR7 remains similar upon stimulation, but CD163 was reduced and cell expressing both markers were increased. The percentage of M2 macrophages was higher in Col-PLA PLGA-nkd on top compared to PLGA-Ibuf on top. The highest M2 macrophage percentage was observed when macrophages were cultured in Col-PLA with free ibuprofen (Figure 18B).

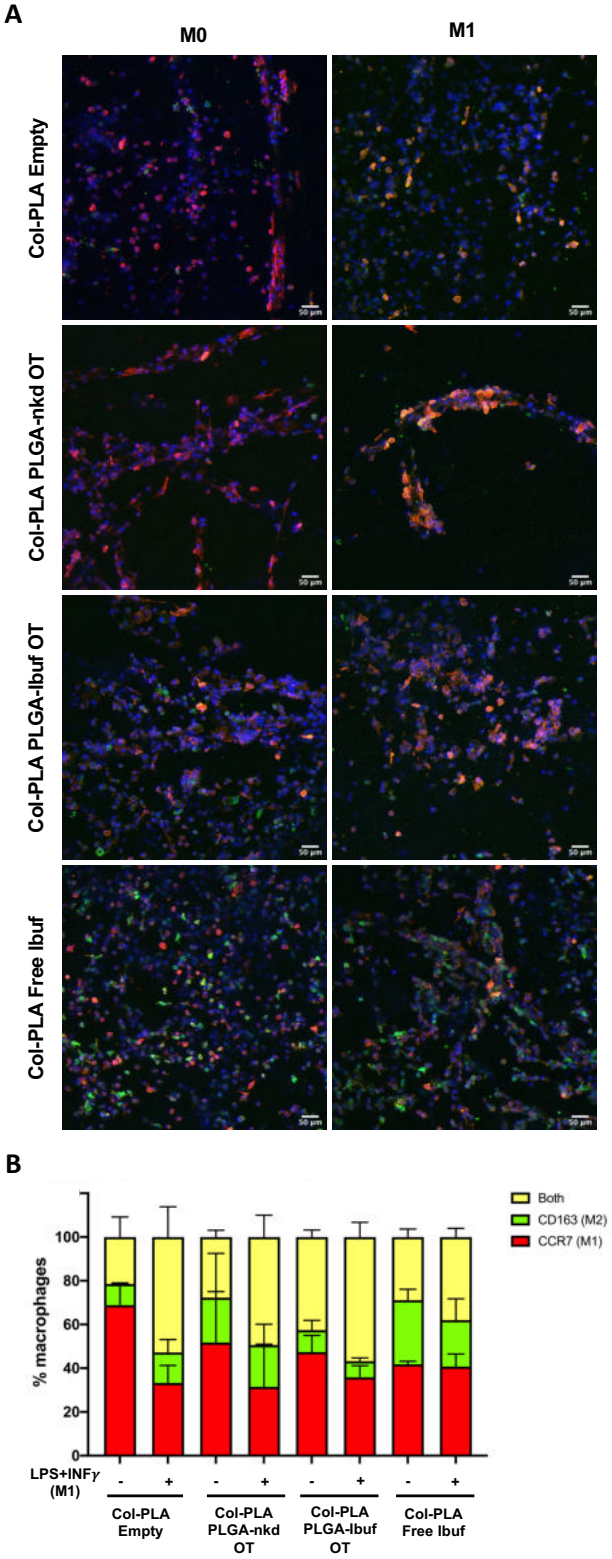

Figure 18. Polarization of macrophages seeded at day 10 in Col-PLA scaffolds nanoenabled with PLGA NPs and Col-PLA scaffolds with PLGA NPs on top with and without M1 stimulation. Monocytes were previously isolated, cultured on Petri dishes for 10 days and allowed to differentiate towards macrophages prior to seeding in empty, PLGA-nkd, PLGA-Ibuf, PLGA-nkd on top, PLGA-Ibuf on top and free ibuprofen Col-PLA scaffolds. M1 stimulation (LPS+INFγ) was performed at day 11. Macrophages in the scaffolds were fixed at day 13, stained for M1 marker CCR7 (red), M2 marker CD163 (green) and nuclei (blue) and visualized using Confocal Laser Scanning Microscopy. **A.** Representative confocal microscope of 2 independent experiments. **B.** Quantification of the results illustrated in A. The number of macrophages positive for M1, M2 or both markers were counted for each condition and expressed as a percentage of the total of stained cells. A total of 5 images per scaffold were acquired (n=2). ***Abbreviations:*** *naked, nkd; ibuprofen, ibuf; on top, OT, collagen-polylactic acid, Col-PLA.*

Analyzing the culture supernatants, on Col-PLA scaffolds with entrapped PLGA NPs without or with ibuprofen, M1 macrophage stimulation resulted in increased PGE2 levels, albeit the results were not statistically significant. In Col-PLA scaffolds with NPs on top M1 stimulation led to a significant increase in PGE2 levels, when NPs did not have ibuprofen, but no increase in PGE2 in Col-PLA with PLGA-Ibuf NPs on top (Figure 18B). Indeed, in both unstimulated and stimulated conditions, PGE2 concentration was similar to basal levels. Concerning Col-PLA scaffolds with free ibuprofen, we observed a decrease of PGE2 in M1 stimulated scaffolds compared to unstimulated ones, albeit not statistically significant (Figure 19A).

On the other hand, M1 stimulation on scaffolds with PLGA-Ibuf NPs on top resulted in the highest increase of IL-1 β, compared to unstimulated ones. This was not the case when free ibuprofen was present in the scaffolds, where the increase in IL-1 β levels upon M1 stimulation was not significant (Figure 19B).

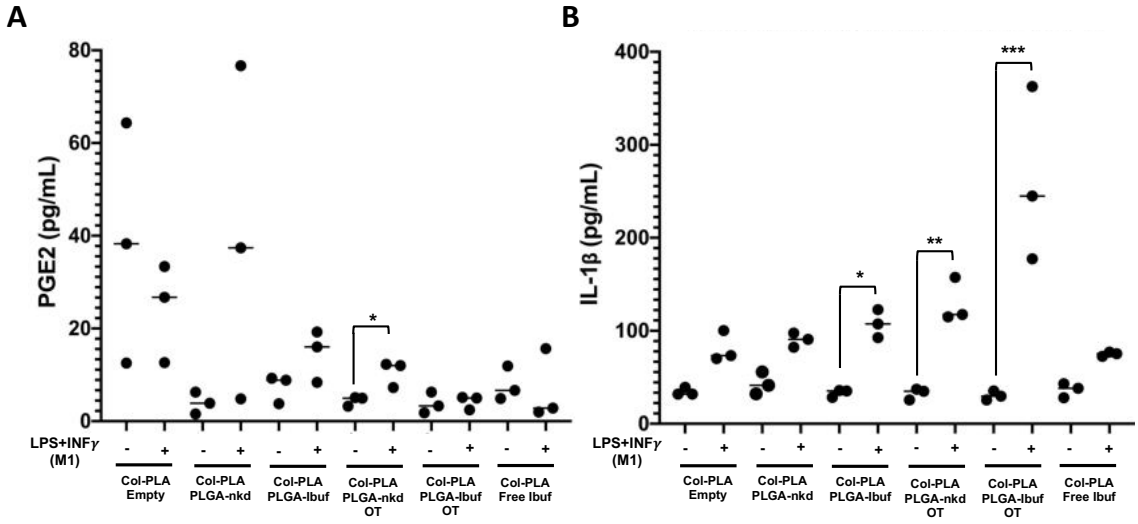

Figure 19. Anti-inflammatory potential of Col-PLA scaffolds nanoenabled with PLGA NPs and Col-PLA scaffolds with PLGA NPs on top on macrophages seeded at day 10 with and without M1 stimulation. Monocytes were previously isolated, cultured on Petri dishes for 10 days and allowed to differentiate towards macrophages prior to seeding in empty, PLGA-nkd, PLGA-Ibuf, PLGA-nkd on top, PLGA-Ibuf on top and free ibuprofen Col-PLA scaffolds. M1 stimulation (LPS+INFγ) was performed at day 11. **A. PGE2 concentration.** PGE2 was quantified in the medium at day 13 by ELISA. *p<0.05 (n=3, RM one-way ANOVA, with Geisser-Greenhouse correction, followed by Uncorrected Fisher's LSD). **B. Concentration of the pro-inflammatory cytokine IL-1β.** IL-1β was quantified in the medium at day 13 by ELISA. *p<0.05, **p<0.01, ***p<0.001 (n=3, Friedman test, followed by Uncorrected Dunn's test). Horizontal bars represent the mean for each condition. ***Abbreviations:*** *naked, nkd; ibuprofen, ibuf; on top, OT, collagen-polylactic acid, Col-PLA.*

Taken together, these results indicate that PLGA NPs entrapped in Col-PLA scaffolds may not be as effective as expected in promoting an anti-inflammatory macrophage phenotype.

3.3. Macrophages cultured on Col-PLA scaffolds influence MSC recruitment in vitro

Strategies that modulate immune cells to attract endogenous stem cell are appealing for effective tissue regeneration. MSCs support the regenerative process due to their ability to migration, differentiation and immunomodulatory properties[123]. Therefore, we sought to understand the functional consequences of Col-PLA-macrophage interactions on human MSC recruitment.

The capacity of macrophages cultured on nanoenabled Col-PLA scaffolds to recruit MSCs was evaluated. Monocytes were seeded at day 0 on empty, PLGA-nkd and PLGA-Ibuf Col-PLA scaffolds and allowed to differentiate for 13 days. We also assessed the effect of M1 macrophage stimulation on cell recruitment. Seeded scaffolds were placed on a well of a 24 well plate and Boyden chambers with Matrigel-coated membranes were inserted on top of it to investigate MSCs invasion capacity. MSCs were allowed to migrate for 24h towards the bottom well. To ensure that the paracrine effect was due to macrophages, assays were performed in serum free media.

Figure 20A illustrates an example of invading MSCs in control conditions, versus using macrophages seeded on Col-PLA with PLGA-Ibuf NPs and M1 stimulated, with nuclei stained in blue (DAPI). The number of cells migrated per membrane was counted for each condition and are presented as relative to the negative control (serum free media only) (Figure 20B). Col-PLA scaffolds by themselves promoted MSCs migration to a certain extent, particularly those with PLGA NPs with and without ibuprofen (Figure 20B). As expected, the presence of macrophage seeded scaffolds in the bottom compartment of the transwell assays influenced MSC invasion, since scaffolds without cells show lower mean value of migrated cells. In scaffolds with M1 stimulated macrophages migration was slightly higher, except for the Col-PLA empty, although no statistically significant differences were found between the conditions. As mentioned, to avoid the interference of unknown molecules, experiments were performed under serum free conditions. However, macrophages were initially cultured in serum containing media and proteins adsorbed to the material surface can impact invasion capacity.

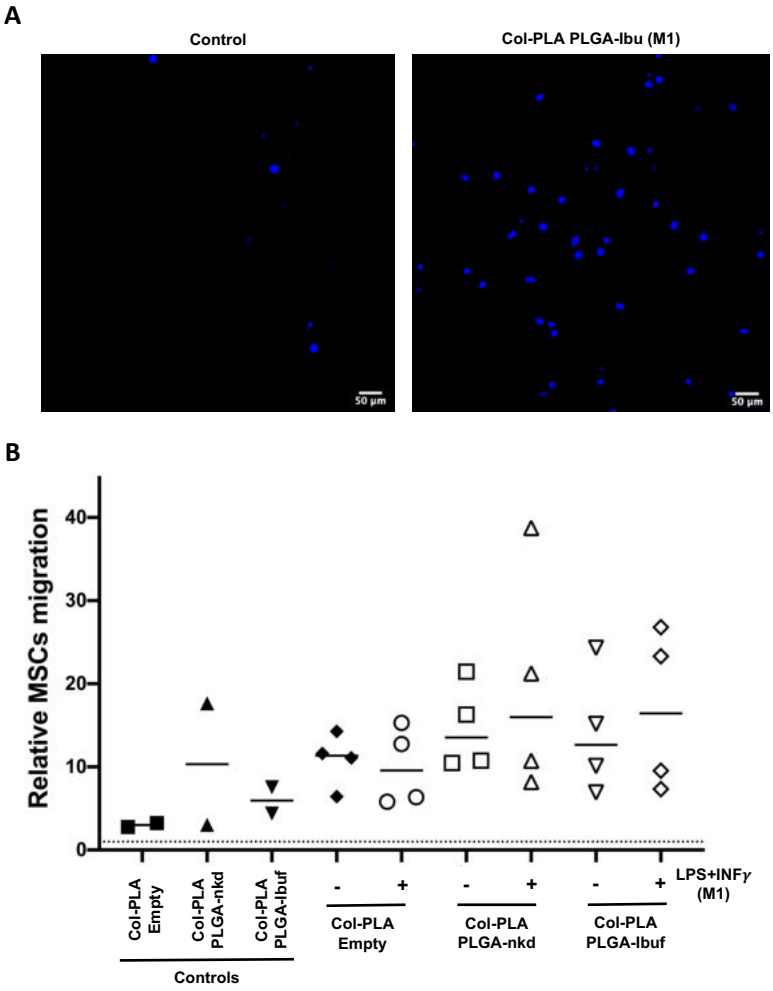

Figure 20. Macrophages cultured on Col-PLA scaffolds promote MSC invasion capacity. Serum free media was used as the negative control. Results are presented as relative to the negative control. Empty, PLGA-nkd and PLGA-Ibu Col-PLA scaffolds with macrophages cultured for 13 days were placed in the bottom compartments of Boyden chambers. Unseeded scaffolds were used as controls. MSCs were seeded on top of transwells with Matrigel-coated membranes with 8 μm pore size. **A.** Representative images of invading MSCs with nuclei stained with DAPI (blue). **B.** Quantification of the number of cells migrated per membrane (n=2-4). Horizontal bars represent the mean for each condition. No statistically significant differences were found (n=2-4, Friedman test, followed by Uncorrected Dunn's test). ***Abbreviations:*** *naked, nkd; ibuprofen, ibuf; collagen-polylactic acid, Col-PLA.*

3.4. Macrophage morphology and polarization state in CNT functionalized COPLA® Scaffolds

Stimuli-responsive nanobiomaterials might have the ability to enhance cartilage regeneration through external remote stimulation. These materials are designed to respond to external stimuli that efficiently penetrate biological tissues in a non-invasive way, allowing the control of the extracellular environment. Among stimuli-responsive nanomaterials, CNTs are lightweight and exhibit excellent properties, including mechanical strength, durability, flexibility, and biocompatibility[124]. Incorporating CNTs in biomaterials for cartilage tissue engineering improves their mechanical strength, which is necessary in the field of orthopedic surgery, where tissues are subjected to mechanical stress[125].

Thus, for the second part of this thesis macrophage response to CNT functionalized collagen-PLA scaffold (COPLA® Scaffold) was investigated. Confocal microscopy images of primary human macrophages cultured on empty and CNT functionalized COPLA® Scaffolds show that macrophages attached and populated the scaffolds after 13 days of culture (Figure 21). Macrophages cultured on both scaffolds showed no significant morphological differences, even after M1 macrophage activation. However, it appears that CNT functionalized scaffolds have a lower cell density than empty ones.

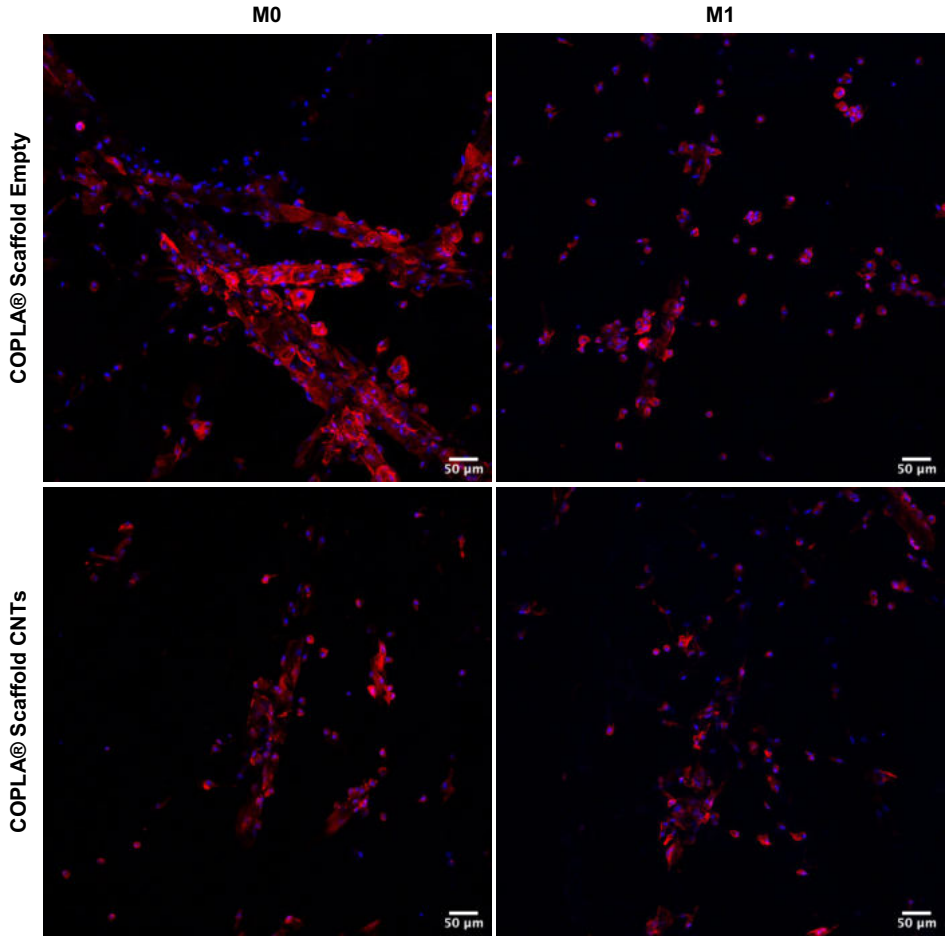

Figure 21. CNT functionalized COPLA® Scaffolds allow macrophage scaffold population. Representative confocal microscope images of macrophage morphology. Macrophages were cultured in empty and CNT functionalized COPLA® Scaffolds for 13 days of culture, with and without M1 stimulation at day 10. Macrophages in the scaffolds were fixed and stained for cytoskeleton (red) and nuclei (blue). Images are representative of 1 experiment.

Macrophage morphology after culture in CNT functionalized COPLA® Scaffolds and the influence of CNTs on cellular ultrastructure was also analyzed by TEM. We further investigated macrophage interaction and internalization of CNTs. Functionalization of COPLA® Scaffolds with CNTs is clearly shown in Supplementary Figure A2. The tubular structure of CNTs is very evident and CNTs appear well distributed in the scaffold mesh. Figure 22A shows representative TEM images of macrophages cultured for 13 days on empty and CNT functionalized COPLA® Scaffolds, with and without M1 activation. A normal macrophage morphology can be observed in empty COPLA® Scaffolds

Furthermore, macrophages seem to adhere and interact with CNT functionalized scaffolds as represented by the yellow arrows (Figure 22A). Macrophage M1 activation resulted in the appearance of membrane projections (pseudopodia) in both types of COPLA® Scaffolds, which are typical of this type of stimuli. The entrance of single CNTs was repeatedly observed by TEM and is represented in more detail in Figure 22B. In some images, the integrity of the cell membrane seemed compromised by CNT penetration, as represented in the green circle in Figure 22B. We also observed the presence of CNTs inside mitochondrias, which have a characteristic double membrane (blue circle). In these cases, the mitochondria lost their characteristic cristae and appeared in stress. Further ultrastructural analysis is ongoing to confirm possible interferences of CNTs with macrophage metabolism and induction of oxidative stress.

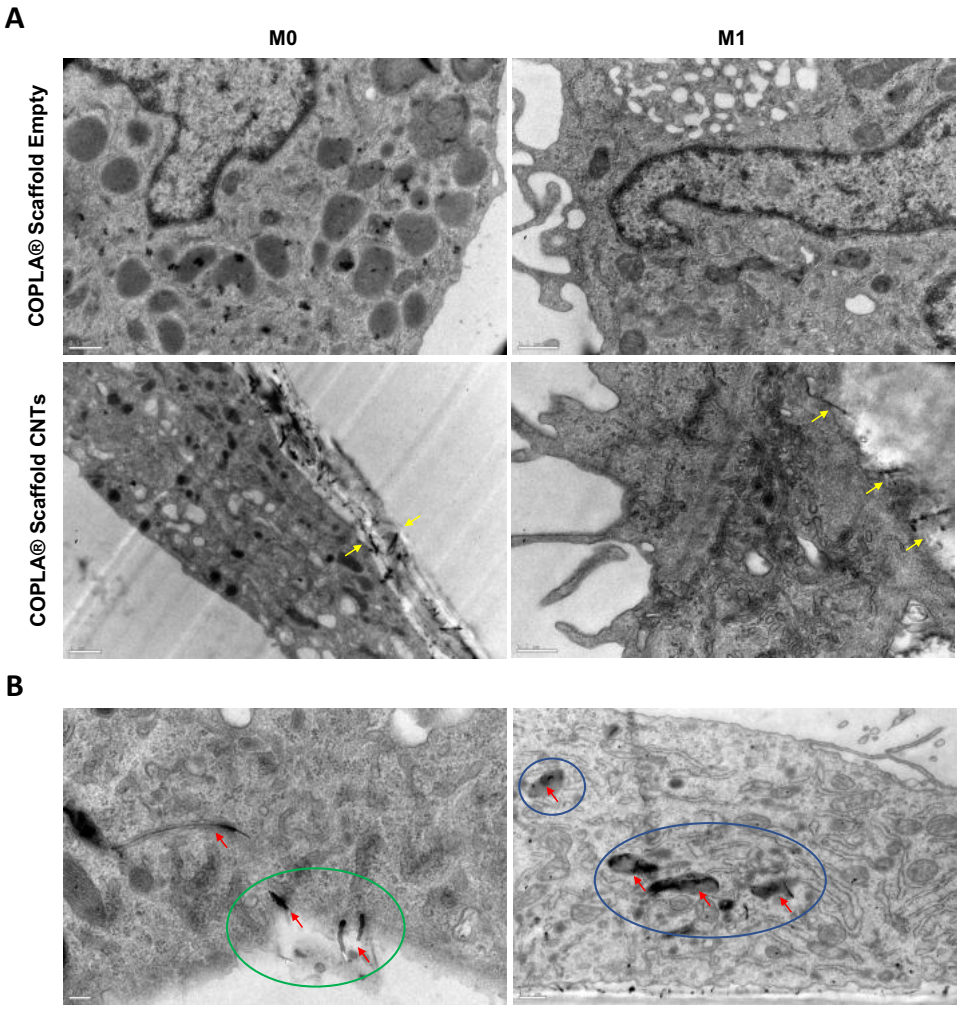

Figure 22. Transmission electron microscopy (TEM) images of macrophages cultured on empty and CNT functionalized COPLA® Scaffolds. Macrophages were cultured in empty and CNT functionalized COPLA® Scaffolds for 13 days, with and without M1 stimulation at day 10. **A.** Ultrastructure of M1 stimulated and unstimulated macrophages cultured on empty and CNT functionalized COPLA® Scaffolds. Macrophages interact and adhere to CNT functionalized scaffolds (yellow arrows). **B.** Images showing CNT penetration (green circle) and their internalization by macrophages. Some CNTs were also found inside mitochondrias (blue circle). Red arrows represent CNTs.

To further characterize if the incorporation of CNT in the scaffolds had a detrimental pro-inflammatory effect on macrophage polarization, monocytes were seeded on empty and CNT functionalized COPLA® Scaffolds. Then, macrophages were M1 stimulated at day 10, and at day 13 scaffolds were fixed and stained for specific macrophage markers: M1 marker CCR7 and M2 marker CD163 and analyzed using confocal microscopy.

Figure 23A shows representative confocal images of empty and CNT functionalized COPLA® Scaffolds, with or without M1 activation, showing a very mixed staining for M1 and M2 markers. Cells positive for each marker or for both were counted and are presented as a percentage of the total of stained cells for each condition (Figure 23B). A decrease was observed in the percentage of macrophages stained for just M1 or M2 markers between unstimulated empty and CNT functionalized COPLA® Scaffolds, while the proportion of cells positive for both markers increased (Figure 23B). M1 stimulation resulted in lower percentages of M2 cells for both scaffolds, but while empty COPLA® Scaffold led to increased proportion of cell labelling for both markers, CNT functionalized COPLA® Scaffold led to statistically significant increase of CCR7+ M1 cells. Collectively, these results indicate that CNT functionalized COPLA® Scaffolds may cause an *in vitro* pro-inflammatory macrophage response. It would be important to complement this phenotypic analysis with the cytokine secretion profile of these cells.

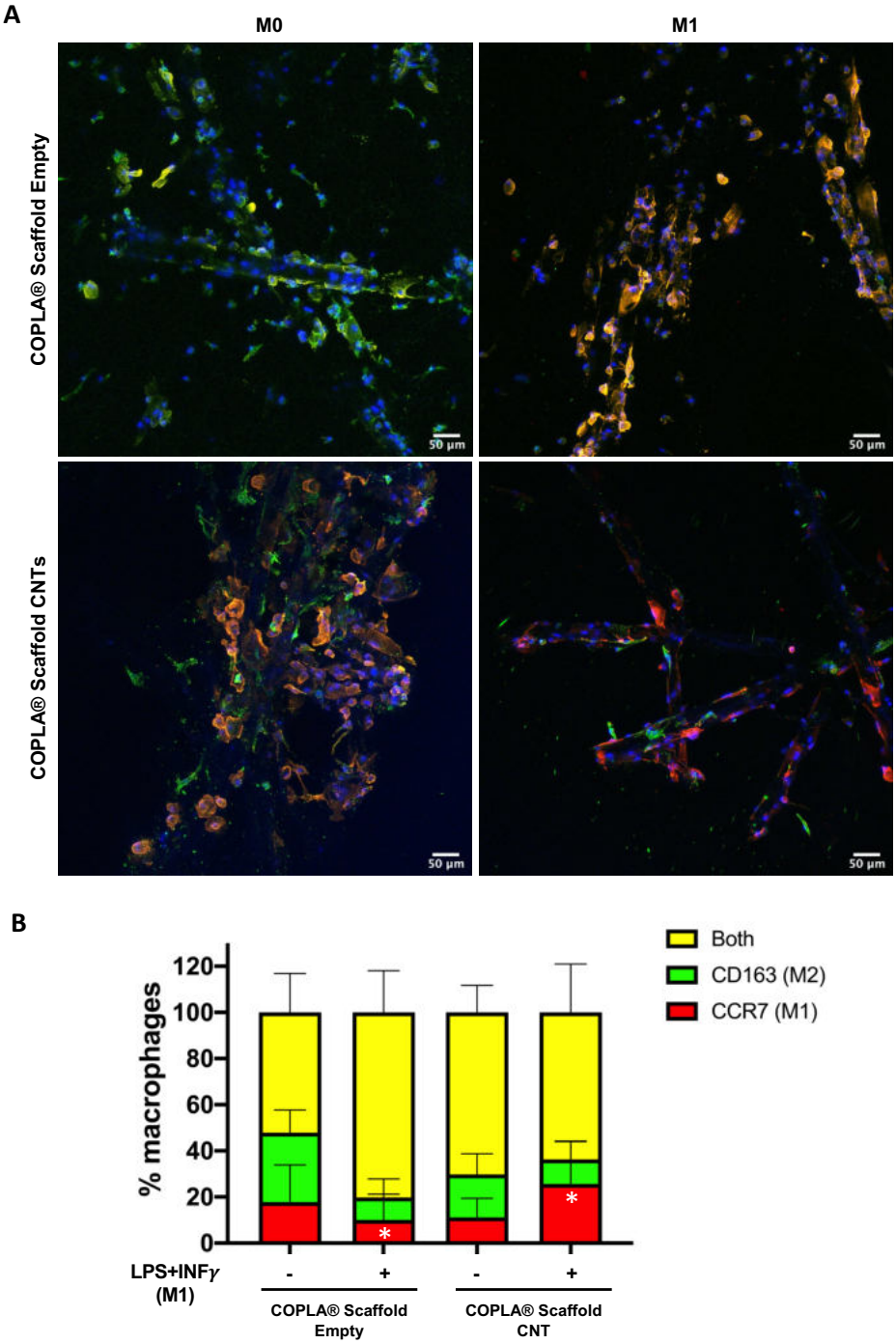

Figure 23. Macrophage polarization after 13 days of culture in empty and CNT functionalized COPLA® Scaffolds with and without M1 stimulation. Macrophages in the scaffolds were fixed and stained for M1 marker CCR7 (red), M2 marker CD163 (green) and nuclei (blue). **A.** Representative confocal microscope images of 5 experiments. **B.** The number of macrophages positive for M1, M2 or both markers were counted for each condition. A total of 5 images per scaffold was considered representative. Significant differences were found between M1 stimulated empty and CNT functionalized COPLA® Scaffolds for M1 macrophage proportion, *p<0.05 (n=5, Friedman test, followed by Uncorrected Dunn's test).

CHAPTER 4. Discussion

In this work, we started by confirming macrophage internalization of PLGA NPs in 2D and then in 3D conditions, after incorporating the NPs in a collagen-PLA scaffold (Col-PLA). Next, we studied the capacity of PLGA-Ibuf NPs incorporated in Col-PLA to revert M1 activated macrophages towards an M2-like phenotype. We also investigated MSCs recruitment capacity of macrophages cultured on these scaffolds. Lastly, we evaluated the inflammatory response of macrophages cultured on CNT functionalized COPLA® Scaffolds.

Throughout this work, primary human macrophages and MSCs were used. Macrophages were differentiated from primary human monocytes, freshly isolated before every experiment. Human monocyte-derived macrophages are a more physiologically relevant model than cell lines, such as human THP-1 or murine J774 and RAW 264.7 since they are not tumorigenic, like most cell lines, and have functional polarization pathways. Additionally, they are relatively easy to isolate and differentiate *in vitro* from human blood and can be obtained from buffy coats, which are waste products from blood donations, thus posing less ethical concerns. The genetic variability underling the use of human donors is at the same time the greatest advantage and disadvantage. While it often complicates results interpretation[126], it is also the most representative of the general human population. On the other hand, cell lines are considered more homogenous and easier to maintain in the laboratory but acquire genetic and phenotypic differences in comparison to primary cells that are related to the transformation or immortalization procedure. Chamberlain et al. demonstrated that activation of three different cell line macrophages with LPS resulted in reduced cytokine expression compared to primary-derived macrophages. Furthermore, the authors also found a limited correlation between primary and immortalized cells in phenotypic activation states with relevance for *in vitro* testing of novel biomaterials and in anti-inflammatory drug activity assays[127]. Thus, in the current study, primary human macrophages were used.

Macrophages have been shown to efficiently internalize NPs by phagocytosis[128]. More importantly, NPs have been successfully used as a carrier to deliverer drugs and cytokines to macrophages, with or without specific molecular targets[96, 129-131].

PLGA NP internalization was analyzed here by a combination of conventional and imaging flow cytometry. Both clearly show a concentration dependent PLGA NPs internalization by human macrophages, which is in line with previous findings. Xiong et al. reported an increase in fluorescent intensity with increasing coumarin-6-loaded PLGA NPs concentration for RAW264.7 (murine monocyte-derived macrophage cell line)[132]. Increasing the NP concentration resulted in an increased uptake by macrophages albeit with decreased uptake efficiency. These results were expected, considering the phagocytic nature of macrophages, whose role in the organism is to eliminate foreign bodies. Previous studies indicate that PLGA NPs enter the cells through adsorptive-

mediated endocytosis (phagocytosis) and that particles are localized in the phagocytic vesicles of macrophages[132, 133].

The effect of incubation time on macrophage uptake of PLGA NPs was also studied. Our results indicate a slight increase in internalization when the incubation time increased from 1h to 3h, albeit without any statistically significant differences. However, for 24h of incubation, we observed a decrease in the percentage of macrophages positive for FITC fluorescence. These results differ from those previously reported by other authors, where a time-dependent cellular uptake was described[132, 134]. On the other hand, cellular uptake rate of PLGA NPs was previously reported to decline gradually with time in RAW 264.7 macrophage cell line[132]. Another study indicates that initial cellular uptake is relatively high in the first 2h and a saturation plateau is reached after about 4-6h[135].

Uptake of PLGA NPs is an dynamic and energy-dependent process and exocytosis of these particles has also been reported[135]. The decrease in the number of cells positive for FITC fluorescence observed after 24h of incubation could be due to particle exocytosis. On the other hand, FITC fluorescent signal is known to be sensitive to pH changes[136]. The acidic and enzymatic environment of the phagocytic vesicles could result in NPs degradation, and consequently lead to a decrease in FITC fluorescence found inside the cells[137]. FITC is less photostable than other fluorescent dyes and fluorescence decay over time is also reported in the literature, which could explain the decrease of fluorescence found inside the cells at 24h[138, 139].

Two different flow cytometry techniques were used to quantify the percentage of macrophages positive for FITC-PLGA NPs internalization. On one hand, imaging flow cytometry (ImageStream^X) is an innovative and more recent technique that allows imaging each analyzed cell. On the other hand, conventional flow cytometry is a widely used cytometry technique, that besides being more common amongst research laboratories, also provides faster sample acquisition.

Contrary to imaging flow cytometry, the conventional technique does not allow to distinguish NPs associated with the cell membrane from truly internalized ones[140]. By performing a cell surface staining for a macrophage lineage marker (CD14) and applying ImageStream^X internalization algorithm, we were able to quantify the macrophages with internalized nanoparticles with higher detection sensitivity for the same conditions. Indeed, after statistical analysis, for the conventional flow cytometry we only observed statistically significant differences between the control and the higher concentration of FITC-PLGA NPs, whereas for the imaging flow cytometry, statistically significant differences were found between control and 30 μg/mL of FITC-PLGA NPs, for 1h and 3h, as well as control and 15 μg/mL for 1h and 3h. Additionally, the images acquired using ImageStream^X allowed a high throughput confirmation of the results. This technique was revealed to be the most effective to detect NPs uptake. Regardless of the technique,

both flow cytometry methods allow an unbiased quantification, that is independent of the operator, since defined gates are applied to all samples, on thousands of cells.

Overall, FITC was shown to be a suitable fluorochrome to label NPs for macrophage internalization. However, FITC stability should be investigated as well as a more throughout assessment of NPs uptake over time including more time-points.

Internalization of FITC-loaded PLGA NPs incorporated in Col-PLA scaffolds by macrophages was also studied. The observed decrease in fluorescence on scaffolds with seeded cells, compared to an unseeded one, may indicate that macrophages are internalizing and metabolizing FITC-loaded PLGA NPs. These results agree with the decrease in fluorescence found after 24h of incubation of the NPs alone. The fluorescence values between scaffolds with monocytes seeded at day 0 and macrophages seeded after differentiation at day 10 are very similar, indicating that the number of NPs internalized was also comparable. This could be due to the slow scaffold degradation, thus exposing small amounts of NPs. Also, monocytes are known to have a lower phagocytic capacity that is enhanced when these cells receive a stimulus for differentiation towards macrophages[141]. For monocyte seeding, we suppose NP phagocytosis rate was relatively slow during the initial period after seeding and increased after macrophage differentiation. In scaffolds that received the already differentiated and mature macrophages with increased phagocytic capacity, NPs uptake rate was higher, thus resulting in comparable fluorescence values after just 72h of incubation.

Internalization was also confirmed using confocal microscopy. We were only able to observe fluorescent NPs inside macrophages that were seeded at day 10 and cultured in Col-PLA scaffolds for 72h. The absence of detectable fluorescence inside macrophages cultured for 13 days once again agrees with previous results, meaning that FITC can lose its fluorescent activity in with the acidic macrophage phagosomes and is not detected after a longer period[142]. Nevertheless, the number of experiments performed was not significative (n=1-2) and further work should be done to assess scaffold fluorescence decrease over culture time, both with and without cells to confirm these results.

The success of tissue repair/ regeneration after biomaterial implantation widely depends on its inflammatory response in the body. An emerging approach is to use immunomodulatory biomaterials to promote immune-mediated tissue repair[143, 144]. In particular, manipulation and modulation of macrophage's immune response to nanoenabled biomaterials is considered a crucial and attractive step towards endogenous regeneration[145].

Our results show that the incorporation of PLGA-Ibuf NPs carrying an anti-inflammatory drug (ibuprofen) entrapped in a collagen-PLA scaffold (Col-PLA) was not as effective as expected in shifting macrophage polarization towards a more anti-inflammatory M2 phenotype. These results differ from those previously described by our group, where a

decrease in cell surface levels of M1 markers CD86 and HLA-DR upon macrophage M1 polarization was observed, after treatment with ibuprofen loaded PLGA NPs, when compared with untreated M1 stimulation and free ibuprofen treatment (unpublished). Furthermore, the levels of secreted PGE2 by macrophages, in response to M1 stimulation, were effectively reduced after incubation with ibuprofen loaded PLGA NPs alone.

The difference found between both studies was that maybe the ibuprofen in the PLGA NPs inside the Col-PLA scaffolds would not be accessible for macrophages. During manufacturing of nanoenabled Col-PLA scaffolds, there is a step that involves crosslinking of the amine and carboxylic acid groups present in the collagen component. However, both PLGA and ibuprofen can have free carboxylic acid groups for the reaction[146, 147]. This means that NPs can be chemically bond to the structure and not just entrapped in the mesh, which may hinder drug release. Additionally, Minardi et al. reported that PLGA microspheres embedded in a highly structured collagen-based scaffold are concealed from macrophages, therefore preventing their detection and extending the delivery of the payload[148].

However, adding the PLGA-Ibuf NPs on top did revert M1 activated macrophages towards an M2-like phenotype. Ma et al. recently reported that PLGA NPs degradation products induce an acidic environment that results in an up-regulation macrophage M1 surface markers and pro-inflammatory cytokines[149]. This pro-inflammatory M1 polarization state was more exacerbated when pH value decreased and authors also showed that the degradation of PLGA NPs in RPMI media significantly reduced the pH value after 3 weeks[149]. Additionally, Caires et al. noticed that macrophages cultured in 3D PLA matrices lowered the pH of culture media, correlated to high levels of metabolic activity and abundant mitochondrial reactive oxygen species production by macrophages interacting with the scaffolds[150]. Moreover, ibuprofen is an acid drug which can further contribute to a decrease in pH values and aggravate M1 macrophage polarization. Thus, it could be worth analyzing the pH of cell culture media from macrophages cultured on nanoenabled Col-PLA scaffolds. Although this effect was not observed in unstimulated scaffolds, M1 macrophage activation might have synergistically contributed to it, hampering the expected anti-inflammatory effect.

Macrophages are highly heterogenous and plastic cells with a great diversity of functional subsets[151]. It has been shown previously that 3D PLA scaffolds lead to a production of cytokines characteristic of both M1 and M2 macrophages[152]. Indeed, their phenotype is very difficult to define and an oversimplistic M1 or M2 classification remains controversial. The high percentage of macrophages expressing both M1 and M2 markers in our results confirms this finding.

As evidence accumulates, the M1/M2 dichotomy is being further expanded to include more subcategories such as M2a, M2b and M2c[153, 154]. Additionally, macrophage

phenotype is been recognized as a dynamic and not static process[155]. As a result, their phenotype is very hard to accurately define and comprehensively characterize. Common assays used to study macrophages, such as the ones used in this work, only capture a snapshot at the moment of sampling or end-point, which does not reflect the constant adaptation to the changing environment and phenotype plasticity[155].

Therefore, multiple aspects need to be described to capture the full picture of macrophage polarization and we suggest a taking closer look at the macrophage-biomaterial interaction and resulting changes in macrophage phenotype. It is also widely recognized that a desired promotion of macrophage phenotype also depends on material composition and scaffold physical properties, such as porosity, stiffness and hydrophobicity that have not been explored in this work[145].

The role of joint-resident MSCs in the repair of damage associated with OA remains poorly understood but research suggests that synovium-derived MSCs might be the primary drivers of cartilage repair in adults[156]. Moreover, it has been reported that anti-inflammatory M2 macrophages enhance the chondrogenic capacity of human BM-derived MSCs[157]. Therefore, we investigated the capacity of macrophages cultured on nanoenabled Col-PLA scaffolds to recruit MSCs.

Our results indicate that macrophages cultured on all Col-PLA scaffolds increased the invasion capacity of MSCs. Simulation the joint inflammatory environment with macrophage M1 activation led to a trend for increased recruitment of MSCs. Pro-inflammatory cytokines secreted by macrophages during the early inflammatory phase are well known to promote MSC migration and activation their immunoregulatory properties[158, 159]. Vallés et al. described a higher migratory activity of MSCs treated with conditioned media of pro-inflammatory stimulated macrophages, compared to non-activated ones, which supports the involvement of cytokines in MSC recruitment[160]. Upon biomaterial interaction, macrophages can produce several pro-inflammatory cytokines and chemokines that are known to exacerbate the expression of CCR2, CCR3 and CCR4 receptors on MSCs[161, 162]. This could be the basis for monocyte-derived macrophages to recruit MSC upon interaction with 3D biomaterials[150].

Moreover, macrophages are known to be potent inducers of MSC recruitment mainly through chemokine RANTES production[117, 163]. Besides impacting MSC chemotaxis, RANTES also influences other key functions linked with their regenerative potential. Indeed, it has been shown that the immunosuppressive ability of MSCs relies of STAT-1 signaling, which is specifically activated by RANTES[162, 164]. Therefore, future work should investigate the presence of this chemokine.

The second part of this work consisted in evaluating the inflammatory response of macrophages cultured on CNT functionalized COPLA® Scaffolds. Several studies report the successful combination of CNTs with scaffolds, using different materials that include

collagen, chitosan, gelatin, and hyaluronic acid for tissue engineering applications[165-170]. TEM images clearly showed the homogenous presence of CNTs in COPLA® Scaffold.

A major concern for the use of CNTs is their safety. The behavior of CNT functionalized biomaterials, especially their immune response is not clearly understood and a careful assessment of their immunotoxicity is still needed. Our results showed that macrophages were able to populate CNT functionalized COPLA® Scaffolds without any visible cytotoxicity or abnormal morphology, as suggested in the literature for other cellular types. Zadehnajar et al. showed that 1% MWCNTs PCL-gelatin scaffolds had no cytotoxicity or caused any adverse effect on chondrocytes viability[104]. Hirata et al. reported that osteoblast-like cells adhered and increased proliferation on MWCNT-coated collagen scaffold than on a non-coated one[171]. In line with these findings, it has been reported that *in vivo* implantation of MWCNT-coated collagen scaffolds did not elicit any severe inflammatory response, but foreign body giant cells were observed around uncoated and MWCNT-coated collagen scaffolds. More importantly, some MWCNTs seemed to be engulfed by macrophages[172].

Indeed, cells cultured in CNT-containing medium are estimated to uptake CNTs[173, 174]. Here, we observed macrophage uptake of CNTs when cultured on a CNT functionalized COPLA® Scaffold. In line with previous studies, CNTs penetrated the plasma membrane and were observed in the cytoplasm. Direct penetration is suggested to be one of the routes to deliver CNTs into the cytoplasm[174]. Hirata et al. reported that after 3 days of culture in MWCNT-coated scaffolds, MWCNTs were clearly observed inside the cells, after penetrating the plasma membrane. After 7 days, MWCNTs were also observed in the cytoplasm, and some were in the nuclei[175]. Mu et al. reported that bundled CNTs tend to enter the cells through endocytosis and can be found inside intra-cellular endosomes and lysosomes[174]. They can then penetrate the endosomal membrane and escape into the cytoplasm, providing another route for CNTs to enter the cytoplasm.

Most importantly, we also found CNTs inside the mitochondria. The absence of the characteristic mitochondrial internal cristae is indicative of organelle stress. Others have observed the presence of CNTs in the mitochondria of macrophages[176, 177]. These organelles are relatively sensitive in response to stress induced by external agents. Chen et al. reported that CNTs lead to mitochondrial injury in RAW 264.7 cells, which could be a possible pathway of apoptotic cell induction[178]. Their results indicated that CNTs produced a dose-dependent cytotoxicity and mitochondria damage that included a decrease of mitochondrial membrane potential and release of cytochrome c. Mitochondria metabolic activities were also inhibited[178]. A systematic TEM analysis of our results still needs to be done to further elucidate possible oxidative stress and metabolic changes caused by CNT functionalized scaffolds in macrophages.

Macrophages cultured on CNT functionalized scaffolds revealed higher proportion of cells expressing both M1 and M2 markers, compared to empty COPLA® Scaffold. It has

been previously reported by Meng and colleagues that incubation of RAW264.7 cells with MWCNTs activates macrophages towards a M1/M2 mixed status. Moreover, higher concentrations of MWCNTs promoted macrophages recruitment trough the release of macrophage inflammation protein 1-α (MIP-1 α) and MIP-2[179]. On the other hand, it was recently showed that CNT-coated polymer nanofibers resulted in accelerated adhesion and osteogenic differentiation of MSCs[180]. Therefore, in future studies, we suggest evaluating the MSCs recruitment capacity of macrophages cultured on CNT functionalized COPLA® Scaffolds.

The cytotoxicity of nanoenabled Col-PLA and COPLA® Scaffolds was quantified using a commercial LDH release kit. LDH is a soluble cytoplasmatic enzyme present in almost every cell type that is released into the extracellular space when plasma membrane is damaged[181]. LDH release is a standard colorimetric cytotoxicity assay that is quantified spectrophotometrically and is considered a well-established and reliable indicator of cellular toxicity. However, there was an interference between the assay and our materials and so we did not include the results in this dissertation. Several studies report aberrant values of measured LDH levels in the media caused by certain engineered nanomaterials, resulting in inaccurate toxicity assessments. These include SWCNTs, carbon nanohorns and different types of NPs[182-184], such as PLGA-polyethylene oxide NPs[185]. It is reported that the intrinsic absorbance of CNT and the adsorption of LDH at the surface of CNTs result in the presence of artifacts in LDH readings[186]. This type of cellular tests, usually based on colorimetric measurements may not be suitable for all the materials since their physicochemical properties interfere with the assays and bias the results.

CHAPTER 5. Conclusions and Future Prospects

In this work, we started by demonstrating PLGA NPs internalization by primary human macrophages under 2D culture conditions. Macrophages readily internalized FITC-loaded NPs and our results revealed a concentration-dependent increase of FITC fluorescence intensity inside the cells. Complementing these results, FITC-loaded PLGA NPs internalization by primary human macrophages was also confirmed in 3D conditions, when these NPs were incorporated in Col-PLA scaffolds.

Previous work by our group showed that ibuprofen loaded PLGA NPs alone were effective promoters of M1 to M2 macrophage shift. Combining these findings and our internalization results, we hypothesized that Col-PLA scaffolds nanoenabled with PLGA-Ibuf NPs would have a positive anti-inflammatory and immunomodulatory effect. However, our results indicate that these nanoenabled scaffolds were not effective in promoting an anti-inflammatory macrophage phenotype or reducing the macrophage inflammatory response. M1 macrophage stimulation resulted in an increase of PGE2 levels and pro-inflammatory cytokine IL-1β. Col-PLA scaffolds alone or nanoenabled with empty or ibuprofen-loaded PLGA NPs failed to modulate macrophage inflammatory phenotype, for monocyte seeding at day 0 or after macrophage differentiation, at day 10. Having the loaded PLGA NPs added on top of the scaffolds, instead of entrapped in the biomaterial mesh resulted in partial reduction of PGE2 levels, but not of IL-1b or the M1 marker CCR7, while scaffolds with free ibuprofen on top promoted a less M1 pro-inflammatory profile.

These results would benefit from further experiments to clearly demonstrate the influence of nanoenabled scaffolds, particularly due to the great variability among donors. This variability was greater in the macrophage polarization assessment and when cells were previously differentiated in Petri dishes and then re-cultured. Also, a more throughout analysis of pro- and anti-inflammatory cytokines released by macrophages would complete the profiling results. Lastly, future work should include testing a different NP system/entrapping methodology to improve macrophage access to ibuprofen. It would also be interesting to compare with a different anti-inflammatory drug, such as diclofenac.

Herein, we also investigated the capacity of macrophages cultured on nanoenabled Col-PLA scaffolds to recruit MSCs. Invasion capacity of MSCs was greater when macrophages received a pro-inflammatory stimulus (M1 activation). The scaffolds alone also seem to recruit MSCs to a certain extent, however more experiments should be done for confirmation. It would also be interesting to compare the influence of macrophages alone *versus* seeded on Col-PLA scaffolds. Since MSCs are known to have an immunomodulatory capacity over macrophages, this effect on M1/M2 polarization should also be investigated for macrophages within Col-PLA after their cross talk. Additionally, studies to detect the expression and activity of MMPs involved in MSCs invasion should be performed by gelatin zymography, as well as a careful screening of

the soluble mediators involved in the crosstalk, both in the top and bottom compartment of the transwell assays.

Lastly, we investigated the effects of CNT functionalized COPLA® Scaffolds on macrophage morphology and phenotype after 13 days of culture. Confocal microscope images show that macrophages populate the scaffolds and appear normal morphologically. We observed the presence of CNTs inside macrophages using TEM and we also found some evidence of mitochondrial stress induced by the carbon materials. A more systematic analysis of the macrophage ultrastructure is ongoing to confirm these findings and further investigate the possible inflammatory effect of CNTs. Since CNTs seem to interfere with LDH readings of commercially available kits as well as other ELISA based assays, future work should evaluate cytotoxicity using alternative quantitative methods such as a live-dead assay. The release of pro-inflammatory mediators should also be assessed. Furthermore, the effect of the magnetic stimulation of these stimuli responsive materials should also be investigated regarding macrophage polarization.

During this work, the first steps were taken towards the development of a nanoenabled scaffold for cartilage repair. NPs loaded with an anti-inflammatory drug were used to investigate the ability to modulate macrophage phenotype, and CNT were used to obtain a stimuli-responsive material. Although several aspects remain to be optimized and further developed, this work shows the ability of macrophages to colonize the scaffolds over time and highlights the need to ensure that scaffold functionalization allows for availability of NPs and their encapsulated drugs.

CHAPTER 6. References

1. Firestein, G.S., Kelley, W.N., Budd, R.C., McInnes, I.B. & O'Dell, J.R. Kelley's Textbook of Rheumatology. (Elsevier/Saunders, 2012).
2. Wieland, H.A., Michaelis, M., Kirschbaum, B.J. & Rudolphi, K.A. Osteoarthritis - an untreatable disease? *Nat Rev Drug Discov* **4**, 331-344 (2005).
3. Martel-Pelletier, J. et al. Osteoarthritis. *Nat Rev Dis Primers* **2**, 16072 (2016).
4. Kou, L. et al. Biomaterial-engineered intra-articular drug delivery systems for osteoarthritis therapy. *Drug Deliv* **26**, 870-885 (2019).
5. Pap, T. & Korb-Pap, A. Cartilage damage in osteoarthritis and rheumatoid arthritis-two unequal siblings. *Nat Rev Rheumatol* **11**, 606-615 (2015).
6. Zhang, L., Hu, J. & Athanasiou, K.A. The role of tissue engineering in articular cartilage repair and regeneration. *Crit Rev Biomed Eng* **37**, 1-57 (2009).
7. Bedi, A., Feeley, B.T. & Williams, R.J., 3rd Management of articular cartilage defects of the knee. *J Bone Joint Surg Am* **92**, 994-1009 (2010).
8. Johnstone, B. et al. Tissue engineering for articular cartilage repair--the state of the art. *Eur Cell Mater* **25**, 248-267 (2013).
9. Falah, M., Nierenberg, G., Soudry, M., Hayden, M. & Volpin, G. Treatment of articular cartilage lesions of the knee. *Int Orthop* **34**, 621-630 (2010).
10. Hunter, D.J., Schofield, D. & Callander, E. The individual and socioeconomic impact of osteoarthritis. *Nat Rev Rheumatol* **10**, 437-441 (2014).
11. Vos, T. et al. Years lived with disability (YLDs) for 1160 sequelae of 289 diseases and injuries 1990-2010: a systematic analysis for the Global Burden of Disease Study 2010. *Lancet* **380**, 2163-2196 (2012).
12. United Nations - Department of Economic and Social Affairs Word Population Prospects 2019: Highlights. (2019).
13. Thomas, E., Peat, G. & Croft, P. Defining and mapping the person with osteoarthritis for population studies and public health. *Rheumatology (Oxford)* **53**, 338-345 (2014).
14. Slattery, C. & Kweon, C.Y. Classifications in Brief: Outerbridge Classification of Chondral Lesions. *Clin Orthop Relat Res* **476**, 2101-2104 (2018).
15. Madry, H., Ochi, M., Cucchiarini, M., Pape, D. & Seil, R. Large animal models in experimental knee sports surgery: focus on clinical translation. *J Exp Orthop* **2**, 9 (2015).
16. van den Bosch, M.H.J. Osteoarthritis year in review 2020: biology. *Osteoarthritis Cartilage* **29**, 143-150 (2021).
17. Hunter, D.J. & Bierma-Zeinstra, S. Osteoarthritis. *Lancet* **393**, 1745-1759 (2019).
18. Sharma, L. Osteoarthritis of the Knee. *N Engl J Med* **384**, 51-59 (2021).
19. Nagase, H. & Kashiwagi, M. Aggrecanases and cartilage matrix degradation. *Arthritis Res Ther* **5**, 94-103 (2003).
20. Burrage, P.S., Mix, K.S. & Brinckerhoff, C.E. Matrix metalloproteinases: role in arthritis. *Front Biosci* **11**, 529-543 (2006).
21. Marcu, K.B., Otero, M., Olivotto, E., Borzi, R.M. & Goldring, M.B. NF-kB signaling: multiple angles to target OA. *Curr Drug Targets* **11**, 599-613 (2010).
22. Goldring, M.B. et al. Roles of inflammatory and anabolic cytokines in cartilage metabolism: signals and multiple effectors converge upon MMP-13 regulation in osteoarthritis. *Eur Cell Mater* **21**, 202-220 (2011).

23. Loeser, R.F. Aging and osteoarthritis: the role of chondrocyte senescence and aging changes in the cartilage matrix. *Osteoarthritis Cartilage* **17**, 971-979 (2009).
24. Bondeson, J. et al. The role of synovial macrophages and macrophage-produced mediators in driving inflammatory and destructive responses in osteoarthritis. *Arthritis Rheum* **62**, 647-657 (2010).
25. Fahy, N. et al. Human osteoarthritic synovium impacts chondrogenic differentiation of mesenchymal stem cells via macrophage polarisation state. *Osteoarthritis Cartilage* **22**, 1167-1175 (2014).
26. O'Brien, K. et al. Enumeration and Localization of Mesenchymal Progenitor Cells and Macrophages in Synovium from Normal Individuals and Patients with Pre-Osteoarthritis or Clinically Diagnosed Osteoarthritis. *Int J Mol Sci* **18** (2017).
27. Scanzello, C.R. & Goldring, S.R. The role of synovitis in osteoarthritis pathogenesis. *Bone* **51**, 249-257 (2012).
28. Locati, M., Curtale, G. & Mantovani, A. Diversity, Mechanisms, and Significance of Macrophage Plasticity. *Annu Rev Pathol* **15**, 123-147 (2020).
29. Molgora, M. et al. The yin-yang of the interaction between myelomonocytic cells and NK cells. *Scand J Immunol* **88**, e12705 (2018).
30. Wu, C.L., Harasymowicz, N.S., Klimak, M.A., Collins, K.H. & Guilak, F. The role of macrophages in osteoarthritis and cartilage repair. *Osteoarthritis Cartilage* **28**, 544-554 (2020).
31. Ummarino, A., Gambaro, F.M., Kon, E. & Torres Andon, F. Therapeutic Manipulation of Macrophages Using Nanotechnological Approaches for the Treatment of Osteoarthritis. *Nanomaterials (Basel)* **10** (2020).
32. Zhu, X. et al. Phenotypic alteration of macrophages during osteoarthritis: a systematic review. *Arthritis Res Ther* **23**, 110 (2021).
33. Culemann, S. et al. Locally renewing resident synovial macrophages provide a protective barrier for the joint. *Nature* **572**, 670-675 (2019).
34. Wenham, C.Y. & Conaghan, P.G. The role of synovitis in osteoarthritis. *Ther Adv Musculoskelet Dis* **2**, 349-359 (2010).
35. Watanabe, S., Alexander, M., Misharin, A.V. & Budinger, G.R.S. The role of macrophages in the resolution of inflammation. *J Clin Invest* **129**, 2619-2628 (2019).
36. Yona, S. et al. Fate mapping reveals origins and dynamics of monocytes and tissue macrophages under homeostasis. *Immunity* **38**, 79-91 (2013).
37. Dreier, R., Wallace, S., Fuchs, S., Bruckner, P. & Grassel, S. Paracrine interactions of chondrocytes and macrophages in cartilage degradation: articular chondrocytes provide factors that activate macrophage-derived pro-gelatinase B (pro-MMP-9). *J Cell Sci* **114**, 3813-3822 (2001).
38. Fernandes, T.L. et al. Macrophage: A Potential Target on Cartilage Regeneration. *Front Immunol* **11**, 111 (2020).
39. Harding, C.V. & Geuze, H.J. Class II MHC molecules are present in macrophage lysosomes and phagolysosomes that function in the phagocytic processing of Listeria monocytogenes for presentation to T cells. *J Cell Biol* **119**, 531-542 (1992).

40. Kanno, S. et al. Scavenger receptor MARCO contributes to cellular internalization of exosomes by dynamin-dependent endocytosis and macropinocytosis. *Sci Rep* **10**, 21795 (2020).
41. Stanley, E.R. & Chitu, V. CSF-1 receptor signaling in myeloid cells. *Cold Spring Harb Perspect Biol* **6** (2014).
42. Kapoor, M., Martel-Pelletier, J., Lajeunesse, D., Pelletier, J.P. & Fahmi, H. Role of proinflammatory cytokines in the pathophysiology of osteoarthritis. *Nat Rev Rheumatol* **7**, 33-42 (2011).
43. Zhang, H. et al. Synovial macrophage M1 polarisation exacerbates experimental osteoarthritis partially through R-spondin-2. *Ann Rheum Dis* **77**, 1524-1534 (2018).
44. Griffin, T.M. & Scanzello, C.R. Innate inflammation and synovial macrophages in osteoarthritis pathophysiology. *Clin Exp Rheumatol* **37 Suppl 120**, 57-63 (2019).
45. Murray, P.J. Macrophage Polarization. *Annu Rev Physiol* **79**, 541-566 (2017).
46. Tarique, A.A. et al. Phenotypic, functional, and plasticity features of classical and alternatively activated human macrophages. *Am J Respir Cell Mol Biol* **53**, 676-688 (2015).
47. Krausgruber, T. et al. IRF5 promotes inflammatory macrophage polarization and TH1-TH17 responses. *Nat Immunol* **12**, 231-238 (2011).
48. Cook, A.D., Braine, E.L. & Hamilton, J.A. The phenotype of inflammatory macrophages is stimulus dependent: implications for the nature of the inflammatory response. *J Immunol* **171**, 4816-4823 (2003).
49. Huang, X., Li, Y., Fu, M. & Xin, H.B. Polarizing Macrophages In Vitro. *Methods Mol Biol* **1784**, 119-126 (2018).
50. Platanitis, E. & Decker, T. Regulatory Networks Involving STATs, IRFs, and NFkappaB in Inflammation. *Front Immunol* **9**, 2542 (2018).
51. Manferdini, C. et al. Adipose stromal cells mediated switching of the pro-inflammatory profile of M1-like macrophages is facilitated by PGE2: in vitro evaluation. *Osteoarthritis Cartilage* **25**, 1161-1171 (2017).
52. Alvarez, M.M. et al. Delivery strategies to control inflammatory response: Modulating M1-M2 polarization in tissue engineering applications. *J Control Release* **240**, 349-363 (2016).
53. Haltmayer, E. et al. Co-culture of osteochondral explants and synovial membrane as in vitro model for osteoarthritis. *PLoS One* **14**, e0214709 (2019).
54. Manferdini, C. et al. From osteoarthritic synovium to synovial-derived cells characterization: synovial macrophages are key effector cells. *Arthritis Res Ther* **18**, 83 (2016).
55. Dai, M., Sui, B., Xue, Y., Liu, X. & Sun, J. Cartilage repair in degenerative osteoarthritis mediated by squid type II collagen via immunomodulating activation of M2 macrophages, inhibiting apoptosis and hypertrophy of chondrocytes. *Biomaterials* **180**, 91-103 (2018).
56. Mahon, O.R., Kelly, D.J., McCarthy, G.M. & Dunne, A. Osteoarthritis-associated basic calcium phosphate crystals alter immune cell metabolism and promote M1 macrophage polarization. *Osteoarthritis Cartilage* **28**, 603-612 (2020).
57. Liu, B., Zhang, M., Zhao, J., Zheng, M. & Yang, H. Imbalance of M1/M2 macrophages is linked to severity level of knee osteoarthritis. *Exp Ther Med* **16**, 5009-5014 (2018).

58. Ji, X. et al. Cartilage repair mediated by thermosensitive photocrosslinkable TGFbeta1-loaded GM-HPCH via immunomodulating macrophages, recruiting MSCs and promoting chondrogenesis. *Theranostics* **10**, 2872-2887 (2020).
59. Pittenger, M.F. et al. Multilineage potential of adult human mesenchymal stem cells. *Science* **284**, 143-147 (1999).
60. De Bari, C. et al. Skeletal muscle repair by adult human mesenchymal stem cells from synovial membrane. *J Cell Biol* **160**, 909-918 (2003).
61. Harrell, C.R., Markovic, B.S., Fellabaum, C., Arsenijevic, A. & Volarevic, V. Mesenchymal stem cell-based therapy of osteoarthritis: Current knowledge and future perspectives. *Biomed Pharmacother* **109**, 2318-2326 (2019).
62. Dominici, M. et al. Minimal criteria for defining multipotent mesenchymal stromal cells. The International Society for Cellular Therapy position statement. *Cytotherapy* **8**, 315-317 (2006).
63. Waterman, R.S., Tomchuck, S.L., Henkle, S.L. & Betancourt, A.M. A new mesenchymal stem cell (MSC) paradigm: polarization into a pro-inflammatory MSC1 or an Immunosuppressive MSC2 phenotype. *PLoS One* **5**, e10088 (2010).
64. Nair, A. et al. Biomaterial implants mediate autologous stem cell recruitment in mice. *Acta Biomater* **7**, 3887-3895 (2011).
65. Fibbe, W.E., Nauta, A.J. & Roelofs, H. Modulation of immune responses by mesenchymal stem cells. *Ann N Y Acad Sci* **1106**, 272-278 (2007).
66. Choi, H., Lee, R.H., Bazhanov, N., Oh, J.Y. & Prockop, D.J. Anti-inflammatory protein TSG-6 secreted by activated MSCs attenuates zymosan-induced mouse peritonitis by decreasing TLR2/NF-kappaB signaling in resident macrophages. *Blood* **118**, 330-338 (2011).
67. Heldens, G.T. et al. Catabolic factors and osteoarthritis-conditioned medium inhibit chondrogenesis of human mesenchymal stem cells. *Tissue Eng Part A* **18**, 45-54 (2012).
68. Kruger, J.P. et al. Chondrogenic differentiation of human subchondral progenitor cells is affected by synovial fluid from donors with osteoarthritis or rheumatoid arthritis. *J Orthop Surg Res* **7**, 10 (2012).
69. Machado, G.C. et al. Efficacy and safety of paracetamol for spinal pain and osteoarthritis: systematic review and meta-analysis of randomised placebo controlled trials. *BMJ* **350**, h1225 (2015).
70. da Costa, B.R. et al. Effectiveness of non-steroidal anti-inflammatory drugs for the treatment of pain in knee and hip osteoarthritis: a network meta-analysis. *The Lancet* **390**, e21-e33 (2017).
71. Wainwright, C., Theis, J.C., Garneti, N. & Melloh, M. Age at hip or knee joint replacement surgery predicts likelihood of revision surgery. *J Bone Joint Surg Br* **93**, 1411-1415 (2011).
72. Sutton, P.M. & Holloway, E.S. The young osteoarthritic knee: dilemmas in management. *BMC Med* **11**, 14 (2013).
73. Kwon, H. et al. Surgical and tissue engineering strategies for articular cartilage and meniscus repair. *Nat Rev Rheumatol* **15**, 550-570 (2019).
74. Totlis, T. et al. Arthroscopic debridement for focal articular cartilage lesions of the knee: A systematic review. *Surgeon* (2021).

75. Kreuz, P.C. et al. Results after microfracture of full-thickness chondral defects in different compartments in the knee. *Osteoarthritis Cartilage* **14**, 1119-1125 (2006).
76. Goyal, D., Keyhani, S., Lee, E.H. & Hui, J.H. Evidence-based status of microfracture technique: a systematic review of level I and II studies. *Arthroscopy* **29**, 1579-1588 (2013).
77. Makris, E.A., Gomoll, A.H., Malizos, K.N., Hu, J.C. & Athanasiou, K.A. Repair and tissue engineering techniques for articular cartilage. *Nat Rev Rheumatol* **11**, 21-34 (2015).
78. Bernhard, J.C. & Vunjak-Novakovic, G. Should we use cells, biomaterials, or tissue engineering for cartilage regeneration? *Stem Cell Res Ther* **7**, 56 (2016).
79. Wasyleczko, M., Sikorska, W. & Chwojnowski, A. Review of Synthetic and Hybrid Scaffolds in Cartilage Tissue Engineering. *Membranes (Basel)* **10** (2020).
80. Cucchiarini, M. et al. A vision on the future of articular cartilage repair. *Eur Cell Mater* **27**, 12-16 (2014).
81. Muir, H. The chondrocyte, architect of cartilage. Biomechanics, structure, function and molecular biology of cartilage matrix macromolecules. *Bioessays* **17**, 1039-1048 (1995).
82. Pascual-Garrido, C. et al. Current and novel injectable hydrogels to treat focal chondral lesions: Properties and applicability. *J Orthop Res* **36**, 64-75 (2018).
83. Hu, G. et al. Nanoparticles Targeting Macrophages as Potential Clinical Therapeutic Agents Against Cancer and Inflammation. *Front Immunol* **10**, 1998 (2019).
84. Liu, P. et al. Intra-articular injection of etoricoxib-loaded PLGA-PEG-PLGA triblock copolymeric nanoparticles attenuates osteoarthritis progression. *Am J Transl Res* **11**, 6775-6789 (2019).
85. Martins, C., Sousa, F., Araujo, F. & Sarmento, B. Functionalizing PLGA and PLGA Derivatives for Drug Delivery and Tissue Regeneration Applications. *Adv Healthc Mater* **7** (2018).
86. Makadia, H.K. & Siegel, S.J. Poly Lactic-co-Glycolic Acid (PLGA) as Biodegradable Controlled Drug Delivery Carrier. *Polymers (Basel)* **3**, 1377-1397 (2011).
87. Niazvand, F. et al. Curcumin-loaded poly lactic-co-glycolic acid nanoparticles effects on mono-iodoacetate -induced osteoarthritis in rats. *Vet Res Forum* **8**, 155-161 (2017).
88. Frohlich, E. The role of surface charge in cellular uptake and cytotoxicity of medical nanoparticles. *Int J Nanomedicine* **7**, 5577-5591 (2012).
89. Sadtler, K. et al. Design, clinical translation and immunological response of biomaterials in regenerative medicine. *Nature Reviews Materials* **1** (2016).
90. Fahy, N., Farrell, E., Ritter, T., Ryan, A.E. & Murphy, J.M. Immune modulation to improve tissue engineering outcomes for cartilage repair in the osteoarthritic joint. *Tissue Eng Part B Rev* **21**, 55-66 (2015).
91. Franz, S., Rammelt, S., Scharnweber, D. & Simon, J.C. Immune responses to implants - a review of the implications for the design of immunomodulatory biomaterials. *Biomaterials* **32**, 6692-6709 (2011).
92. Dougados, M. Why and how to use NSAIDs in osteoarthritis. *J Cardiovasc Pharmacol* **47 Suppl 1**, S49-54 (2006).

93. Adatia, A., Rainsford, K.D. & Kean, W.F. Osteoarthritis of the knee and hip. Part II: therapy with ibuprofen and a review of clinical trials. *J Pharm Pharmacol* **64**, 626-636 (2012).
94. Schjerning, A.M., McGettigan, P. & Gislason, G. Cardiovascular effects and safety of (non-aspirin) NSAIDs. *Nat Rev Cardiol* **17**, 574-584 (2020).
95. Mazaleuskaya, L.L. et al. PharmGKB summary: ibuprofen pathways. *Pharmacogenet Genomics* **25**, 96-106 (2015).
96. Goncalves, R.M., Pereira, A.C., Pereira, I.O., Oliveira, M.J. & Barbosa, M.A. Macrophage response to chitosan/poly-(gamma-glutamic acid) nanoparticles carrying an anti-inflammatory drug. *J Mater Sci Mater Med* **26**, 167 (2015).
97. Richards, M.M., Maxwell, J.S., Weng, L., Angelos, M.G. & Golzarian, J. Intra-articular treatment of knee osteoarthritis: from anti-inflammatories to products of regenerative medicine. *Phys Sportsmed* **44**, 101-108 (2016).
98. Cardea, S., Baldino, L., Scognamiglio, M. & Reverchon, E. 3D PLLA/ibuprofen composite scaffolds obtained by a supercritical fluids assisted process. *J Mater Sci Mater Med* **25**, 989-998 (2014).
99. Yuan, Z. et al. Ibuprofen-loaded electrospun fibrous scaffold doped with sodium bicarbonate for responsively inhibiting inflammation and promoting muscle wound healing in vivo. *Biomater Sci* **2**, 502-511 (2014).
100. Riggin, C.N. et al. Electrospun PLGA Nanofiber Scaffolds Release Ibuprofen Faster and Degrade Slower After In Vivo Implantation. *Ann Biomed Eng* **45**, 2348-2359 (2017).
101. Kumar, P., Dehiya, B.S. & Sindhu, A. Ibuprofen-Loaded CTS/nHA/nBG Scaffolds for the Applications of Hard Tissue Engineering. *Iran Biomed J* **23**, 190-199 (2019).
102. Amiryaghoubi, N. et al. Recent advances in polymeric scaffolds containing carbon nanotube and graphene oxide for cartilage and bone regeneration. *Materials Today Communications* **26** (2021).
103. Eatemadi, A. et al. Carbon nanotubes: properties, synthesis, purification, and medical applications. *Nanoscale Res Lett* **9**, 393 (2014).
104. Zadehnajar, P., Akbari, B., Karbasi, S. & Mirmusavi, M.H. Preparation and characterization of poly ε-caprolactone-gelatin/multi-walled carbon nanotubes electrospun scaffolds for cartilage tissue engineering applications. *International Journal of Polymeric Materials and Polymeric Biomaterials* **69**, 326-337 (2019).
105. Li, Y. & Cao, J. The impact of multi-walled carbon nanotubes (MWCNTs) on macrophages: contribution of MWCNT characteristics. *Sci China Life Sci* **61**, 1333-1351 (2018).
106. Zhu, Y. et al. Designed composites for mimicking compressive mechanical properties of articular cartilage matrix. *J Mech Behav Biomed Mater* **36**, 32-46 (2014).
107. Iwasa, J., Engebretsen, L., Shima, Y. & Ochi, M. Clinical application of scaffolds for cartilage tissue engineering. *Knee Surg Sports Traumatol Arthrosc* **17**, 561-577 (2009).
108. Rutgers, M. et al. Effect of collagen type I or type II on chondrogenesis by cultured human articular chondrocytes. *Tissue Eng Part A* **19**, 59-65 (2013).
109. Shen, Y. et al. Biomaterial and mesenchymal stem cell for articular cartilage reconstruction. *Curr Stem Cell Res Ther* **9**, 254-267 (2014).

110. Vinatier, C. et al. Cartilage tissue engineering: towards a biomaterial-assisted mesenchymal stem cell therapy. *Curr Stem Cell Res Ther* **4**, 318-329 (2009).
111. Haaparanta, A.M. et al. Preparation and characterization of collagen/PLA, chitosan/PLA, and collagen/chitosan/PLA hybrid scaffolds for cartilage tissue engineering. *J Mater Sci Mater Med* **25**, 1129-1136 (2014).
112. Askel Healthcare (2020).
113. Rajam, A.M., Jithendral, P., Mandal, A.B. & Rose, C. Evaluation of in vitro macrophage response and in vivo host response to growth factors incorporated chitosan nanoparticle impregnated collagen-chitosan scaffold. *J Biomed Nanotechnol* **10**, 508-518 (2014).
114. Oliveira, M.I. et al. Adsorbed Fibrinogen stimulates TLR-4 on monocytes and induces BMP-2 expression. *Acta Biomater* **49**, 296-305 (2017).
115. Bessa-Goncalves, M. et al. Fibrinogen and magnesium combination biomaterials modulate macrophage phenotype, NF-kB signaling and crosstalk with mesenchymal stem/stromal cells. *Acta Biomater* **114**, 471-484 (2020).
116. StemCell Technologies (2011).
117. Almeida, C.R., Vasconcelos, D.P., Goncalves, R.M. & Barbosa, M.A. Enhanced mesenchymal stromal cell recruitment via natural killer cells by incorporation of inflammatory signals in biomaterials. *J R Soc Interface* **9**, 261-271 (2012).
118. Barbosa, J.P. et al. Nanostructured lipid carriers loaded with resveratrol modulate human dendritic cells. *Int J Nanomedicine* **11**, 3501-3516 (2016).
119. Song, G., Petschauer, J.S., Madden, A.J. & Zamboni, W.C. Nanoparticles and the mononuclear phagocyte system: pharmacokinetics and applications for inflammatory diseases. *Curr Rheumatol Rev* **10**, 22-34 (2014).
120. Barrios-Rodiles, M. & Chadee, K. Novel regulation of cyclooxygenase-2 expression and prostaglandin E2 production by IFN-gamma in human macrophages. *J Immunol* **161**, 2441-2448 (1998).
121. Kato, M., Nishida, S., Kitasato, H., Sakata, N. & Kawai, S. Cyclooxygenase-1 and cyclooxygenase-2 selectivity of non-steroidal anti-inflammatory drugs: investigation using human peripheral monocytes. *J Pharm Pharmacol* **53**, 1679-1685 (2001).
122. Nakatsugi, S., Sugimoto, N. & Furukawa, M. Effects of non-steroidal anti-inflammatory drugs on prostaglandin E2 production by cyclooxygenase-2 from endogenous and exogenous arachidonic acid in rat peritoneal macrophages stimulated with lipopolysaccharide. *Prostaglandins Leukot Essent Fatty Acids* **55**, 451-457 (1996).
123. Caplan, A.I. & Correa, D. The MSC: an injury drugstore. *Cell Stem Cell* **9**, 11-15 (2011).
124. Saito, N. et al. Safe clinical use of carbon nanotubes as innovative biomaterials. *Chem Rev* **114**, 6040-6079 (2014).
125. Aoki, K., Ogihara, N., Tanaka, M., Haniu, H. & Saito, N. Carbon nanotube-based biomaterials for orthopaedic applications. *J Mater Chem B* **8**, 9227-9238 (2020).
126. Andreu, N. et al. Primary macrophages and J774 cells respond differently to infection with Mycobacterium tuberculosis. *Sci Rep* **7**, 42225 (2017).
127. Chamberlain, L.M., Godek, M.L., Gonzalez-Juarrero, M. & Grainger, D.W. Phenotypic non-equivalence of murine (monocyte-) macrophage cells in biomaterial and inflammatory models. *J Biomed Mater Res A* **88**, 858-871 (2009).

128. Chellat, F., Merhi, Y., Moreau, A. & Yahia, L. Therapeutic potential of nanoparticulate systems for macrophage targeting. *Biomaterials* **26**, 7260-7275 (2005).
129. Vieira, A.C. et al. Targeted macrophages delivery of rifampicin-loaded lipid nanoparticles to improve tuberculosis treatment. *Nanomedicine (Lond)* **12**, 2721-2736 (2017).
130. Amarnath Praphakar, R., Munusamy, M.A., Sadasivuni, K.K. & Rajan, M. Targeted delivery of rifampicin to tuberculosis-infected macrophages: design, in-vitro, and in-vivo performance of rifampicin-loaded poly(ester amide)s nanocarriers. *Int J Pharm* **513**, 628-635 (2016).
131. Wang, Y. et al. Polymeric nanoparticles promote macrophage reversal from M2 to M1 phenotypes in the tumor microenvironment. *Biomaterials* **112**, 153-163 (2017).
132. Xiong, S., Zhao, X., Heng, B.C., Ng, K.W. & Loo, J.S. Cellular uptake of Poly-(D,L-lactide-co-glycolide) (PLGA) nanoparticles synthesized through solvent emulsion evaporation and nanoprecipitation method. *Biotechnol J* **6**, 501-508 (2011).
133. Murakami, H., Kobayashi, M., Takeuchi, H. & Kawashima, Y. Preparation of poly(DL-lactide-co-glycolide) nanoparticles by modified spontaneous emulsification solvent diffusion method. *Int J Pharm* **187**, 143-152 (1999).
134. Lutsiak, M.E., Robinson, D.R., Coester, C., Kwon, G.S. & Samuel, J. Analysis of poly(D,L-lactic-co-glycolic acid) nanosphere uptake by human dendritic cells and macrophages in vitro. *Pharm Res* **19**, 1480-1487 (2002).
135. Panyam, J. & Labhasetwar, V. Dynamics of endocytosis and exocytosis of poly(D,L-lactide-co-glycolide) nanoparticles in vascular smooth muscle cells. *Pharm Res* **20**, 212-220 (2003).
136. Ritter, S.C., Milanick, M.A. & Meissner, K.E. Encapsulation of FITC to monitor extracellular pH: a step towards the development of red blood cells as circulating blood analyte biosensors. *Biomed Opt Express* **2**, 2012-2021 (2011).
137. Onoshita, T. et al. The behavior of PLGA microspheres containing rifampicin in alveolar macrophages. *Colloids Surf B Biointerfaces* **76**, 151-157 (2010).
138. Abuknesha, R.A., al-Mazeedi, H.M. & Price, R.G. Reduction of the rate of fluorescence decay of FITC- and carboxyfluorescein-stained cells by anti-FITC antibodies. *Histochem J* **24**, 73-77 (1992).
139. Mahmoudian, J. et al. Comparison of the Photobleaching and Photostability Traits of Alexa Fluor 568- and Fluorescein Isothiocyanate- conjugated Antibody. *Cell J* **13**, 169-172 (2011).
140. Phanse, Y. et al. Analyzing cellular internalization of nanoparticles and bacteria by multi-spectral imaging flow cytometry. *J Vis Exp*, e3884 (2012).
141. Uribe-Querol, E. & Rosales, C. Phagocytosis: Our Current Understanding of a Universal Biological Process. *Front Immunol* **11**, 1066 (2020).
142. Canton, J. Phagosome maturation in polarized macrophages. *J Leukoc Biol* **96**, 729-738 (2014).
143. Rice, J.J. et al. Engineering the regenerative microenvironment with biomaterials. *Adv Healthc Mater* **2**, 57-71 (2013).
144. Yu, Y., Wu, R.X., Yin, Y. & Chen, F.M. Directing immunomodulation using biomaterials for endogenous regeneration. *J Mater Chem B* **4**, 569-584 (2016).

145. Liu, Y. & Segura, T. Biomaterials-Mediated Regulation of Macrophage Cell Fate. *Front Bioeng Biotechnol* **8**, 609297 (2020).
146. Felix Lanao, R.P. et al. Physicochemical properties and applications of poly(lactic-co-glycolic acid) for use in bone regeneration. *Tissue Eng Part B Rev* **19**, 380-390 (2013).
147. Ullah, N. et al. NSAIDs do not require the presence of a carboxylic acid to exert their anti-inflammatory effect - why do we keep using it? *J Enzyme Inhib Med Chem* **31**, 1018-1028 (2016).
148. Minardi, S. et al. Biomimetic Concealing of PLGA Microspheres in a 3D Scaffold to Prevent Macrophage Uptake. *Small* **12**, 1479-1488 (2016).
149. Ma, S. et al. The pro-inflammatory response of macrophages regulated by acid degradation products of poly(lactide-co-glycolide) nanoparticles. *Engineering in Life Sciences* (2021).
150. Caires, H.R. et al. Macrophage interactions with polylactic acid and chitosan scaffolds lead to improved recruitment of human mesenchymal stem/stromal cells: a comprehensive study with different immune cells. *J R Soc Interface* **13** (2016).
151. Wynn, T.A., Chawla, A. & Pollard, J.W. Macrophage biology in development, homeostasis and disease. *Nature* **496**, 445-455 (2013).
152. Almeida, C.R. et al. Impact of 3-D printed PLA- and chitosan-based scaffolds on human monocyte/macrophage responses: unraveling the effect of 3-D structures on inflammation. *Acta Biomater* **10**, 613-622 (2014).
153. Mantovani, A. et al. The chemokine system in diverse forms of macrophage activation and polarization. *Trends Immunol* **25**, 677-686 (2004).
154. Martinez, F.O., Sica, A., Mantovani, A. & Locati, M. Macrophage activation and polarization. *Front Biosci* **13**, 453-461 (2008).
155. Mosser, D.M. & Edwards, J.P. Exploring the full spectrum of macrophage activation. *Nat Rev Immunol* **8**, 958-969 (2008).
156. McGonagle, D., Baboolal, T.G. & Jones, E. Native joint-resident mesenchymal stem cells for cartilage repair in osteoarthritis. *Nat Rev Rheumatol* **13**, 719-730 (2017).
157. Sesia, S.B. et al. Anti-inflammatory/tissue repair macrophages enhance the cartilage-forming capacity of human bone marrow-derived mesenchymal stromal cells. *J Cell Physiol* **230**, 1258-1269 (2015).
158. Saldana, L. et al. Immunoregulatory potential of mesenchymal stem cells following activation by macrophage-derived soluble factors. *Stem Cell Res Ther* **10**, 58 (2019).
159. Wang, Y. et al. TNF-alpha-induced LRG1 promotes angiogenesis and mesenchymal stem cell migration in the subchondral bone during osteoarthritis. *Cell Death Dis* **8**, e2715 (2017).
160. Valles, G. et al. Influence of inflammatory conditions provided by macrophages on osteogenic ability of mesenchymal stem cells. *Stem Cell Res Ther* **11**, 57 (2020).
161. Honczarenko, M. et al. Human bone marrow stromal cells express a distinct set of biologically functional chemokine receptors. *Stem Cells* **24**, 1030-1041 (2006).

162. Ponte, A.L. et al. The in vitro migration capacity of human bone marrow mesenchymal stem cells: comparison of chemokine and growth factor chemotactic activities. *Stem Cells* **25**, 1737-1745 (2007).
163. Anton, K., Banerjee, D. & Glod, J. Macrophage-associated mesenchymal stem cells assume an activated, migratory, pro-inflammatory phenotype with increased IL-6 and CXCL10 secretion. *PLoS One* **7**, e35036 (2012).
164. Mounayar, M. et al. PI3kalpha and STAT1 Interplay Regulates Human Mesenchymal Stem Cell Immune Polarization. *Stem Cells* **33**, 1892-1901 (2015).
165. Hirata, E. et al. 3D collagen scaffolds coated with multiwalled carbon nanotubes: initial cell attachment to internal surface. *J Biomed Mater Res B Appl Biomater* **93**, 544-550 (2010).
166. Im, O., Li, J., Wang, M., Zhang, L.G. & Keidar, M. Biomimetic three-dimensional nanocrystalline hydroxyapatite and magnetically synthesized single-walled carbon nanotube chitosan nanocomposite for bone regeneration. *Int J Nanomedicine* **7**, 2087-2099 (2012).
167. Tanaka, M. et al. In Vitro and In Vivo Evaluation of a Three-Dimensional Porous Multi-Walled Carbon Nanotube Scaffold for Bone Regeneration. *Nanomaterials (Basel)* **7** (2017).
168. Cancian, G., Tozzi, G., Hussain, A.A., De Mori, A. & Roldo, M. Carbon nanotubes play an important role in the spatial arrangement of calcium deposits in hydrogels for bone regeneration. *J Mater Sci Mater Med* **27**, 126 (2016).
169. Gholizadeh, S. et al. Preparation and characterization of novel functionalized multiwalled carbon nanotubes/chitosan/beta-Glycerophosphate scaffolds for bone tissue engineering. *Int J Biol Macromol* **97**, 365-372 (2017).
170. Abarrategi, A. et al. Multiwall carbon nanotube scaffolds for tissue engineering purposes. *Biomaterials* **29**, 94-102 (2008).
171. Hirata, E. et al. Development of a 3D collagen scaffold coated with multiwalled carbon nanotubes. *J Biomed Mater Res B Appl Biomater* **90**, 629-634 (2009).
172. Hirata, E. et al. Multiwalled carbon nanotube-coating of 3D collagen scaffolds for bone tissue engineering. *Carbon* **49**, 3284-3291 (2011).
173. Kostarelos, K. et al. Cellular uptake of functionalized carbon nanotubes is independent of functional group and cell type. *Nat Nanotechnol* **2**, 108-113 (2007).
174. Mu, Q., Broughton, D.L. & Yan, B. Endosomal leakage and nuclear translocation of multiwalled carbon nanotubes: developing a model for cell uptake. *Nano Lett* **9**, 4370-4375 (2009).
175. Hirata, E. et al. Transmission electron microscopic observation of cells cultured on multiwalled carbon nanotube-coated sponges. *J Electron Microsc (Tokyo)* **59**, 447-450 (2010).
176. Battigelli, A. et al. Peptide-based carbon nanotubes for mitochondrial targeting. *Nanoscale* **5**, 9110-9117 (2013).
177. Fujita, K., Obara, S., Maru, J. & Endoh, S. Cytotoxicity profiles of multi-walled carbon nanotubes with different physico-chemical properties. *Toxicol Mech Methods* **30**, 477-489 (2020).
178. Chen, T. et al. Water-soluble taurine-functionalized multi-walled carbon nanotubes induce less damage to mitochondria of RAW 264.7 cells. *J Nanosci Nanotechnol* **12**, 8008-8016 (2012).

179. Meng, J. et al. Carbon nanotubes activate macrophages into a M1/M2 mixed status: recruiting naive macrophages and supporting angiogenesis. *ACS Appl Mater Interfaces* **7**, 3180-3188 (2015).
180. Patel, K.D. et al. Coating biopolymer nanofibers with carbon nanotubes accelerates tissue healing and bone regeneration through orchestrated cell- and tissue-regulatory responses. *Acta Biomater* **108**, 97-110 (2020).
181. Burd, J.F. & Usategui-Gomez, M. A colorimetric assay for serum lactate dehydrogenase. *Clin Chim Acta* **46**, 223-227 (1973).
182. Wang, G. et al. Understanding and correcting for carbon nanotube interferences with a commercial LDH cytotoxicity assay. *Toxicology* **299**, 99-111 (2012).
183. Han, X. et al. Validation of an LDH assay for assessing nanoparticle toxicity. *Toxicology* **287**, 99-104 (2011).
184. Kroll, A., Pillukat, M.H., Hahn, D. & Schnekenburger, J. Interference of engineered nanoparticles with in vitro toxicity assays. *Arch Toxicol* **86**, 1123-1136 (2012).
185. Guadagnini, R. et al. Toxicity screenings of nanomaterials: challenges due to interference with assay processes and components of classic in vitro tests. *Nanotoxicology* **9 Suppl 1**, 13-24 (2015).
186. Forest, V. et al. Adsorption of lactate dehydrogenase enzyme on carbon nanotubes: how to get accurate results for the cytotoxicity of these nanomaterials. *Langmuir* **31**, 3635-3643 (2015).

CHAPTER 7. Annex

7.1. FITC-loaded nanoparticle internalization by human macrophages as analyzed by imaging flow cytometry (Image Stream^X)

Figure A1 illustrates the workflow used in IDEAS software with the "Internalization Wizard". First, a histogram representing the gradient RMS of channel 1 (brightfield) was created. It enables the discrimination between focused and out of focus cells by enumerating changes in pixel values. A gate was applied to ensure that the events under analysis were in focus (population named "Focused"). Next, a dot plot according to the area and aspect ratio of the cells previously gated (population "Focused") was made in order to select only the events that corresponded to single cells (population named "Focused & Single"). After that, cell events from "Focused & Single" were gated according to the CD14 fluorescence intensity (blood-monocyte derived macrophages express CD14). The defined CD14 positive macrophage population was named "Focused & Single & CD14 positive". Finally, gated events were displayed in a dot plot for the intensity of the fluorescence acquired in channel 2 versus the maximum florescence values (Max Pixel Ch02), where FITC is visible. Gated events defined in this graph represent cells positive for NP internalization (population named "Focused & Single & CD14 positive & FITC positive").

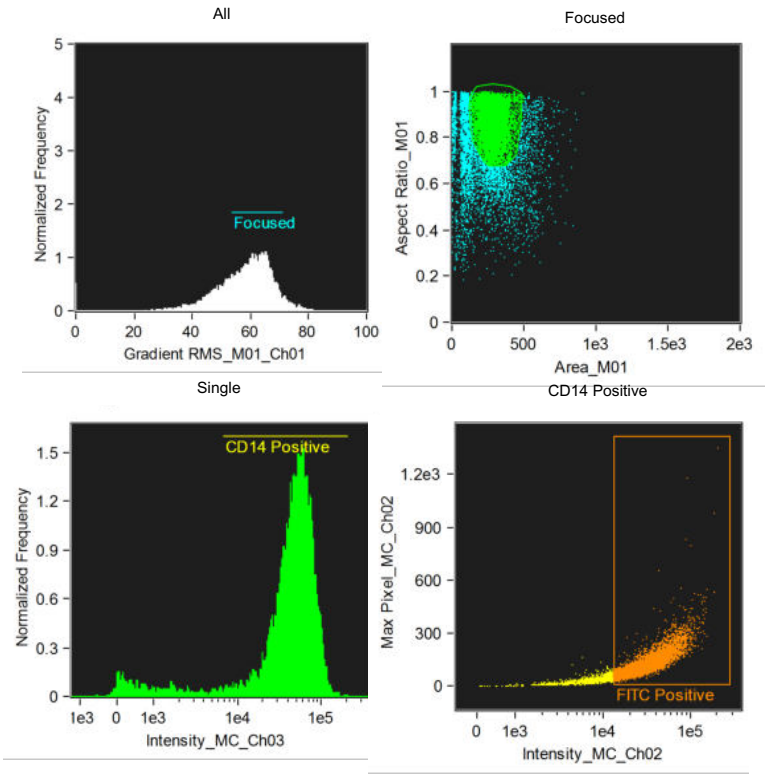

Figure A1. Workflow for the determination of FITC-loaded NP internalization. Gates define focused events (top left), single cells (excluding cell duplets or other complexes) (top right), define CD14 positive cells (bottom left) and positive events for FITC-loaded NP internalization (bottom right). The gates correspond to cells showing FITC-loaded NP internalization. In the control, macrophages show FITC intensity values out of the internalization gate defined, while all samples where FITC-PLGA NPs were used fall inside the defined gate.

7.2. CNT functionalized COPLA® Scaffold observed by transmission electron microscopy (TEM)

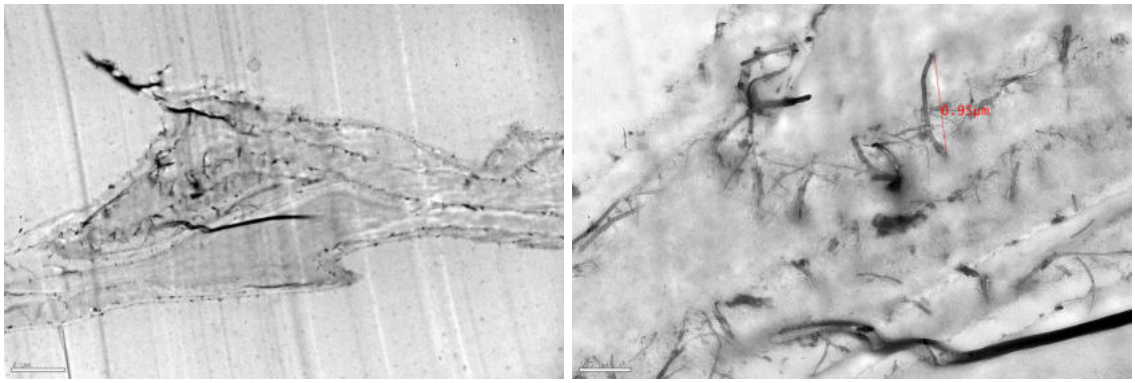

Figure A2. Transmission electron microscopy (TEM) images of CNT functionalized COPLA® Scaffold. TEM images of a nanoenabled COPLA® Scaffold clearly show the incorporation and dispersion of CNTs throughout the scaffold.